AB INITIO STUDIES OF SYSTEMS CONTAINING ACTINIDES USING RELATIVISTIC EFFECTIVE CORE POTENTIALS

DISSERTATION

Presented in Partial Fulfillment of the Requirements for

the Degree Doctor of Philosophy in the Graduate

School of The Ohio State University

By

Rajni Tyagi

*****

The Ohio State University
2005

Dissertation Committee:

Professor Russell M. Pitzer, Advisor

Professor Sherwin J. Singer

Professor James V. Coe

Approved by

Advisor
Graduate Program in Chemistry

ABSTRACT

The major part of this dissertation deals with quantum chemical calculations on atoms, molecules and clusters containing actinide elements. The calculations for these systems are challenging because: (1) correlation, relativistic and spin-orbit (SO) effects are significant and in many cases they are also strongly coupled; (2) three open shells (5f, 6d and 7s) with different angular quantum numbers are close in energy with substantial differences in radial extent and all are involved in bonding and excitations, not only increasing the size of the calculation but also the multireference character of the electronic states; (3) with many low- as well as high-lying (up to near ultraviolet) electronic states lying a few hundred cm^{-1} from others arising from the same and different electron configurations, a calculation involving higher-order electron correlation needs to be performed; (4) high core-valence correlation is present in many cases among 5s-5f and 6s-6d shells; and, finally (5) the coupling scheme is highly complicated.

In spite of the complexities inherent in studying the systems containing actinides, significant developments in theoretical models have resulted in the successful prediction of the electronic properties of systems containing actinides ranging from small systems like UH to large systems like $Pu(C_8H_8)_2$.

This work is another attempt to apply relativistic *ab intio* methodology to the study of the electronic structure of systems containing actinides not only in different regions of spectroscopy but also under different chemical environments. In all the systems studied in this work the relativistic effects, correlation effects and spin-orbit effects are strongly coupled. As a result our multireference configuration interaction method (MRCI) is an ideal choice to study these systems. In this work we have analyzed the electronic structure of systems like UO, UO_2, UO_2^{2+}, ThO and $Cs_2UO_2Cl_4$ among many others for which significant amounts of experimental data are present. In addition we have presented theoretical studies of systems like ThO^+ and UO^+ for which experimental work is currently in progress and our work has been used to guide the search for the transitions of interest. Our calculated results are in good agreement with the experimentally obtained results, when available.

To my mother

ACKNOWLEDGMENTS

The completion of my Ph.D. has been a long journey and I would like to take this opportunity to thank all the people who have helped make it a most memorable one.

Words cannot adequately express the encouragement and mentorship that I received from my advisor, Professor Russell Pitzer. I am indeed lucky to have interacted with someone who has the depth of scientific and general knowledge that he possesses (and so willingly imparts to his students). I will miss being a part of his research group. He also stood by me in all my diverse academic endeavors and was a constant pillar of support. Thank you, Dr. Pitzer.

My thanks to Professor Sherwin Singer, whose knowledge of and passion for the subject ensure that students such as me leave Ohio State with a much richer appreciation of research in physical chemistry.

I would also like to thank my parents, for having provided me with an environment that helped me to pursue all my dreams. They may be miles away, but I know they will always be by my side. Thanks are also due to my sisters: Neelam, who was always there for me (even though she is at that University up north), and Seema and Devyani for their moral support.

My very special thanks to Sumant Kulkarni, whose friendship is something I treasure the most in this world. I don't think I would have come this far in my life without him.

Thanks to Fersi Hannan, a very good friend. She almost single-handedly ensured that there was never a dull moment in my life in Columbus, Ohio. Finally, while the demands placed by my research were high, my colleagues in the Pitzer Group: Tianxiao Yang, Jean Blaudeau, Scott Brozell, Yang Yang, and friends in the Chemistry Department here at Ohio State: Jose Lopez, Ilias Sioutis and Jason Sonnenberg, considerably lightened the load by virtue of their company – my sincere thanks to all of them.

Finally I want to acknowledge Ali Hassanali, who I met in the last year of my PhD. His dedication towards his work has inspired me a lot. Because of him the last four months of my PhD, the most stressful time of my life turned out be the time I enjoyed a lot at Ohio State.

VITA

1998	M.Sc. – Indian Institute of Technology, Bombay Bombay, India
2001-2003	M.B.A. – Fisher College of Business, Ohio State University
1999-2004	Graduate Teaching Associate, Ohio State University
2004-2005	Graduate Research Associate, Ohio State University

FIELDS OF STUDY

Major Field: Chemistry
Division: Physical

TABLE OF CONTENTS

Page

Abstract ... ii

Dedication ... iv

Acknowledgments ... v

Vita ... vii

List of Tables ... xi

List of Figures ... xv

Chapters:

1. INTRODUCTION ... 1

1.1 COLUMBUS Package ... 1
1.2 Relativistic Effective Core Potentials ... 4
1.3 Basis Sets ... 8
1.3.1 Actinide Basis Sets ... 10
1.3.2 Basis Set Optimization ... 14
1.4 Theory ... 16

2. ELECTRONIC SPECTRUM OF THE GAS PHASE UO_2 MOLECULE ... 31

2.1 Introduction ... 31
2.2 Computational Details ... 34

2.3 Results and Discussion 38
2.3.1 Electronic-Structure Calculations 43
2.3.2 Coupling Scheme 50
2.2 Conclusions 54
2.3 Future Work 55

3. ELECTRONIC SPECTRUM OF THE UO AND UO^+ MOLECULES 68

3.1 Introduction 68
3.2 Computational Details 71
3.3 Results and Discussion 72
3.3.1 Electronic Spectrum of UO 75
3.3.2 Electronic Spectrum of UO^+ 84
3.4 Conclusions 89

4. ELECTRONIC SPECTRUM OF THE ThO AND ThO^+ MOLECULES 101

4.1 Introduction 101
4.2 Computational Details 102
4.3 Electronic Spectrum of ThO^+ 103
4.4 Electronic Spectrum of ThO 109
4.5 Conclusions 112

5. IONIZATION POTENTIAL STUDY OF OXIDES OF ACTINIDES 118

5.1 Introduction 118
5.2 Methods 120
5.3 Results and Discussion 121
5.4 Ionization Potential Study of UO 127
5.5 First Ionization Potential Study of Uranium 128
5.6 Ionization Potential Study of Thorium 130
5.7 Ionization Potential Study of ThO 131
5.8 Ionization Potential Study of ThO_2 133
5.9 Conclusions 134

6. THEORETICAL CALCULATIONS FOR THE HIGH-LYING EXCITED LEVELS AT THE OXYGEN K-EDGE FOR $Cs_2UO_2Cl_4$ 142

6.1 Introduction 142
6.2 Calculation Details 144
6.3 Results and Discussion 150
6.3.1 Ionization Potential 151
6.3.2 Hole State Calculation 152
6.3.3 Free-Ion Results 153
6.3.4 Crystal Calculation 154
6.3.5 Transition Assignments For Bands Below the Ionization Threshold 157
6.3.6 Assignments Above the Ionization Threshold 158

6.4 Conclusions 161

Bibliography 171

LIST OF TABLES

Table Page

1.1 Uranium cc-pVTZ Basis Set 24

1.2 Neptunium cc-pVDZ Basis Set 25

2.1 Bond lengths R_e (Å) for UO_2 in the gas phase 57

2.2 Partial Gross Population Analysis for selected MOs of the average of wave functions of the $^3\Phi_u$ ($5f^17s^1$) and the $^3\Delta_u$ ($5f^17s^1$) states at R_e = 1.803 Å 57

2.3 Partial Gross Population Analysis for selected MOs of the MCSCF wave functions from the average of the ^{3}Hg ($5f^2$) and $^3\Pi_g$ ($5f^2$) states at R_e = 1.803 Å........ 58

2.4 Mulliken Population Analysis for the average of wave functions of the $^3\Phi_u$ and $^3\Delta_u$ states at R_e = 1.803 Å using the 68-electron RECP........ 58

2.5 Mulliken Population Analysis for the MCSCF wave functions from the ^3H_g ($5f^2$) and $^3\Pi_g$ ($5f^2$) states at R_e = 1.803 Å using the 68-electron RECP........ 58

2.6 Mulliken Population Analysis for the average of wave functions of the $^3\Phi_u$ and $^3\Delta_u$ states at R_e = 1.809 Å using the 60-electron RECP........ 59

2.7 Mulliken Population Analysis for the MCSCF wave functions from the average of ^3H_g ($5f^2$) and $^3\Pi_g$ ($5f^2$) states at R_e = 1.809 Å using the 60-electron RECP........ 59

2.8 Comparison of the calculated and experimentally observed electronic structure for gaseous UO_2 in the UV-visible range........ 59

2.9 Non spin-orbit results for the low and high-lying states of UO_2 for triplet states (U68-electron RECP) 60

2.10 Electronic Spectrum Results for the low and high-lying of UO_2 using the cc-pVTZ basis set and 68-electron core potential........ 61

2.11 Electronic Spectrum Results for the low and high-lying states of UO_2 using the cc-pVDZ basis set and 68-electron core potential 63

2.12 Atomic character for the MOs listed in the Tables 2.9-2.11 66

3.1 Bond lengths of the UO molecule for the three low-lying states with $\Omega = 4$ using the cc-pVTZ Basis Set 91

3.2 Bond lengths of the UO molecule for the three low-lying states with $\Omega = 4$ using the cc-pVDZ Basis Set 91

3.3 Bond length of the UO^+ molecule for the ground state and two excited states using the cc-pVTZ basis set 92

3.4 Bond length of the UO^+ molecule for the ground state and the excited states in the absence of spin-orbit using the cc-pVDZ basis set 92

3.5 Electronic states of the UO^+ molecule without spin-orbit using the cc-pVDZ basis set at $R_e = 1.845$ Å 93

3.6 Electronic states of the UO^+ molecule with the cc-pVDZ basis set 93

3.7 Partial Gross Population Analysis for the bonding MOs for the $^4I + {}^4\Gamma + {}^4\Delta + {}^4\Sigma$ ($5f\varphi^1 5f\delta^1 5f\pi^1$) states for UO^+ at $R_e = 1.845$ Å 94

3.8 Partial Gross Population Analysis for the bonding MOs for the $^4H + {}^4\Pi$ ($5f\varphi^1 5f\delta^1 7s\sigma^1$) states for UO^+ at $R_e = 1.845$ Å 94

3.9 Partial Gross Population Analysis for the bonding MOs for the $^4H + {}^4\Pi$ ($5f\varphi^1 5f\delta^1 7s\sigma^1$) states for UO^+ at $R_e = 1.803$ Å 94

3.10 Partial Gross Population Analysis for selected MOs for the $^5I + {}^5\Gamma + {}^5\Delta + {}^5\Sigma$ ($5f\varphi^1 5f\delta^1 5f\pi^1 7s\sigma^1$) state for UO at $R_e = 1.879$ Å 95

3.11 Partial Gross Population Analysis for selected MOs for $^3H + {}^3\Pi$ ($5f\varphi^1 5f\delta^1 7s\sigma^2$) states for UO at $R_e = 1.879$ Å 95

3.12 Partial Gross Population Analysis for selected MOs for the $^5K + {}^5\Phi + {}^5\Pi$ ($5f\varphi^1 5f\delta^1 7s\sigma^1 6d\delta^1$) states for UO at $R_e = 1.879$ Å 95

3.13 Partial Gross Population Analysis for selected MOs for the $^3H + {}^3\Pi$ ($5f\varphi^1 5f\delta^1 7s\sigma^2$) states for UO at $R_e = 1.826$ Å 96

3.14 Vertical Transition Energies and Intensities for UO from the $\Omega'' = 4$ ground state 97

3.15 Adiabatic Transition Energies for the UO molecule 98

3.16 High-lying excited-state calculations with intensities from the $\Omega'' = 4$ ground state at its equilibrium geometry 99

3.17 High-lying excited-state calculations from the $\Omega'' = 3$ first excited state at the equilibrium geometry of the ground state 99

3.18 Tentative Assignments 99

4.1 Electronic States of the ThO^+ molecule at the equilibrium geometry of the ground state using the cc-pVDZ basis set and based on excitation from the 6σ MO........ 113

4.2 Charge-transfer transitions at the equilibrium geometry of the ground state based on the excitations from the 5σ or 3π bonding MOs 113

4.3 Transition Energies and Intensities for ThO^+ in the absence of spin-orbit............ 114

4.4 Atomic character for the ThO and ThO^+ MOs listed in Tables 4.1-4.3 and 4.6-4.7 114

4.5 Transition Energies and Intensities for ThO... 115

4.6 Experimental and theoretical T_e (cm^{-1}) results for ThO using different methods . 116

4.7 Mulliken Population Analysis for the $^2\Sigma^+$ ($7s\sigma^1$) wavefunction of ThO^+ at R_e = 1.825 Å 117

4.8 Mulliken Population Analysis for the $^1\Sigma^+$ ($7s\sigma^2$) wavefunction of ThO at R_e = 1.861 Å 117

5.1 Ionization Energy of AnO and AnO_2 systems using different experimental techniques (Refs [117-120], [131,132].. 136

5.2 Adiabatic Ionization Energy (eV) for UO_2 (gas phase).. 137

5.3 Ionization energies (eV) for UO_2 (gas phase) with different levels of electron correlation 137

5.4 CISD (spin-orbit) and CISD (non-spin-orbit) equilibrium bond length and ionization energy results for the UO_2 molecule using the cc-pVTZ Basis Set 138

5.5 CISD (spin-orbit) and CISD (non-spin-orbit) equilibrium bond length and ionization energy results for the UO_2 molecule using the cc-pVDZ Basis Set 138

5.6 CISD (spin-orbit) result for the Ionization Energy (eV) of the UO_2 molecule from the f^2 electron configuration using the cc-pVTZ Basis Set 138

5.7 Ionization Energy (eV) for the UO molecule using the cc-pVTZ Basis Set 139

5.8 Energy (eV) for the UO molecule using the cc-pVDZ Basis Set 139

5.9 Partial Gross Population Analysis for selected MOs of the $^1A_1$ state of ThO_2 using the Gaussian geometry (Th-O = 1.906 Å, O-Th-O = 118.75°) 139

5.10 Partial Gross Population Analysis for selected MOs of the $^2B_2$ state of ThO_2^+ using the Gaussian geometry (Th-O = 1.906 Å, O-Th-O = 118.75°) 139

5.11 Mulliken Population Analysis for the SCF wave function of the $^1A_1$ state of ThO_2 using the Gaussian geometry (Th-O = 1.906 Å, O-Th-O = 118.75°)................... 140

5.12 Mulliken Population Analysis for the SCF wave function of the $^2B_2$ state of ThO_2^+ using the Gaussian geometry (Th-O = 1.906 Å, O-Th-O = 118.75°)................... 140

5.13 Vertical Ionization Energy (eV) for ThO_2 based on Hartree-Fock calculations ... 141

5.14 Vertical Ionization Energy (eV) for ThO_2 based on single reference CISD calculations without spin-orbit 141

6.1 Mulliken Population analysis for U and O centers of UO_2^{2+} for a U-O distance of 3.155 bohr 163

6.2 Oxygen 1s Ionization energies at the SCF approximation 164

6.3 Vertical excitations energies of the UO_2^{2+} ion at U(R-O) = 3.155 bohr. (symmetry-broken solution) 165

6.4 Vertical excitations energies of the UO_2^{2+} ion at U(R-O) = 3.155 bohr. (symmetry-restricted solution) 166

6.5 Comparison of Excitation Energies for UO_2^{2+} (symmetry-broken results)........... 167

6.6 Assignment of Peaks for Perpendicular Polarization (symmetry-broken results). 167

6.7 Assignment of peaks for Parallel Polarization (symmetry-broken results) 168

LIST OF FIGURES

Figure Page

1.1 Vertical excitation energies from Oxygen K-edge of H_2O vs. the quality of basis set 26

1.2 Oxygen 1s ionization energies for H_2O vs. the quality of basis set 27

1.3 Energy level diagram of the LS and jj coupling scheme for the p^2 electron configuration and for the states arising from the $6p^2$ electron configuration of lead 28

1.4 Energy level diagram of the LS and jj coupling scheme for the p^3 electron configuration and for the states arising from the $6p^3$ electron configuration of bismuth 29

1.5 Energy level diagram of the LS and jj coupling scheme for the p^4 electron configuration 30

2.1 Energy level diagram of the (ω-ω) and (Λ-S) coupling schemes for the $\sigma^1\varphi^1$ electron configuration 67

3.1 Potential energy curves for three low-lying $\Omega = 4$ states of UO using the cc-pVDZ quality basis set 100

6.1 X-ray absorption spectrum at the oxygen K-edge for $Cs_2UO_2Cl_4$ 170

6.2 Orbital Energies of the valence orbitals of U^{+2} ion from relativistic Hartree-Fock wave functions 171

CHAPTER 1

INTRODUCTION

The calculations in this work are performed using the COLUMBUS package of codes [1-4]. This is one of the most flexible Multi-Reference Configuration Interaction (MRCI) programs, which has the capability to include relativistic effects, correlation effects and spin-orbit effects simultaneously under the double group symmetry of the molecule. This program is also one of the most efficient for studying the electronic structure of polyatomic molecules with very large spin-orbit interactions and high multireference character. The relativistic effects are treated with core and spin-orbit potentials derived from relativistic atomic calculations.

1.1 COLUMBUS Package

COLUMBUS is a collection of programs that deals with all aspects of MRCI calculations, from evaluating integrals over atomic orbitals to finally calculating the electric-dipole transition moments using the resulting wave functions. The atomic integrals are obtained using the ARGOS program, which has the capability to compute integrals up to angular momentum functions of h (l=5). Earlier this program was limited to just 256 basis functions, but it has been since modified to work with a calculation size of 1000 basis functions. The orthogonal atomic/molecular orbitals are generated using the Self-Consistent Field (SCF) or the Multi-Configuration Self-Consistent Field (MCSCF) method. In the SCF program [4], P-matrix extrapolation, level shifting and DIIS extrapolation [5] are the algorithms used for energy minimization. In addition the flexibility built into the program allows us to use the MO coefficient file of a previous run as starting orbitals. The atomic orbitals are converted to molecular integrals using the TRAN program. The multireference spin-orbit Configuration Interaction (CI) is performed using the Graphical Unitary Group Approach (GUGA). In addition to the GUGA CI program, there is one more flexible CI program to obtain the ground- and excited-state energies and wave functions. This program is a collection of two programs, namely, CGDBG, which generates the list of configurations for use in the CI, and CIDBG, which carries out CI calculation over double-group-adapted configuration functions. This program is more flexible than the GUGA CI program in the selection of the classes of configurations that should be included in the calculation, which is the most important facet of increasing the efficiency/quality of the CI calculation. The one major shortcoming of this program is that it is limited to expansions of several thousand configurations, whereas the serial GUGA version of the program itself can handle millions of configurations. But, on a positive note, there has been considerable ongoing work on the parallel version of CIDBG. The COLUMBUS system also has the capability to calculate transition moments using the transition density matrices of the CI wave functions. The oscillator strengths are calculated under the electric-dipole approximation, where the higher terms in the expansion of the electromagnetic vector potential are ignored. For degenerate levels, the oscillator strength is calculated by averaging over all the initial states and summing over all the final states making up the transition.

Using the COLUMBUS code with the GUGA CI program, all the calculations are carried out with D_{2h} symmetry and its subgroups, due to complications in CI code in using higher symmetry. The flexibility of using the fractional population in the SCF calculations, however, allows us to compute solutions with higher symmetry. As we are not performing the full CI, care should be taken in choosing the configuration expansion space so as to avoid breaking the symmetry. With less than a full CI, symmetry-adapted solutions are not necessarily the lowest energy solutions. The breaking of symmetry as a result of relaxation of the constraints can result in lower energy solutions. This behavior has been commonly observed in systems with core hole states (O_2^+ [6-7], UO_2^{3+} (this work), N_2^+ [8] etc.) and valence hole states (SF_6^+ [9], Cu_2^+ [10], CrO_4^{2-} [11], etc.). In these cases a lower SCF energy was obtained if the symmetry restrictions were released, but in the event that full CI is performed, both the symmetry-adapted and symmetry-broken solutions will give the same result, as there will then be an equal probability for the hole to be on any symmetry-equivalent center.

In our calculation, the effects of spin-orbit coupling are included explicitly by including the one-electron spin-orbit operator as a part of the Hamiltonian. The spin-orbit operator changes the Hamiltonian symmetry into the double group symmetry. We know that the Schrödinger Hamiltonian is invariant under point-group symmetry operations, which act on the spatial coordinates of the molecule, but such is not the case with its relativistic analogue, the Dirac Hamiltonian. The latter is invariant under double-group symmetry operations, which act on both the spatial and spin coordinates.

1.2 Relativistic Effective Core Potentials

For theoretical investigation of complexes containing heavy elements, not only a relatively large number of electrons have to be correlated but relativistic effects have also to be taken into account. The relativistic effects are so large in these heavy elements that a perturbation treatment is not feasible.

Relativistic effects for heavy elements can be categorized as: 1) indirect effects, 2) direct effects, and 3) spin-orbit effects. The direct effects result in the contraction of the orbitals due to the mass-velocity term. This effect is most obvious for the s and $p_{1/2}$ type orbitals as these orbitals tend to have a greater density near the nucleus, and therefore experience a greater fraction of the full nuclear charge. For the element Db (Z=105), the 7s orbital is contracted 25% relativistically [12]. The orbital shrinking experienced by s and p orbitals results in the expansion of outer d and f orbitals. The greater density of the s and p orbitals in the nuclear vicinity effectively crowds out the d and f orbitals through shielding effects. The resultant expansion of the d and f orbitals, and the associated shift of the orbital energies, is classified as an indirect relativistic effect often called the self-consistent expansion. The relativistic 5f orbital for uranium is expanded 20% in comparison to its non-relativistic counterpart [13]. Finally the relativistic expansion of d and f orbitals results in a small stabilization of the outermost s and p-orbitals. Finally, the SO interaction splits degenerate levels by the coupling of the electron's intrinsic spin angular momentum with its orbital angular momentum. All three relativistic effects grow roughly as Z^2 for isoelectronic valence shells [12].

Relativistic effects are incorporated implicitly in our calculation into the relativistic effective core potential (RECP), which is the part of the Hamiltonian in addition to the usual non-relativistic kinetic energy and Coulomb energy for the valence electrons and the approximate one-electron spin-orbit operator. The spin-orbit part of the core potential includes the spin-orbit interaction of the valence electrons with the nucleus and the core electrons. It also includes an approximation to the spin-orbit coupling between the valence electrons, which is very small in magnitude due to the $1/r^3$ dependence of the operator. Along similar lines, if RECPs are used, the SO coupling operators differ from those used without RECPs. This is because the valence orbitals now used are pseudo-orbitals, which remain the same in the valence region but then go nodelessly to zero in the core region. The effective spin-operators, derived simultaneously with the RECPs, compensate for the pseudo-orbital property.

The use of RECPs in the calculations drastically reduces the computational expenses of the calculations in comparison to the all-electron calculations, but at the same time allows us to incorporate all the important relativistic effects. The main idea behind this method is to replace the relatively inert atomic core (in accordance with the frozen-core approximation) with an effective potential, which takes into account the scalar relativistic effects, but ignores the core polarization in response to excitations or bonding. In the event the core-valence correlation and core polarization effects are negligible, this method can produce electronic structure results of great accuracy for atomic and molecular systems.

To date several schemes have been suggested to derive these RECPs [14-16]. In our calculation we have used RECPs generated by the shape-consistent procedure proposed by Christiansen *et al.* [17]. The shape-consistent RECPs with spin-orbit operators derived from the all-electron Dirac equation have been generated by

Christiansen, Ermler and coworkers [18-23]. The shape-consistent method for generating RECPs produces pseudo-orbitals that are equal to the corresponding all-electron orbitals in the valence region where the chemical bonding takes place.

The RECP approach allows us to include both relativistic effects and electron correlation simultaneously. This is quite important in the study of complexes, especially those containing heavy elements, as in these systems correlation effects and relativistic effects can be strongly coupled.

One of the important aspects of a calculation employing RECPs is to decide on the size of the core. This is very important especially for heavy elements in which there are large numbers of electrons that need to be correlated and the relativistic effects are not only significant for the core electrons but also for the electrons in the valence space. For actinides, RECP and SO operators of three core sizes are commonly used: large core (78e), medium core (68e) and small core (60e). The core space of 78-, 68- and 60-electron RECP is 1s-5d, 1s-5p and 1s-4f, respectively. In actinides, the small-core RECP (60e) provides better estimates of the electronic properties if the excitation/ionization involves change in the 5f occupation number. The change in the 5f occupation number results in the effective nuclear charge experienced by 5s, 5p, 5d, 6s, 6p, 6d and 7s orbitals due to their similar or larger radial extent. As a result, intershell correlations between these orbitals are significant. In the event this core-valence correlation effect is small and the 5s and 5p inner orbitals could be frozen in their atomic form, the 68-electron core was used in this work. For the 68-electron potential, the 5s and 5p shells are in the core, and the 5d shell is a part of the valence space. Although one might argue that the core-valence separation should be based on the principal quantum number (PQN), as the orbitals with the same PQN have similar radial extent and hence the higher coulomb and exchange interactions. This is valid in non-relativistic calculations, but it breaks down when relativistic effects are included. As discussed earlier, relativistic effects result in the contractions of s and p and the expansion of d and f orbitals, which results in a decrease the exchange interactions between s-d and p-d pairs.

The smaller the size of the core, the better will be the estimate for valence correlation energy (core-valence, valence-valence and valence-virtual) [24-25]. This is due to the fact that with small core, the radial nodal structure of the pseudo-valence orbital becomes more similar to the original valence orbitals. As a result, with a better description of the radial nodal structure, there will be an improvement in the exchange interactions involving these orbitals. But a drawback associated with using a small core size potential stems from the fact that when the RECPs are used to incorporate relativistic effects, the valence electrons are treated non-relativistically with traditional techniques. As a result, one-electron mass-velocity (MV) and one- and two-electron Darwin correction type relativistic effects are not included in the calculation for the orbitals that are not part of the core space. For calculations using the U 60 core, the 5s and 5p orbitals are out of the core and are treated non-relativistically. The 5s and 5p orbitals have significant electron density near the nucleus. So, the relativistic effects such as the MV correction are expected to be quite significant for the electrons in these shells. Thus, as a result in the calculations where the intershell correlation effects between the 5s, 5p and 5f orbitals is not significant, the medium size core potential (68e) might give better results than the small size core potential (60e). Beck *et al.* [26] performed calculations on the low-lying excitation energies of U^{4+} and U^{5+} with RECP sizes of 60e, 68e and 78e.

According to their calculations, the excitation-energy results obtained with the 68e RECP are in better agreement with experimental values than are those obtained with the 60e RECP. The important point to consider is that in their work all the low-lying excitations that are studied are 5f → 5f excitations. As a result there is no significant change in the 5f occupation number upon excitation.

1.3 Basis Sets

The ATMSCF atomic self-consistent field program [27-30] was used to generate the atomic basis sets to be used in conjunction with the RECP's in atomic/molecular calculations. The basis set used in conjunction with core potentials must describe pseudo-orbitals, which are small in the core region but equal to all-electron orbitals in the valence region.

In virtually all the *ab initio* calculations carried out currently, a basis set of contracted Gaussians is used. The use of Gaussian basis sets is strongly motivated by the fact that the three- and four-center two-electron repulsion integrals are relatively inexpensive to compute in comparison to those with Slater orbitals [31]. This is because the product of two Gaussian functions centered at different points is equal to a Gaussian function centered at an intermediate point. Hence, all the three- and four-center two-electron repulsion integrals are reduced to two-center integrals.

In our calculations, we have used basis sets that follow Dunning's correlation-consistent procedure [32-39]. The basic idea behind the correlation-consistent basis sets is that functions that contribute approximately the same amount of correlation energy should be grouped together when considering sets of basis functions to use. The main advantages in working with this class of basis set is that, firstly, it uses fewer primitive functions than the atomic natural orbital (ANO) basis sets without any loss in accuracy of the calculation and secondly, extrapolation is possible so as to approach the basis set limit [32]. These basis sets are labeled as cc-pVXZ, which stands for correlation-consistent polarized valence X-(X=D, double; X=T, triple; X=Q, quadruple) zeta with polarization.

For the calculations performed in this work, we have used basis sets up to the triple-zeta level for the actinide complexes, but for calculations involving only light elements, such as the x-ray absorption study of water (this work), basis sets of even cc-pV5Z quality were used. But as can seen from the Figures 1.1-1.2, the convergence of the excitation and ionization energy results for water is quite fast with the increase in the quality of the basis set. Thus care should be taken in using the optimum quality basis set to achieve a given level of accuracy, as the number of configurations increases very rapidly with the number of basis functions.

In basis-set optimization procedures, the atomic set is obtained by optimizing the exponents in an atomic Hartree-Fock (HF) calculation. In order to obtain the basis functions that are efficient in describing the molecular and atomic correlation, the following steps needs to be taken:

1. Extra contractions are added by freeing the most diffuse exponent of the respective symmetries so as to allow for the distortion of the atomic orbitals in the molecular environment.

2. For alkali and alkaline elements, where the core-valence correlation are significant, the additional s and p contractions are added that are meant to be at most singly occupied

in correlated calculations [40,41], thus providing core polarization effects not included in the RECP

3. An additional s contraction is added to the basis set, which is large in the core region. This contraction is then available to reduce the amplitude, in the core region, of orbtials centered on the neighboring atoms [42]. This contraction is useful only in molecular SCF or MCSCF calculations. It contributes to a very high energy virtual which makes little contribution to in correlated calculations and may be omitted from them.

(4) In the event a p inner shell has been replaced by a core potential, the uncontracted diffuse p primitives are augmented with a higher exponent primitive such that this contraction has a zero first derivative at the nucleus [42]. Basis sets for the first-row elements thus do not have these augmented p contractions. No improvement in correlation energy was observed in augmenting uncontracted d functions [42] such that the second derivative is zero at the nucleus.

5. An additional primitive of higher angular momentum but similar radial extent is added to account for the polarization of the orbitals involved in bonding, due to the fact that the exchange integral is large between two orbitals with high radial overlap and a small difference in the angular quantum number. In this work the polarization set is obtained by performing energy-based optimization of the exponent using the CISD calculation.

1.3.1 Actinide Basis Sets

In actinyl systems where the ground state and lower excited states are mostly $5f^n$ states and the contribution of the 7s and 7p is very little, the atomic set is obtained by optimizing the exponents in Hartree-Fock calculations on the $5f^2 6d^2$ average of configurations with the idea of obtaining a d and f basis close to optimum for a U(II) or higher oxidation-state ion. In addition, for these systems the g polarization set is added to correlate the f shell electrons. For like ThO and UO, such as are studied in this work, the 7s, 7p and 6d make a significant contribution to the ground state and the lower excited states, so we must think about these states carefully and be sure that we are developing our basis sets to include the proper functions. The 7s is mainly polarized and correlated by 7p, also 6d (outer contraction); the 6d is mainly polarized and correlated by the diffuse f contraction, so care should be taken that the outer 5f exponent is small enough to correlate the 6d shell electrons.

The cc-pVDZ basis for uranium that goes with the 68-electron core potential has been published by our group [43]. For the work listed in this thesis, however, a higher quality basis set was needed for uranium due to the presence of higher order electron correlation effects in the electronic structure calculations for the CUO, UO and UO_2 molecules. For CUO, there is currently a controversy as to whether the ground state of the molecule is $^1\Sigma^+_0$ or $^3\Phi_2$. With the cc-pVDZ quality basis set the $^1\Sigma^+_0$ - $^3\Phi_2$ difference of 19.08 kJ/mol was obtained. Then, with the cc-pVTZ basis set, the closed-shell $^1\Sigma^+_0$ level was 49.41 kJ/mol lower than the $^3\Phi_2$ state [44]. Also for the UO molecule, two low excited states have the same Ω value as the ground state with energy differences of approximately 300 cm^{-1} and are from the $5f^3s^1$ and $5f^27s^2$ type configurations. Also due to the weak-field approximation, all the low-lying states are highly multi-reference in character making the calculation sensitive to the quality of the basis set. Moreover, in the electronic structure study of $UO_{2,}$ there is strong mixing between states arising from different configurations. Hence not only the excitation energy but also the intensities are quite sensitive to the correlation treatments. According to our calculation the electronic structure results for UO_2 from the triple-zeta basis set are in better agreement with the experimental values then the ones obtained from the cc-pVDZ basis set. In addition, in this work, we were interested in checking the effect of the quality of basis sets on the ionization energy and the bond lengths of selected AnO and AnO_2 molecules. Though no change in the IE was obtained for the molecules studied in this work, the calculations are important from the standpoint that there is currently a significant discrepancy in the value of IE for UO and UO_2 obtained by different experimental and theoretical techniques. The increase in the quality of the basis set results in a bond length for UO just 0.01 Å different from the experimental value, whereas the difference was 0.04 Å with the basis set of cc-pVDZ quality.

The triple-zeta basis set for uranium is shown in Table 1.1. The first, second, and third sd (Cartesian 3d functions, linear combinations give 3s and 3d), the first p, and the first f contractions, represent the 5d, 6s, 6d, 6p, and 5f orbitals respectively. For the cc-pVDZ quality basis set an additional sd function was used to represent 7s whereas in our cc-pVTZ basis set we have added two additional 1s primitives to do this. Following the ideas of Christiansen *et al.* [42], using the high-angular momentum 3s primitives to describe uranium-centered s functions is problematic if the bonding between the metal and ligand is significant. The diffuse functions of the ligands can have significant amplitude close to the nucleus of uranium and they can be cancelled by uranium 1s functions and not the 3s functions as the latter has a zero amplitude close to the nucleus. After adding a 1s primitive of exponent 0.00757, one more 1s primitive was added to the basis set to obtain the proper behavior of the pseudo-orbital close to the nucleus. The triple-zeta basis set was augmented with two g polarization functions, which were optimized in an iterative fashion. There are quite a few local minima associated with this optimization; the best starting point is to take numbers on either side of the optimizated g exponent for the cc-pVDZ basis set. Finally the exponent for the h polarization function was optimized.

We also generated the cc-pVDZ quality basis set for neptunium to be used with 68e core potential; it is listed in Table 1.2. The atomic set was obtained by optimizing the (5sd,4p,4f) set of exponents in a Hartree-Fock calculation on the $5f^3 6d^2$ average of configuration, with the idea of obtaining a d and f basis close to optimum for a Np(II) or higher oxidation-state ion. The 7s and 7p orbitals were obtained by adding one sd primitive and two pf primitives and optimizing them for the $5f^3 6d^2 7s^1 7p^1$ average of configuration. This approach works well for systems in which the contribution of the 7s and 7p is very little for the neptunium complexes with high oxidation states. For neptunium, the optimization of orbital exponents for the p basis functions using the 2p primitives resulted in multiple collapses of adjacent exponents, i.e., the coefficients for the adjacent exponents became very large and equal in magnitude but opposite in sign. As discussed earlier [43, 40], this problem can be solved by using pf (Cartesian 4f) primitives to obtain basis functions for the 6p and 7p orbitals. In this approach, the 4p basis functions and the 4f basis functions share a common set of exponents, which not only takes care of the convergence problem but also reduces the number of total basis functions. Finally, the g polarization set was obtained by optimizing the exponent of a single g primitive by performing all the SO-CISD calculations on the lowest state of $5f^3 6d^2$. During this calculation, we only allowed for correlation of the 5f shell and the 6d orbital was doubly occupied in all the single and double references. The first, second, third and fourth sd and the first, second and the third pf contractions represent the 5d, 6s, 6d, 7s, 6p, 7p, and 5f orbitals respectively. The fifth sd, and third and fifth pf contractions, which give flexibility to the basis set, were obtained by freeing particular exponents of the respective symmetries.

1.3.2 Basis Set Optimization

As seen above, for actinides, the problem of collapse of primitives is quite severe during the exponent optimization. In order to deal with this problem one approach has been to use Cartesian primitives of larger angular momentum [40, 43], as mentioned in the previous paragraph. Another crude approach is to impose a restriction of some minimum difference between the exponents, which usually results in a higher value of the HF energy.

To deal with this problem, many methods of exponent optimization have been suggested in the literature and none of them has been applied so far to actinides and lanthanides. In the simplest approximation, two variational parameters are used to develop the even-tempered basis set [45, 46] (constant ratio of exponents). In the even tempered basis the plot of the logarithms of the exponents ($\ln \alpha_j$) vs. the index j (where $j = 1,2 ..N_{prim}$) is a straight line. This linear behavior is not observed in the exponents of optimized basis sets. For optimized basis sets, the spacing between the exponents is larger at either extreme (i.e., the large and small values of the exponents) than the ones in the middle. This is the reason why the plot of $\ln \alpha_j$ vs j has the resultant shape in the form of a curve [48]. The curve at lower values of j is concave up in shape because of the decrease in the spacing with the increase in the value of j, and similarly the shape is concave down at higher values of j because of the increase in spacing between the exponents at that end. If this curve is approximated by a polynomial, the degree of the polynomial should be at least three since this curve has a point of inflection. To address the shortcomings of the even-tempered basis set Huzinaga *et al*. [47] instead used polynomials with four variational parameters, and atomic total energy results very close to that from numerical HF calculations were obtained.

Finally, the method suggested by Petersson *et al.* [48] is the one used in this work and it has been implemented in the ATMSCF program by Pitzer [30]. In this method, the logarithms of the exponents are written in terms of orthonormal Legendre polynomials of an argument depending on j. This approach for the optimization for the exponents is much more attractive if core potentials are used since now the orbitals are replaced with pseudo-orbitals, which have fewer nodes than the respective valence orbitals. As a result fewer primitive functions are needed for the proper description of the orbitals. And finally fewer Legendre coefficients need to be optimized in order to derive the set of optimized Gaussian exponents. Cases of exponent collapse can be controlled by reducing the length of the Legendre expansion.

This method exploits the fact that the curvature behavior [48] is prominent in case of s, p and d primitives irrespective of atomic number and the size of the basis set. But, for primitives with large angular momentum, the exponents are more evenly spaced and hence the plot is more of a straight line.

1.4 Theory

The work in this thesis has been carried out at the self-consistent-field (SCF), multi-configuration self-consistent-field (MCSCF) and configuration interaction (CI) levels of theory.

The first steps in solving for the many-body problem is the HF approximation where the many-electron wave function is a determinant of single-particle wave functions. The HF wave function is an approximate solution of the many-electron Hamiltonian. There are several HF techniques and each may give a different energy and thereby different correlation energy, where correlation energy is defined as the difference between the HF energy and the exact non-relativistic energy [49]. In our work we perform the HF calculations using Roothaan's [50] analytical self-consistent field method. By definition, the correlation error inherent in the HF wave function is due to the mean-field approximation. The correlation between the electrons with parallel spins is included in the HF methods due to the antisymmetrization of the wave function.

HF is a good approximation if the total wave function is dominated by a single configuration. Thus, the HF wave function is variationally the best single determinant of orbitals for closed-shell systems. Then, care needs to taken since even if the HF wave function is a good approximation close to equilibrium, it will start to break down further away from equilibrium due to the multi-reference character of the states. The HF model also is a poor approximation for systems with multiple bonds, cases where near-degeneracy effects are important and thus the nondynamical correlation needs to be taken into account. In these conditions, the MCSCF wave functions provide a better description. In this method, both the molecular orbitals in the Configuration State

Functions (CSFs, linear combination of Slater determinants that are eigenfunctions of $\hat{S}^2$) and the coefficients of the CSFs are simultaneously optimized variationally. The MCSCF method provides a good starting point to study important chemical porperties if the active space can be represented by a limited number of carefully chosen configurations. The quality of an MCSCF calculation depends on the judicious selection of the configurations. The quality of the MCSCF wave function lies in the percentage of correlation energy included in the total energy obtained from the exact wave function. A frequently used kind of MCSCF is the complete active space SCF (CASSCF).

Dynamical correlation is incorporated into the wave function in our work using the CI approach, in which the variational trial wave function is written as a linear combination of CSFs.

We performed the calculations by including only the symmetry-allowed single and double excitations out of the multireference list of configurations. This accounts for the major part of the correlation energy at least near the equilibrium geometry where double excitations make the major contribution. The quadruple excitations are the next important contributor, but including all quadruples in the calculation is not the most efficient approach to incorporate further correlation effects. Instead, the flexibility built in our CI program can be exploited, which allows us to include single and double excitations out of any number or type of reference configurations. As a result, we can incorporate the important quadruples excitations in our calculation by including the important double excitations as a part of the reference space. This approach to include quadruples is still variational in nature. On the other hand, Langhoff and Davidson [51] formulated a simple correction factor, which gives an estimated value of the energy contribution that will emanate from the quadruple excitations. This approach makes the energies approximately size-consistent, but now the method is no longer variational.

The other popular methods to include electron correlation effects are coupled-cluster (CC) and many-body perturbation theory (MBPT). The CI, CC and MBPT techniques have come a long way in now successfully treating many-electron systems. References 52-57, 58-60, 61-64 are the earliest works in the field of CI, MBPT and CC respectively. The CI method, either full or truncated, is variational in contrast to the nonvariational MBPT and CC techniques. The primary weakness of truncated CI is that it is not size-consistent, which is not an issue for techniques like MBPT, CC and even the full CI.

Efficiency is further achieved in CI calculations by including configurations that make the difference in differential correlation energy upon excitation/ionization. For example, pairs of single excitations from different shells are required to characterize intershell correlation effects. Double excitations make the largest contributions to the total correlation energy, but their contributions to the differential correlation energy may be small. This assumes importance as double excitations account for the major contribution to total numbers of CSFs under the CI Singles and Doubles (CISD) approximation. Similarly, the chemically inert electrons make significant contribution to the total correlation energy but not to the differential correlation energy upon excitation/ionization.

For systems containing actinides, the active space requires at a minimum the distributions of valence electrons between the 5f, 6d and 7s open valence shells, putting a limitation on the size of the computation that can be handled by the currently available computing resources. The increase in the size of the calculation also makes the wave functions difficult to obtain due to the slow convergence of the CI expansion. This becomes a bigger issue when the states are not only multi-reference in character but also nearly degenerate. In case of systems containing heavy elements, even for calculations involving small molecules, the CI expansion space is of the order of millions. In addition, a small increase in the size of the reference space results in a large increase in the size of the calculation. For example, the uranium atom with a 68-electron core potential and the cc-pVDZ basis set has 55 basis functions. With 5s, 5p, 5d as a part of the frozen space, 6s and 6p as part of the inactive space, i.e. doubly occupied in all the references, and the reference space consisting of states arising from the $f^3d^1s^2$ type configuration and in addition the references incorporating $7s^2 \rightarrow 7p^2$ and $7s^2 \rightarrow 6d^2$ near-degeneracy excitations the size of the calculation was ca. 47 million CSFs. Now the attempt with a 60-electron RECP to correlate 5s, 5p and 5d electrons will result in a size of calculation that will be too large for currently available computing resources. On a positive note, now the working massively-parallel version of the MR-CISD program is also available as a part of the COLUMBUS package [67].

As discussed in the previous paragraph, the theoretical investigation of the electronic structure of complexes is challenging due to the high density of electronic states arising from different configurations and different multiplicities. This becomes quite challenging for systems like UO, where due to the small radial overlap of the metal centered 5f with the oxygen 2p atomic orbitals, the weak-field approximation holds among all the seven 5f MOs. According to our calculation for UO, there lie ~200 electronic states under ~16,000 cm^{-1} (~2eV). Experimentally many bands have been observed in the 16,000 – 21,000 cm^{-1} range [68]. Similar complex electronic spectra have been observed for lanthanide oxides [69]. As a result, the ligand field theory (LFT) approach has been used widely in the literature for lanthanide oxides and has been proven quite useful. A similar approach has been applied to a few oxides of actinides [68,70]. Thus a part of this work deals with testing the effectiveness of the LFT approach in predicting the electronic structure of systems containing actinides.

The CI calculations performed in this work are dependent upon the quality of the reference MOs. In the event full CI is performed, the final solution is independent of the initial MOs. For limited CI, however, the calculation is strongly dependent on the choice of the MOs that are optimized for particular reference configurations. But, then at the same time, the flexibility inherent in the CI program allows us to perform excited-state calculations in which appropriate reference CSFs can be provided for all states using a given set of MOs. For UO_2, the ground state and the excited states have different 5f occupation numbers and further complications arise from the mixing between states arising from f^1 and f^2 configuration. In order to represent the f^1 and f^2 configurations in a balanced fashion, we included the requisite 5f virtual orbitals ($2\delta_u$, $2\varphi_u$) as a part of the reference space such that a desired linear combination is created to represent an f orbital suitable for the particular occupation number of 5f. For example, the molecular orbitals may be generated for the ground state $5f(\varphi,\delta)^1 7s^1$ configuration. Then, in order to represent the excited ^3H_g states arising from $5f\delta^1 5f\varphi^1$ configuration, the reference space should include configurations: $1\varphi_u^1 1\delta_u^1$, $2\varphi_u^1 1\delta_u^1$, $1\varphi_u^1 2\delta_u^1$ and $2\varphi_u^1 2\delta_u^1$.

For systems containing actinides, the 5f, 7s and 6d orbitals can participate in bonding based on the energetic and spatial extents. But then as a result of relativistic stabilization/destabilization, the relative energy differences of the 5f, 7s and 6d changes as we go across the series, which is further evident in the electron configuration of the actinide elements. As a result, the ground-state configuration varies considerably among the An^{n+}, AnO and AnO_2 isoelectronic systems, which are the main focus of this work. For example for 2-e isoelectronic systems like UO_2, NpO_2^+, PuO_2^{2+} and AmO_2^{3+}, the ground-state configuration is $1\varphi_u^1 5\sigma_g^1$ ($5f\varphi_u^1 7s\sigma_g^1$) for UO_2 and $1\varphi_u^1 1\delta_u^1$ ($5f\varphi_u^1 5f\delta_u^1$) for the others. Similarly, for 3-e isoelectronic systems like UO_2^-, NpO_2, PuO_2^+, AmO_2^{2+}, the ground-state electronic configuration is $1\varphi_u^1 1\delta_u^1 5\sigma_g^1$ ($5f\varphi_u^1 5f\delta_u^1 7s\sigma_g^1$) for UO_2^- and NpO_2 and $1\varphi_u^1 1\delta_u^1 5\sigma_g^1$ ($5f\varphi_u^1 5f\delta_u^1 7s\sigma_g^1$) for PuO_2^+ and AmO_2^{2+}. Further the isoelectronic systems like UO_2^{2+} and ThO_2 have the same closed-shell ground state configuration, but then UO_2^{2+} is linear in structure whereas ThO_2 is bent with an experimentally obtained O-Th-O angle of 122±2° [71].

The multireference method is further necessitated by the fact that for systems containing heavy elements, the spin-orbit interaction is significant. For atoms, the L-S coupling scheme prevails among the lighter atoms. As a result the spin-orbit effects in these systems can be treated pertubatively. In the periodic table, the ground states of all the elements lower than platinum (Pt) can be treated under the framework of LS coupling. The ground-state electron configuration for Pt is $5d^9 6s^1$. After platinum, the next few elements in the periodic table are gold (Au), mercury (Hg) and thallium (Th) with the ground electron configuration of $5d^{10} 6s^1$, $5d^{10} 6s^2$ and $5d^{10} 6s^2 6p^1$ respectively. Since Au and Th are one-electron systems and Hg is a closed-shell system, the coupling scheme for these elements is indeterminate. The next element in the periodic table is lead (Pb) with a ground electron configuration of $5d^{10} 6s^2 6p^2$, which is the first element for which the ground state can best be described by the jj-coupling coupling scheme [74]. This is due to the large SO coupling constant associated with the 6p orbital. Along the same lines, bismuth (Bi) and polonium (Po), which arise from $5d^{10}6s^2 6p^3$ and $5d^{10}6s^2 6p^4$, are also governed by the jj coupling scheme. The ground state of neutral Pb, Bi, and Po is multireference in character [12] with the leading wave functions of $6p^2_{1/2}$ (J=0), $6p^2_{1/2}6p_{3/2}$ (J=3/2), and $6p^2_{1/2}6p^2_{3/2}$ (J=2) respectively. The direct approach to figuring out the coupling scheme comes from the relative size of the spin-orbit and exchange integrals. A semi-quantitative method to figure out the coupling schemes in atoms is the energy level pattern followed by the states under the two extreme coupling schemes, which is displayed in Figures 1.3-1.5 for p^2, p^3 and p^4 systems [72 - 74].

Currently there are two theoretical methods to incorporate spin-orbit effects into *ab initio* configuration interaction (CI) calculations. The commonly used term for both the techniques is the “one-step” and “two-step” approaches [12, 65-66]. As evident from the names, the one-step approach involves simultaneous consideration of electron repulsion and spin-orbit effects, but in the two-step approach, the computational effort is reduced considerably by first introducing the correlation effects and second adding the spin-orbit interaction. The two approaches will result in very similar results for electronic structure calculation if at least these two conditions are satisfied: (1) if either the ω-ω or Λ-S limit coupling scheme is a good approximation and (2) if there is no mixing between states arising from different coupling schemes. In this case, the two-step approach is more efficient in comparison to the one-step approach. But in cases of intermediate coupling and heavy mixing between states described with different coupling schemes, the one-step CI-SO approach is superior. In the event the extreme coupling scheme prevails, both the one-step and the two-step approach will give a similar value of bond length and vibrational mixing, but then in the presence of intermediate coupling also the two methods might coincidentally give the same value of r_e in the event that the spin-orbit mixing is between the two states with almost the same values of the internuclear distance. For the ground state of ThO, which stems from the $6\sigma^2$ ($7s\sigma^2$) configuration, r_e of 1.861 Å (this work) and 1.862 Å [75] is obtained using the one-step and two-step approach respectively.

The coupling scheme in actinyl ions has been studied quite extensively in the literature [76-78]. The ground and excited states cannot be described well within the framework of one coupling scheme (ω-ω, Λ-S and intermediate). For UO_2, whose electronic structure is studied extensively in this work, for the ground state configuration ω-ω coupling is a better approximation but then all the three coupling schemes are present among excited states. Above all, there is a strong mixing between the states that are best described in the framework of different coupling schemes. Under the single-configuration approximation, the transition moment is independent of correlation. Heavy mixing between the states of the same and different multiplicities makes the transition moment values sensitive to the accuracy of the correlation and spin-orbit treatment. In these cases the more balanced description of the spin-orbit, relativistic and electron correlation effects is needed, which is one of the most prominent features of the COLUMBUS package of codes.

orbital	primitives	contractions					
sd	16.04	-0.0220169	0.0014641	0.0062287	-0.0004537	0.0	0.0
	2.688	0.7131844	-0.1093208	-0.2750109	0.0396668	0.0	0.0
	1.071	0.3571578	0.6588099	-0.0529771	-0.3297919	0.0	0.0
	0.4678	0.0159465	0.4618666	0.4298592	-0.0747694	0.0	0.0
	0.1556	0.0070934	0.0185132	0.5988588	0.6543130	1.0	0.0
	0.0550	-0.0021820	0.0018716	0.1756525	0.4681155	0.0	1.0
s	2.688	1.0					
s	0.007566	1.0					
p	7.579	-0.0022720	0.0000000	0.0009548	0.0000000		
	1.391	-0.3312456	0.0000000	0.0929973	0.0000000		
	0.6237	0.7820047	-0.3114600	-0.2522302	0.0000000		
	0.2453	0.4894980	1.0000000	-0.1664635	0.0000000		
	0.05872	0.0198571	0.0000000	0.5430849	-0.2752451		
	0.02092	-0.0028652	0.0000000	0.5773948	1.0000000		
	0.005328	0.0006100	0.0000000	0.0192379	0.0000000		
f	7.299	0.0685408	0.0	0.0			
	2.940	0.2994046	0.0	0.0			
	1.404	0.3884397	0.0	0.0			
	0.6741	0.3226422	1.0	0.0			
	0.3113	0.1742962	0.0	1.0			
	0.1306	0.0456812	0.0	0.0			
g	2.922	1.0					
g	0.9207	1.0					
h	1.825	1.0					

Table 1.1: Uranium cc-pVTZ Basis Set

orbital	primitives	contractions				
sd	13.24	-0.0426918	-0.0001850	0.0126673	0.0005991	0.0
	2.937	0.6828050	-0.1314906	-0.2609691	0.0522590	0.0
	1.215	0.3851901	0.5929210	-0.0874958	-0.2987080	0.0
	0.5332	0.0302773	0.5344052	0.4112376	-0.1262166	0.0
	0.1695	0.0060190	0.0308034	0.6256602	0.6425674	0.0
	0.05792	-0.0017369	-0.0008087	0.1878609	0.5079069	1.0
pf	5.292	-0.0083521	0.0023053	0.0	0.1531555	0.0
	2.227	0.0276818	-0.0088938	0.0	0.4315985	0.0
	0.9412	0.6574724	-0.1860092	0.0	0.4286991	0.0
	0.3717	0.4219143	-0.0180497	0.0	0.2366999	1.0
	0.01136	0.0275201	0.5235156	0.0	0.0410615	0.0
	0.03762	-0.0010256	0.6197986	1.0	-0.0041099	0.0
g	1.800	1.0				

Table 1.2: Neptunium cc-pVDZ Basis Set

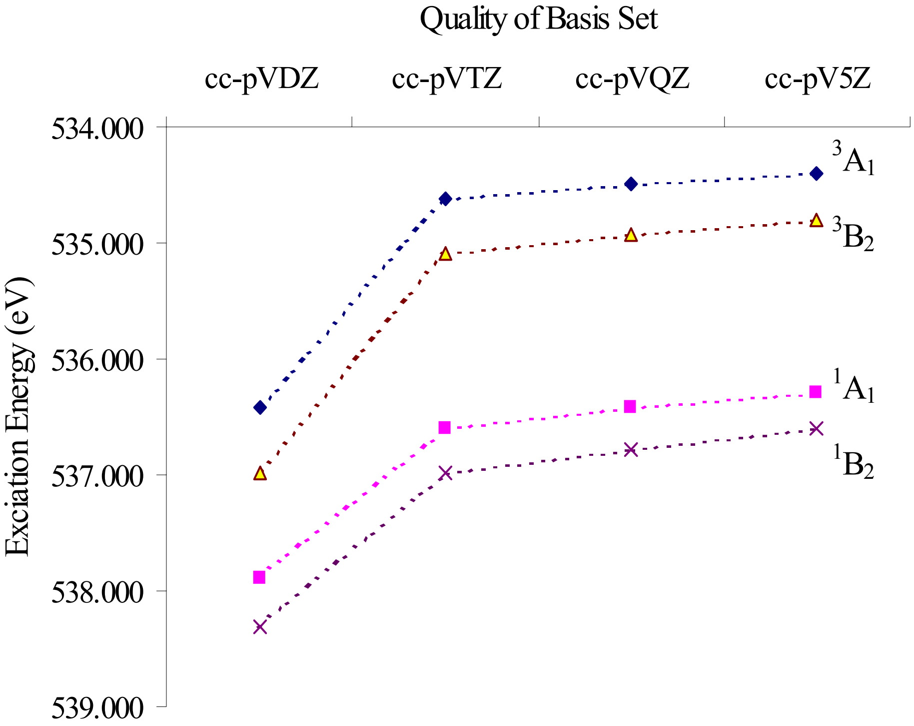

Figure 1.1: Vertical excitation energies from Oxygen K-edge of H_2O vs. the quality of the basis set

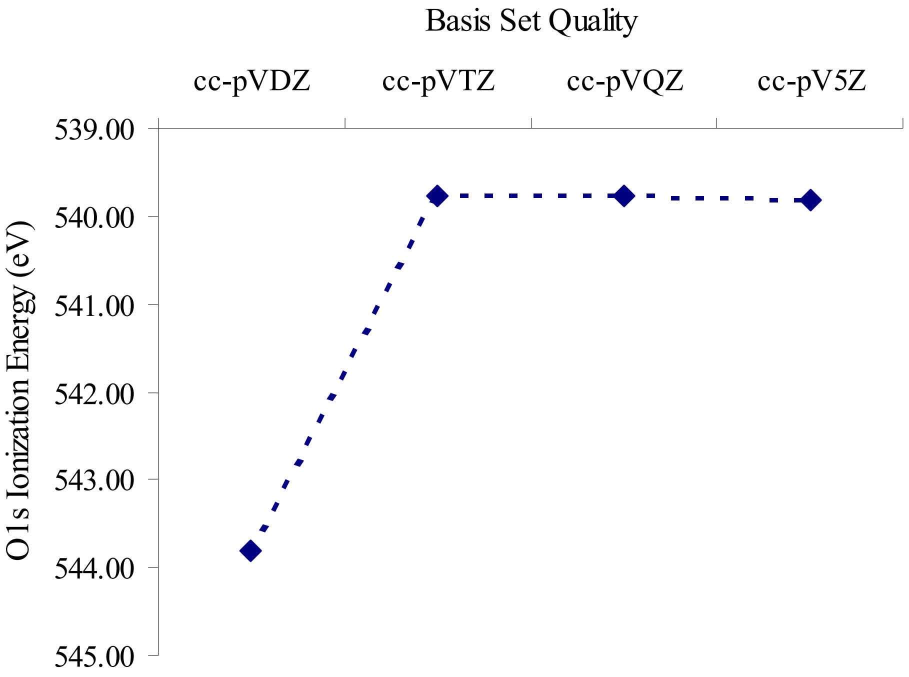

Figure 1.2: Oxygen 1s ionization energies for H_2O vs. the quality of the basis set

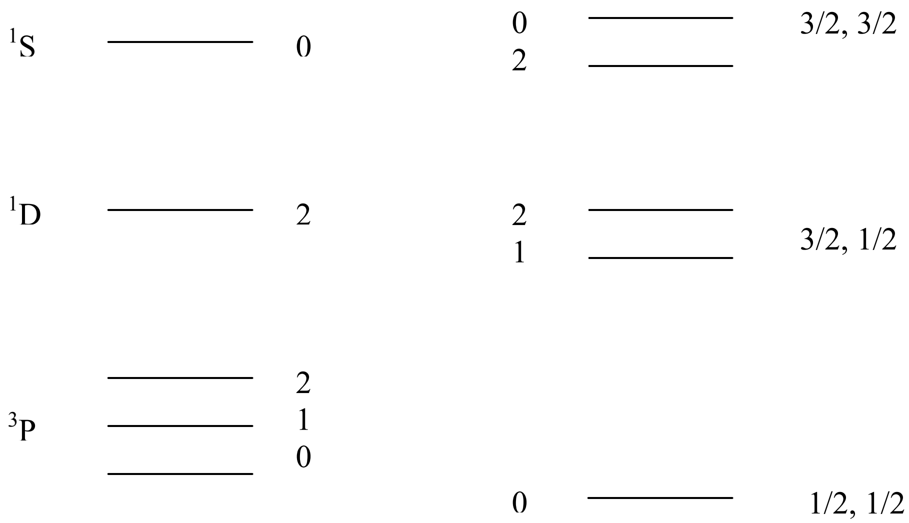

LS Coupling (3,1,1) jj Coupling (1,2,2)

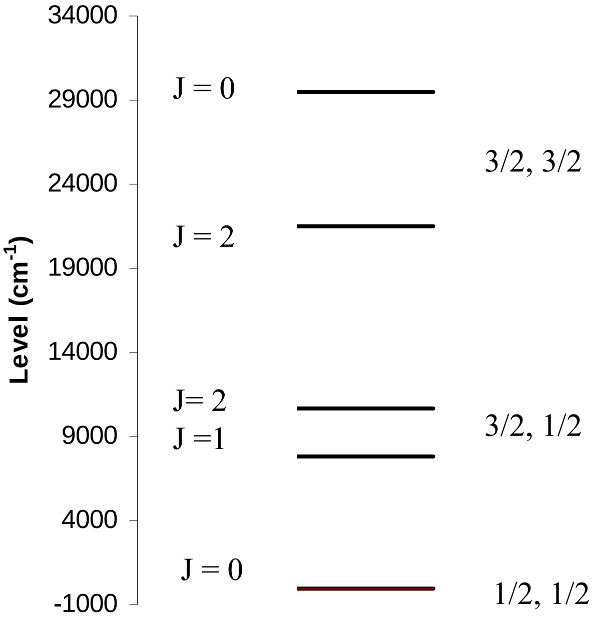

Energy Level Diagram for Pb (6p^2 conf.)

Figure 1.3: Energy level diagram of the LS and jj coupling scheme for the p^2 electron configuration and for the states arising from the 6p^2 electron configuration of lead

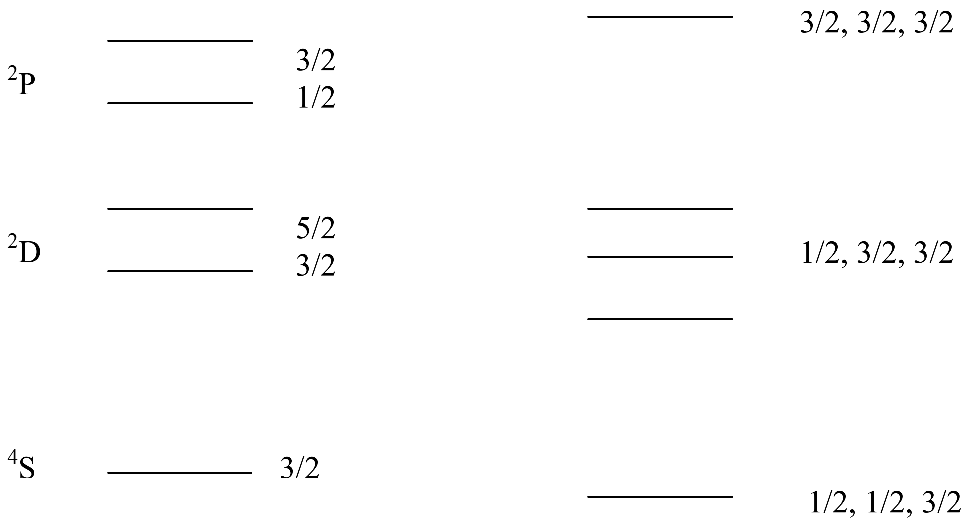

LS Coupling (1,2,2)　　　*jj* Coupling (1,3,1)

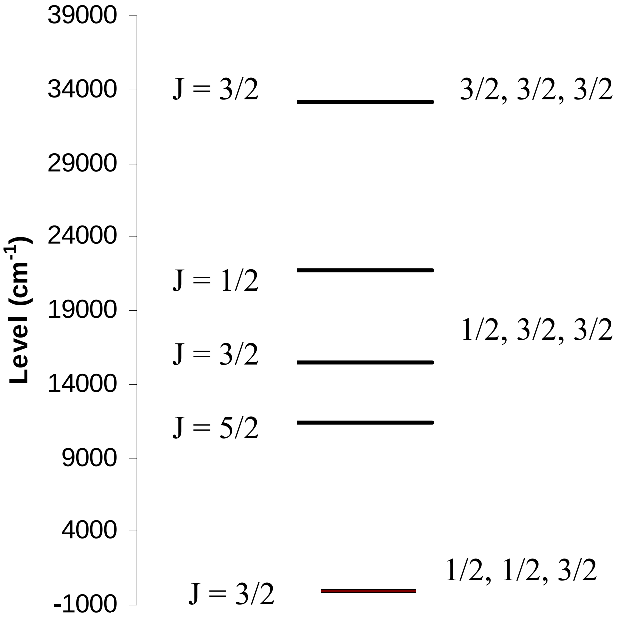

Energy Level Diagram for Bi (6p^3 conf.)

Figure 1.4: Energy level diagram of the LS and jj coupling scheme for the p^3 electron configuration and for the states arising from the 6p^3 electron configuration of bismuth

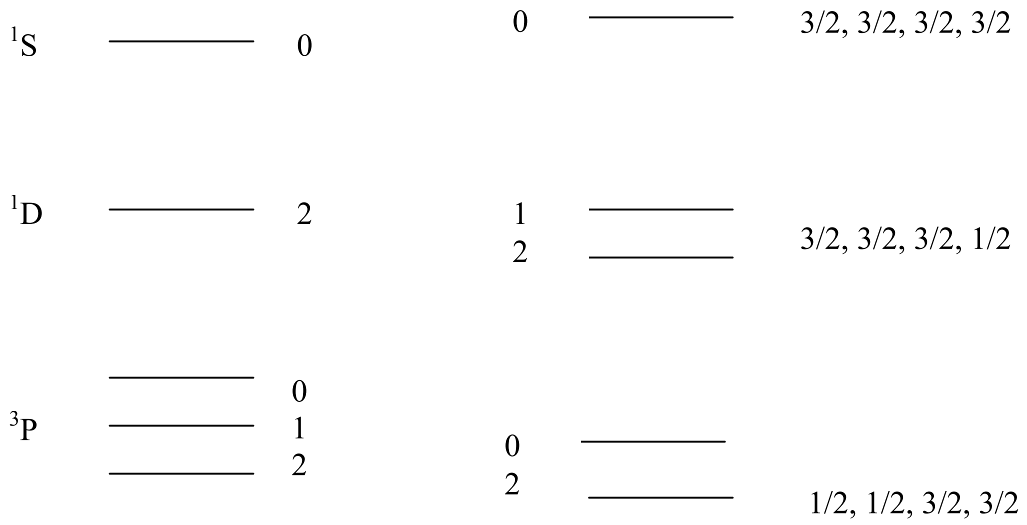

LS Coupling (3,1,1)

jj Coupling (2,2,1)

Figure 1.5: Energy level diagram of the LS and jj coupling scheme for the p^4 electron configuration

CHAPTER 2

ELECTRONIC SPECTRUM OF THE GAS PHASE UO_2 MOLECULE

2.1 Introduction

Heaven *et al*. [79] have recently reported 22 vibronic bands of UO_2 in the ultraviolet and visible range using resonantly enhanced multiphoton ionization techniques (REMPI). Transitions originating from excited states have also been explored using dispersed fluorescence techniques for UO_2 trapped in solid argon [80]. Currently, infrared absorption spectra are available for UO_2 in isolated neon and argon matrices [81] but not for gaseous UO_2. A large shift in the asymmetric stretching frequency has been observed with the change in host rare gas from Ne to Ar [81]. The change in the ground state from $^3\Phi_{2u}$ to $^3H_{4g}$ is offered as an explanation for this change in the frequency with the change in the rare gas from Ne to Ar. According to our gas-phase calculations, the adiabatic excitation energy between the two states is ~1250cm^{-1}. Finally, the ionization potential of UO_2 data is available from mass spectrometry [82] and enhanced multiphoton ionization techniques (REMPI) [83].

In this chapter, the electronic structure and nature of the excited states of UO_2 are investigated using the multireference configuration interaction approach. This method proves optimal in studying this system as the involvement of 5f, 6d and 7s in bonding results in many states with different open-shell configurations and because the heavy mixing between these states complicates the calculation further. This work involves studying the transition energies and intensities of bands with a much higher level of correlation than previous work [85] and the results are in good agreement with the observed experimental bands in the 17400 – 32000 cm^{-1} region.

In previous theoretical study of the electronic structure of UO_2, calculations have been performed by Chang using multi-reference configuration interaction techniques [85] and by Gagliardi *et al.,* using CASPT2 techniques [84]. Electronic structure calculations of UO_2 are among the calculations where benchmarking can be done not only between experimental and theoretical work but one can also assess the accuracy of different correlation and relativistic methods in studying the complicated excited-state structures of AnO and AnO_2 systems.

Most of the electronic states in the region of the study have less than 50% contribution from the principal term thus making electron correlation and spin-orbit effects very important for these states. We have performed electronic structure calculations using both cc-pVDZ and cc-pVTZ basis sets to study the effect of increased MO accuracy and correlation on transition energy and oscillator strengths for these states. In this work, the important occupied and virtual MOs needed to obtain the proper descriptions and correlation levels of the electronic states are discussed. Many of these MOs were included in the of theoretical calculations performed previously [84,85].

The ground state for UO_2 in the absence of spin-orbit is $^3\Phi_u$, which stems from the $1\varphi_u^1 5\sigma_g^1$ ($5f\varphi^1 7s\sigma^1$) electron configuration and has an equilibrium bond length of 1.774 Å. The study of the electronic spectra of UO_2 in the gas phase shows that the states with the strongest oscillator strength lie in the 27000-30000 cm^{-1} region, where the transitions are a result of excitation of an electron from the $7s\sigma$ MO to an MO with predominantly $7p\pi$ character. The four strongest (oscillator strength > 0.1) electric dipole-allowed transitions are perpendicular transitions at 27259, 28885, 29623 and 29670cm^{-1} with oscillator strengths of 0.1843, 0.1885, 0.1061 and 0.1566 respectively. These transitions correspond to $2_u \rightarrow 3_g$, $3_u \rightarrow 2_g$, $3_u \rightarrow 4_g$ and $2_u \rightarrow 1_g$ excitations, with two arising from the 2_u ground state and the other two being hot bands from the 3_u first excited state. The next sets of computed intense transitions lie in the spectral range of the experiment (17400 – 32000 cm^{-1}) at 16542 and 17328 cm^{-1} with oscillator strengths of 0.0856 and 0.0841 respectively. The transition at 16542 cm^{-1} corresponds to $2_u \rightarrow 1_g$ and the one at 17328 cm^{-1} corresponds to $3_u \rightarrow 4_g$.

The subsequent sections of this chapter are organized as follows. Section 2 details the theoretical approach and computational methods employed. Section 3 reports the results of the calculations performed, along with a discussion of them. Finally, Section 4 provides some conclusions that may be drawn from the results.

2.2 Computational Details

To study the electronic structure of UO_2 and its ions, *ab initio* calculations were performed using D_{2h} symmetry in the COLUMBUS suite of programs. Initial guess molecular orbitals (MOs) were obtained using the SCF and MCSCF programs. The experimental bond length is available for UO_2 in solid neon and argon (given bond lengths and references) but not for UO_2 in the gas phase. This gas-phase bond length for UO_2 was calculated using a 2-reference CI calculation. The reference space consisted of the states arising from $1\varphi_u^1 5\sigma_g^1$ and $1\delta_u^1 5\sigma_g^1$, where the $5\sigma_g$ is principally composed of the U7s orbital. The MOs were generated as the natural orbitals of MCSCF calculations by averaging the wave function for the $^3\Phi_u$ and the $^3\Delta_u$ states. Basis sets of cc-pVDZ and cc-pVTZ quality were used with both the 60e and 68e size uranium core potentials. The bond length calculation was also performed with different numbers of correlated electrons. In one case 14 electrons comprising 12 bonding electrons (C_1(O2p) + C_2(U5f or U6d)) and 2 valence electrons were correlated and in the second case all electrons were correlated. The resulting bond lengths are listed in Table 2.1.

The low-lying electronic structure calculation was performed using both the 68- and 60-electron RECP and SO operators for uranium. The valence spaces for the 68- and 60-electron RECPs for the uranium atom are $5d^{10}6s^{2}6p^{6}5f^{3}6d^{1}7s^{2}$ and $5s^{2}5p^{6}5d^{10}6s^{2}6p^{6}5f^{3}6d^{1}7s^{2}$ respectively.

For the excited state-calculations, the MOs were obtained by using an energy-averaged MCSCF calculation in which the ground state and the excited states that are observed below 36,000 cm^{-1} were averaged. The natural orbitals obtained from this MCSCF calculation were used in the CI calculations with single and double excitations from the multireference list of configurations. In addition, the MOs for these calculations can also be obtained by using the improved virtual orbital (IVO) method on MO generated from f^1 or f^2 configurations. In the event we are performing full CI calculations, it does not matter what set of initial molecular orbitals are used to perform the correlation calculation. Since it is not feasible to perform such a full calculation, limited CIs are performed which include the configurations expected to be necessary to achieve the desired level of accuracy.

The optimum set of MOs for the excited-state calculations are used for two reasons. First, there is a significant mixing between the states with different occupancy of the 5f shell. The 5f orbital needs to be more diffuse in case of states derived from f^2 configurations than the ones derived from f^1 configurations. Second, for transition-moment calculations, we need a common set of MOs for the ground and excited states. Hence, in order to perform the calculation satisfactorily we need to use the MOs and the corresponding reference space such that all states are described in a balanced way.

Between the states arising from f^1 and f^2 configurations there is not an exact increase in the population of the 5f shell by one electron as can be seen from Tables 2.4-2.7. Where there is an increase in population of the nonbonding $1\varphi_u$ and $1\delta_u$ orbitals, there is a decrease in the amount of 5f character in the $3\sigma_u$ bonding molecular as shown in Tables 2.1 and 2.2. As a result, interestingly, the charge on uranium is lower in the case of $^3\Phi_u$ ground state than in the case of the ^3H_g state in which the two electrons are in the nonbonding MOs. From the Mulliken population analysis, the overall charge distribution is $U^{+0.96}(O^{-0.48})_2$ for the $^3\Phi_u$ ground state and $U^{+1.20}(O^{-0.60})_2$ for the ^3H_g state.

In order to represent the f^1 and f^2 configurations on an equal footing, we need to include the requisite 5f virtual orbitals ($2\delta_u$, $2\varphi_u$) such that a desired linear combination is created to represent an f orbital suitable for the particular 5f occupation number. For example, if the MOs are generated from the $5f(\varphi,\delta)^1 7s^1$ configuration, then in order to represent the states of ^3H_g arising from the $5f\delta^1 5f\varphi^1$ configuration, the reference space should include the configurations: $1\varphi_u{}^1 1\delta_u{}^1$, $2\varphi_u{}^1 1\delta_u{}^1$, $1\varphi_u{}^1 2\delta_u{}^1$ and $2\varphi_u{}^1 2\delta_u{}^1$. In the event the molecular orbitals are obtained from the MCSCF technique, the single excitations from the references are the ones that will mix substantially with the main reference wavefunction to modify the MOs. This option for performing the electronic state calculation is quite attractive as including the singles does not scale the computational cost of the calculation substantially.

By including the right virtual orbitals in the references, one can obtain a high-quality wave function for the ground and excited states to account for the diffuseness of the 5f orbital. Along the same line, we do not need to include virtual MOs with 7s, 7p, 6d character in the reference space since all the states under study have either one or zero electrons in these orbitals.

In the case of UO_2, the problem is further intensified by the fact that between the different occupation numbers of the 5f shell, the composition of the $1\sigma_u$ and $2\sigma_u$ bonding molecular orbitals differ significantly. These orbitals are composed primarily of U6pσ and O2sσ atomic orbitals. The change in occupation number of the 5f orbitals changes the effective nuclear charge that is experienced by the electrons in the 6p orbital. The radial overlap of the 5f orbitals is quite significant with the 6s and 6p orbitals. The increase in the 5f population will destabilize the 6p orbital, thereby decreasing the mixing between U6pσ and O2sσ. This is evident from the fact that the bonding MO $1\sigma_u$ that comes out of the mixing between U6pσ and O2sσ orbitals has less 6p character and the corresponding $2\sigma_u$ antibonding orbital has more 6p character. The $2\sigma_u$ orbital further mixes with the O2pσ_u and U5fσ_u orbitals. It is the mixing of the 6p orbital with the oxygen orbitals that is responsible for the "hole" in the 6p shell in systems like UO_2^{2+} and NpO_2^{2+} [87-89]. The participation of the 6p shell in bonding is smaller in the U-O bond in UO_2 than in the U-O bond of UO_2^{2+} due to the longer UO bond distance in the former.

Since the $1\sigma_u$ and $2\sigma_u$ occupied MOs change significantly with the change in the 5f population, these fully occupied orbitals cannot be designated as part of the core orbitals, which would have been possible solely based on energetic arguments. Significant improvements in correlation energy are expected in correlating these electrons. In our calculations, these orbitals were added to the reference space, where they were doubly occupied in all the references but then single and double excitations were allowed out of them. At this stage, the lowest virtual orbtials with the same atomic orbital composition (U6pσ, O2sσ and O2pσ), was added to the active space to allow for the relaxation of these MOs with the change in 5f population.

Further, we have included the states arising from the $6d\delta^1 7s\sigma^1$ configurations in our reference space. These configurations were not included in previous calculations [84,85]. Without spin-orbit, the oscillator strength for the perpendicular transition from the $^3\Phi_u$ ground state to the $^3\Delta_g$ state arising from this configuration is 0.0126. The inclusion of this configuration as a part of the reference space is also important because the states arising from this configuration have substantial mixing with the ones that have the maximum dipole strength in the region of study (0 –36000 cm^{-1}).

We further analyzed the charge-transfer states arising from excitation out of highest occupied $3\sigma_u$ bonding molecular orbital as in the case of isoelectronic NpO_2^+ [89], which start at 23,000cm^{-1}, within the range of our study. In our calculation the low-lying charge-transfer states from the $3\sigma_u$ orbital were the ungerade state from the $3\sigma_u^1 5\sigma_g^1 1\delta_u^1 1\varphi_u^1$ configuration. The first state from this configuration lies at ~30,000 cm^{-1}, still in our region of study, but it was not included in our calculation since it is not dipole allowed from the ground state. The set of dipole allowed gerade states arising from the $3\sigma_u^1 1\delta_u^1 1\delta_u^1 1\varphi_u^1$ and $3\sigma_u^1 1\delta_u^1 1\varphi_u^1 1\varphi_u^1$ configuration start at 45,000 cm^{-1}, which are beyond our region of study.

The vertical transition energies were calculated using cc-pVDZ and cc-pVTZ quality basis sets. Transition-moment calculations are performed from both the $^3\Phi_u$ (2_u) ground state and the $^3\Phi_u$ (3_u) first excited state. As the difference between the $^3\Phi_u$ (2_u) and $^3\Phi_u$ (3_u) states is just 360cm^{-1}, the thermally excited bands are possible from the first excited state [78, 84] at the temperature of interest.

2.3 Results and Discussion

UO_2, unlike its isoelectronic systems NpO_2^+ and PuO_2^{2+}, has its ground state from $\sigma_g^1\varphi_u^1$ instead of the $(1\delta_u, 1\varphi_u)^2$ electronic configuration [79,81,84,85]. The bonding in UO_2 is similar to that of UO_2^{2+} discussed in Chapter 6. The ground state of UO_2 is the $^3\Phi_u$

(2_u) state arising from the $1\varphi_u^1 5\sigma_g^1$ ($5f\varphi^1 7s\sigma^1$) electronic configuration. The $5\sigma_g$ MO is made up of 80% U$7s\sigma_g$ + 17% U$6d\sigma_g$.

The equilibrium bond length for the ground state $^3\Phi_u$ (2_u) is 1.771 Å at the Hartree-Fock level. Subsequently, with added correlation through CI calculations these values are 1.803 Å and 1.777 Å for the cc-pVDZ and cc-pVTZ basis sets respectively. The accuracy of the Hartree Fock wavefunction in predicting the bond length closer to the one that is obtained with a higher level of correlation appears to be a coincidence. The MRCISD calculation with the cc-pVDZ basis set increased the bond length because of the mixing of the main reference with configurations with electrons excited to antibonding orbitals. The increased correlation obtained on using the triple zeta basis set then results in the shortening of the bond length.

According to our calculation, the spin-orbit interaction reduces the bond length by the small amount of 0.007 Å because of the mixing of the ground state with the $^3\Delta_2$ state, which has a shorter bond length than $^3\Phi_{2u}$. Gagliardi *et al.* [86] in their 14/14 large active space CASPT2 calculations also obtained the 0.04 Å decrease in bond length in the presence of spin-orbit. We did not obtain any change in the bond length by decreasing the size of the core to 60e from the 68e size core potential as can be seen from Table 2.1.

In the absence of spin-orbit with the 68-electron core potential for uranium, $^3\Delta_u$ ($5f\delta^1 7s\sigma^1$) is the ground state and the vertical $^3\Delta_u$ - $^3\Phi_u$ separation is 830cm^{-1}. But then with the 60-electron smaller core potential for uranium, the $^3\Phi_u$ is the ground state with the $^3\Delta_u$ being 551cm^{-1} above the ground state at its equilibrium bond length. The vertical $^3\Phi_u$ - $^3\Delta_u$ energy separation is reduced to 511cm^{-1} by including the states arising from

$3\sigma_u^0 1\delta_u^2 1\varphi_u^1$, $3\sigma_u^0 1\delta_u^3 1\varphi_u^0$ and $3\sigma_u^0 1\delta_u^1 1\varphi_u^2$ configurations in the reference space [89]. This is due to the fact that the electrons occupying the $3\sigma_u$ MO, which is the highest MO, is strongly bonding, and has substantial 5f character, are highly correlated with the electrons occupying the non-bonding $1\delta_u$ and $1\varphi_u$ uranium-centered orbitals. Since $1\delta_u$ and $1\varphi_u$ are virtually pure 5f orbitals, under the atomic scenario the spin-orbital lowering of $^3\Phi_u$ is 1.5 times that of $^3\Delta_u$, resulting in the $^3\Phi_{2u}$ ($5f\varphi^1 7s\sigma^1$) as the ground state in the presence of the spin-orbit.

The ground state of UO_2 in the presence of spin-orbit is multi-reference in character where the main reference has the weight of 71%. The wave-function character of the ground state is 71% $^3\Phi_{2u}$ ($5f\varphi^1 7s\sigma^1$) + 13% $^3\Delta_{2u}$ ($5f\delta^1 7s\sigma^1$) + 2% $^1\Delta_{2u}$ ($5f\delta^1 7s\sigma^1$) where the ratio of the coefficients of $^3\Phi_{2u}$ and $^3\Delta_{2u}$ is 5.4:1 The $^3\Phi_{2u}$ and the $^3\Delta_{2u}$ states mix due to the spin-orbit interaction.

According to the experimental results, the first excited state $^3\Phi_u$ (3_u) is just 360 cm^{-1} above the ground state (1) and according to our calculation it has a vertical T_e value of 439 cm^{-1} using the basis set of triple-zeta basis set and the 68-electron core potential. With the small size 60-electron core potential the $^3\Phi_u$ (2_u) - $^3\Phi_u$ (3_u) separation is reduced to 392 cm^{-1}. The zero-point energy correction and the difference between the vertical and adiabatic transition is negligible between the two states since they arise from the same electron configuration. The small difference between the $2_u - 3_u$ arises because of the strong $^3\Phi_{3u} \leftrightarrow {}^1\Phi_{3u}$ mixing in 3_u component of the $^3\Phi_u$ (actually closer to ω-ω coupling) . At the equilibrium bond length of the ground state, the wave function of the 3_u state is composed of 42% $^3\Phi_{3u}$ ($5f\varphi^1 7s\sigma^1$), 26% $^1\Phi_{3u}$ ($5f\varphi^1 7s\sigma^1$) and 18% $^3\Delta_{3u}$ ($5f\delta^1 7s\sigma^1$).

Since the first electronic state $^3\Phi_u$ (3_u) is just 360 cm^{-1} above the ground state, this state is populated thermally and a number of observed observation bands originate from this state [79, 84]. This fact assumes importance in the electronic spectrum calculation of UO_2, because the Ω value for the first excited state is different from that of the ground state. Based on the electric-dipole mechanism the transitions to excited states of the 1_g, 2_g or 3_g types are allowed from the ground state and the 2_g, 3_g or 4_g types from the first excited state. Electric-quadrupole and magnetic-dipole allowed transitions are not being studied as part of this work, which will also allow transitions to ungerade final states.

The next sets of states (1_u, 2_u, 3_u and 1_u) with ungerade symmetry arise from $1\delta_u^1 5\sigma_g^1$ ($5f\delta^1 7s\sigma^1$) configuration. The $^3\Phi_u$ (2_u) → $^3\Delta_u$ (1_u) vertical transition energies of 1037 cm^{-1} and 1893 cm^{-1} are obtained using uranium 68- and 60-electron RECP respectively. The 1_u state is mostly single reference in character with a contribution of 85% from the principal term. The 2_u state, on the contrary, has heavy spin-orbit mixing and has a vertical T_e of 1587 cm^{-1} and 2293 cm^{-1} using uranium 68- and 60-electron RECPs. The CASPT2 results [84] predict that the 1_u and 2_u states lie at 2567 and 2908 cm^{-1} above the ground state. The band positions for $^3\Phi_u(2_u) \leftrightarrow {}^3\Delta_u$ (1_u) and $^3\Phi_u(2_u) \leftrightarrow {}^3\Delta_u$ (2_u) transitions have been observed experimentally at 1094 cm^{-1}and 1401 cm^{-1} for UO_2 isolated in an argon matrix [79].

The lowest excited state of gerade symmetry arises predominantly from the f^2 ($1\varphi^1 1\delta^1$) configuration. This configuration generates the $^3H_{4g,5g,6g}$, $^1H_{5g}$, $^3\Pi_{0^+,0^-,1,2}$ and $^1\Pi_1$ Λ-S states. The equilibrium bond length for $^3H_{4g}$, the first state of gerade symmetry is 1.884 Å and 1.852 Å with the cc-pVDZ and cc-pVTZ basis sets respectively, longer than the corresponding values for the ground state. In the ground state, one electron is in in compact 5f shell and another one is in the diffuse 7s shell. Thus, screening of the nuclear charge is in this case is small for the 5f and large for the 7s in contrast to being moderate for both electrons on the 5fφ, 5fδ case. Thus, the states belonging to the $5f^2$ configuration will have larger equilibrium bond lengths, lower vibrational frequencies and smaller rotational constants compared to the ground state.

According to our results, the vertical $^3H_{4g}$ state has a vertical transition energy of 3974 cm^{-1} and an adiabatic transition energy of 1251 cm^{-1} above the ground level. At the equilibrium geometry of the ground state, the $^3H_{4g}$ – $^3H_{5g}$ and $^3H_{5g}$ - $^3H_{6g}$ separations are 3822 cm^{-1} and 4227 cm^{-1} respectively. In the 5_g component of the ^3H_g state, the $^3H_{5g} \leftrightarrow {}^1H_{5g}$ mixing is very small, with the composition of the ^3H_g (5_g) state being 86% $^3H_{5g}$ ($5f\varphi^1 5f\delta^1$) + 0.9% $^1H_{5g}$ ($5f\varphi^1 5f\delta^1$). Similarly, the ^3H_g (4_g) and the ^3H_g (6_g) state are also mostly single-reference states with reference weights of more than 80%. The ^3H_g (4_g) is 83% $^3H_{4g}$ ($5f\varphi^1 5f\delta^1$) and 3% $^1\Gamma_{4g}$ ($5f\delta^2$). The ^3H_g (6_g) is made up of 88% $^3H_{6g}$ ($5f\varphi^1 5f\delta^1$) and 2% $^1K_{6g}$ ($5f\varphi^2$).

The $^3\Pi_g$ component states arising from the same $5f\varphi^1 5f\delta^1$ configuration do not follow Hund's Rule, in contrast to the components of ^3H_g. The $^3\Pi_g(1_g)$ state is lower than the $^3\Pi_g(0_g^+)$ and $^3\Pi_g(0_g^-)$ states because of the strong $^3\Pi_1 \leftrightarrow {}^1\Pi_1$ mixing and also because of the heavy mixing with the $^3\Sigma_{1g}^-$ ($1\delta_u^2$) and $^3\Sigma_{1g}^-$ ($1\varphi_u^2$) states. The $^3\Pi_g(1_g)$ is composed of 34% $^3\Pi_{1g}$ ($1\varphi_u^1 1\delta_u^1$), 26% $^3\Sigma_{1g}^-$ ($1\delta_u^2$), 7% $^3\Sigma_{1g}^-$ ($1\varphi_u^2$) and 9% $^1\Pi_{1g}$ ($1\varphi_u^1 1\delta_u^1$), where the $^3\Pi_g(0_g^+)$ and $^3\Pi_g(0_g^-)$ states are relatively pure.

In addition to the gerade states arising from $5f\varphi^1 5f\delta^1$ configuration, the other configurations which contribute to the states in the visible and UV region are as follows:

$5f\varphi^1 7p\pi^1$, $5f\delta^1 7p\pi^1$, $5f\varphi^1 5f\pi^1$, $5f\delta^1 5f\pi^1$, $6d\delta^1 7s\sigma^1$, $5f\varphi^1 7p\sigma^1$ and $5f\delta^1 7p\sigma^1$. Among the low and high lying gerade states arising from these configurations, there is also a change in energy ordering from the one advocated by Hund's Rule due to spin-orbit mixing among the following systems: $^3\Pi_1 \leftrightarrow {}^1\Pi_1$, $^3\Delta_2 \leftrightarrow {}^1\Delta_2$, $^3\Phi_3 \leftrightarrow {}^1\Phi_3$ and $^3\Gamma_4 \leftrightarrow {}^1\Gamma_4$ and also because of the heavy mixing between states arising from different configurations.

The spin-orbit mixing between $^3\Pi_1 \leftrightarrow {}^1\Pi_1$ and $^3\Delta_2 \leftrightarrow {}^1\Delta_2$ is far more significant than the systems $^3\Phi_3 \leftrightarrow {}^1\Phi_3$ and $^3\Gamma_4 \leftrightarrow {}^1\Gamma_4$, which have higher omega values. The $^3\Gamma_g$ components of the $5f\varphi^1 7p\pi^1$ configuration follow Hund's rule with the energy ordering of the states being $^3\Gamma_{3g}$, $^3\Gamma_{4g}$, $^3\Gamma_{5g}$. The components of the $^3\Delta$ state which arise from the same configuration ($5f\varphi^1 7p\pi^1$), however, have the following ordering: $^3\Delta_{2g}$, $^3\Delta_{1g}$, $^3\Delta_{3g}$. The $^3\Delta_g$ (2_g) state is made up of 30% $^3\Delta_{2g}$ ($1\varphi_u^1 3\pi_u^1$), 27% $^1\Delta_{2g}$ ($1\varphi_u^1 3\pi_u^1$) and 21% $^3\Pi_{2g}$ ($1\varphi_u^1 1\delta_u^1$). On the other hand, for the $^3\Gamma_g$ (4_g) state, the spin-orbit mixing is negligible, but there is significant mixing with a $^3\Gamma_g$ (4_g) state arising from $5f\varphi^1 5f\pi^1$.

2.3.1 Electronic-Structure Calculations

The electronic spectrum of UO_2 has been obtained by Heaven *et al.* in the regions 17,400-18,600 and 27,000-32,000 cm^{-1} [79], where there are bands with observable intensity outside this region as predicted by our calculation and by work performed by Chang [85] and Gargliardi *et al.* [84]. Tables 2.8-2.11 list the transition energies and the oscillator strengths from the ground state 2_u and the first excited state 3_u for the low- and high-lying electronic states of UO_2 at the equilibrium geometry of the ground state. The atomic character of the MOs listed in Tables 2.8-2.11 is given in Table 2.12. As can be seen from the results tabulated in Tables 2.10 and 2.11, almost all the states are multireference in character with heavy spin-orbit mixing and the increased correlation offered by the better basis set having a significant effect not only on the excitation energy but also on the oscillator strength results. The calculation of oscillator strength involves the evaluation of transition moments, which under a single configuration approximation is independent of correlation. But, as we can see from Tables 2.9-2.11, there is a substantial mixing of the principal term with the term also arising from a different configuration, making the transition moment sensitive to correlation. The zero-point correction is not added to the numbers listed in these Tables. As discussed above, because the states arising from the f^2 configuration have longer equilibrium bond length r_e and a smaller value of vibrational frequency with respect to the ground state, the zero-point correction will result in a small decrease in the excitation energy. A similar situation is also observed when the electron is excited to the states with antibonding 5fπ and 5fσ character.

The transitions in the region below 36,000 cm^{-1} are both metal-to-metal centered transitions (examples, 7sσ → 5fδ or 7sσ → 5fφ, 5fφ → 6dδ or 5fδ and 7sσ → 7pσ) and the charge-transfer excitation involving the excitation of an electron from 7sσ orbital to an antibonding orbital with U5fπ and O2pπ character. Charge-transfer excitations arising from the excitation to the states with 5fσ character lie around 40,000 cm^{-1}, but these are not explored in this work. In the absence of spin-orbit, transitions from $^3\Phi_u$ ($5f\varphi^1 7s\sigma^1$) → $^3\Phi_g$ ($5f\varphi^1 5f\sigma^1$) and $^3\Delta_u$ ($5f\delta^1 7s\sigma^1$) → $^3\Delta_g$ ($5f\delta^1 5f\sigma^1$) lie at 43292 and 48402 cm^{-1} respectively.

Region I (less than 16000 cm^{-1}): Our calculations and those performed by Chang [85] and Gagliardi *et al*. [84], predict few electric-dipole-allowed transitions lower than 16000

cm^{-1}, the region in which no experimental results are currently available. There are two intense peaks at 13411 and 14365 cm^{-1} with oscillator strengths of 0.1047 and 0.0659, respectively. The electronic transition at 13411 cm^{-1} is a $2_u - 3_g$ perpendicular transition, where the 3_g excited state is the mixture of 72% $^3\Gamma_{3g}$ $(1\varphi_u^{\ 1}3\pi_u^{\ 1})$ and 6% $^3\Gamma_{3g}$ $(1\varphi_u^{\ 1}4\pi_u^{\ 1})$. The transition at 13926 cm^{-1} is a perpendicular $3_u \rightarrow 2_g$ transition in which there is some loss of intensity due to $^3\Delta_{2g} \leftrightarrow {}^1\Delta_{2g}$ spin-orbit coupling.

Below 16000 cm^{-1}, there are also two peaks with somewhat smaller oscillator strengths of 0.0282 and 0.0275 at 12042 and 13836 cm^{-1} respectively. The weak transition at 12042 cm^{-1} stems from the $3_u \rightarrow 2_g$ transition where the $^3\Pi_{2g}$ $(1\varphi_u^{\ 1}1\delta_u^{\ 1})$ main term of the excited state undergoes spin-orbit mixing with $^3\Delta_{2g}$ $(1\varphi_u^{\ 1}3\pi_u^{\ 1})$.

Similarly for the experimental observed band at 13836 cm^{-1}, the principal term of the final state is $^1\Gamma_{4g}$ $(1\delta_u^{\ 2})$ which does not contribute to the transition moment from 3_u. This is an example in which the transition probability has no contribution from the main terms but instead from the states that mix with both the initial (3_u) and final state (4_g) through spin-orbit coupling. The contributions to the oscillator strength come from the $^1\Phi_{3u}$ - $^1\Gamma_{4g}$ and $^3\Delta_{3u}$ - $^3\Phi_{4g}$ terms.

Region II (17,400 – 18,600 cm^{-1}): Heaven *et al.* [79], in their experiments have scanned the 17,400 – 18,600 cm^{-1} region of the visible spectrum. According to the experimental result, there are four electronic bands at the transition energies of 17859, 18159, 18227 and 18423 cm^{-1}. Gagliardi *et al.* [84] have assigned these transitions to 15454 ($3_u \rightarrow 2_g$), 16725 ($2_u \rightarrow 1_g$), 17274 ($3_u \rightarrow 4_g$) and 17645 ($3_u \rightarrow 1_g$) respectively. Gagliardi *et al.*(6), have assigned the experimentally observed transition at 17859 cm^{-1} to the 2_g state with their calculated value of 15454 cm^{-1}. According to our calculation, this transition has considerable intensity but it lies at an even lower transition energy of 13,926 cm^{-1}, making this even further from the experimentally observed band at 17859 cm^{-1}. Based on this argument, we have ruled out this transition as lying in the region where the experimental data were recorded. The next transition with significant oscillator strength is the $2_u \rightarrow 1_g$ perpendicular transition, which lies at 16542 cm^{-1}. This is the band we have assigned to the experimental observed band at 17859 cm^{-1}. Next in line is the transition from the first excited state to the 4_g final state, which lies at 17767 cm^{-1}. This $3_u \rightarrow 4_g$ transition is assigned to the observed peak at 18500 cm^{-1}. In this region our calculation further predicts two weak transitions at 18132 and 18935 cm^{-1}.

Region III (20,000 – 27,000 cm^{-1}): Again this is another region where no experimental measurements are available for gas-phase UO_2. In this region there are peaks of significant oscillator strength at 20677, 23634, 24380 and 24118 cm^{-1}, as can be seen from the results obtained using the cc-pVDZ basis set listed in Table 2.11.

Region IV (27,000 – 36,000 cm^{-1}): Heaven *et al.* [79] have obtained a group of bands in the region 27,000 – 30,000 cm^{-1}, in which all the bands have not been fully assigned. According to our calculation, among all the electric-dipole-allowed transitions that are calculated below 36000 cm^{-1}, the most intense transitions are found in this region at 26999, 27661, 29324, 29670 and 30062 cm^{-1}. The oscillator strength for the last four absorptions are greater than 0.1. All the intense electronic transitions in this region are as a result of excitation from an orbital with significant 7sσ character to the one with significant 7pπ character. This is to be expected as the transition comes from the 7s and

7p radial overlap which is large. In this region at 27813 cm^{-1}, there also lies a first transition arising from the 6dδ^{1}7sσ^1 configuration.

The experimental spectrum shows an intense transition at 27290 cm^{-1}. Corresponding to this observed band there are two computed transitions at 26999 and 27661 cm^{-1}. The transition at 26999 cm^{-1} corresponds to the $2_u \rightarrow 1_g$ transition, which is forbidden in the absence of spin-orbit. Moreover, the main contribution to the oscillator strength is from the $^3\Delta_{2u}$ - $^3\Pi_{1g}$ transition, where the $^3\Delta_{2u}$ is coupled to the principal term $^3\Phi_{2u}$ through spin-orbit. The calculated transition at 27661 cm^{-1} is a strong electric-dipole transition from the ground state to the state with predominantly $^3\Gamma_{3g}$ ($1\varphi_u^1 4\pi_u^1$) character. Finally the experimentally observed band at 27259 cm^{-1} is assigned to $2_u \rightarrow 3_g$ perpendicular transitions with the computed value of 27661 cm^{-1}, as the oscillator strength of this transition is almost five times more than the calculated $2_u \rightarrow 1_g$ transition at 26999 cm^{-1}. In addition, this assignment is in line with the fact that the absorption at 27290 cm^{-1} was observed in absorption spectra for matrix isolated UO_2 at 15K. The $2_u \rightarrow 3_g$ perpendicular transition is also a candidate for the emission band observed at 27120 cm^{-1} for UO_2 molecule isolated in solid argon [79].

The next strong experimentally observed band occurs at 29700 cm^{-1}. At 29670 and 29623 cm^{-1}, we have two very intense transitions from the ground state and the first excited state respectively. Since the band at 29700 cm^{-1} was observed in the absorption spectra for matrix-isolated UO_2 at 15K, this absorption will occur from the ground state instead of the thermally excited vibrational or electronic bands. Hence the observed feature at 29700 cm^{-1} has been assigned to the $2_u \rightarrow 1_g$ perpendicular transition.

The unassigned peak at 29623 cm^{-1} from the first excited state to the state with character 59% $^3\Gamma_{4g}$ ($1\varphi_u{}^1 4\pi_u{}^1$) + 5% $^1\Gamma_{4g}$ ($1\delta_u{}^2$), is a peak with considerable transition moment. We think that this transition could be the one associated with the vibronic band that is experimentally observed at 29654 cm^{-1}, which has been assigned by Heaven *et al.* as 1-1 vibrational structure. Also this assignment is in keeping with the argument that it was not observed at 15K, as it is a thermally excited transition.

The next set of experimentally observed transitions lies in the 28600-28800 cm^{-1} region. The transition in this region is assigned to the one from the first excited state to the 2_g final state that is made up of 36% $^3\Delta_{2g}$ ($1\varphi_u{}^1 4\pi_u{}^1$) + 26% $^1\Delta_{2g}$ ($1\varphi_u{}^1 4\pi_u{}^1$) + 5% $^3\Delta_{2g}$ ($2\delta_g{}^1 5\sigma_g{}^1$). This assignment is consistent with the one made by Gagliardi *et al.* [84]. Their calculated value is ~2083 cm^{-1} lower than the experimental value and our result differs by just ~200cm^{-1}. Also this excited state with its heavy singlet-triplet mixing might be the upper level for the emission band with a slow decay rate observed at 28169 cm^{-1} (355 nm). It was suggested by Heaven *et al.* [79] that this emission band undergoes decay by non-radiative relaxation.

The next set of experimentally observed bands at 31,478 cm^{-1} and 31838 cm^{-1} are separated by 360 cm^{-1} ($\Delta T_e = 2_u - 3_u$), which is the difference between the ground state and the first excited state. This has been explored earlier in literature [79, 84] that the two transitions are to the excited state that is optically accessible from both the ground state and the first excited state [79], or that the transitions are to the two closely spaced excited states from the 2_u and 3_u states respectively [84]. Transitions in this region have previously been assigned to the 2_g and 3_g states, which were found to arise predominantly from the $5f\varphi^1 7p\sigma^1$ configuration.

According to our calculation, the 2_g excited state at 34126 cm^{-1} has significant oscillator strength from both the 2_u ground state and the 3_u first excited state through parallel and perpendicular polarization. Then, at just a few cm^{-1} above this state, however, there are two closely spaced peaks ($\Delta T_e = 59$ cm^{-1}) with excited states at 34245 and 34625 cm^{-1}. The oscillator strength to these two states is four to five times more than to the one at 34126 cm^{-1}. The transition at 34245 cm^{-1} is a result of $3_u \rightarrow 3_g$ parallel excitation. The 3_g state is a heavily mixed state with the following composition: 32% ${}^3\Phi_{3g}$ ($1\varphi_u{}^1 4\sigma_u{}^1$) + 26% ${}^1\Phi_{3g}$ ($1\varphi_u{}^1 4\sigma_u{}^1$) + 9% ${}^3\Delta_{3g}$ ($1\delta_u{}^1 4\sigma_u{}^1$). The coupling scheme for the states arising from $1\varphi_u{}^1 4\sigma_u{}^1$ ($5f\varphi^1 7p\sigma^1$) is closer to the ω-ω limit (further explained in the section 2.3.2 of this chapter) thus there is significant ${}^3\Phi_{3g}$ - ${}^1\Phi_{3g}$ mixing, resulting in the spreading of intensity between various states. Still the $3_u \rightarrow 3_g$ parallel transition has oscillator strength of 0.0882 because the contribution to the oscillator strength comes from the ${}^3\Phi_{3u} \leftrightarrow {}^3\Phi_{3g}$, ${}^3\Delta_{3u} \leftrightarrow {}^3\Delta_{3g}$ and ${}^1\Phi_{3u} \leftrightarrow {}^1\Phi_{3g}$ pairs of initial and final wave-function components. The electronic transition at 34625 cm^{-1} is from the 2_u ground state to the 2_g excited state, where the 2_g state is made up of 56% ${}^3\Phi_{2g}$ ($1\varphi_u{}^1 4\sigma_u{}^1$) + 5% ${}^1\Delta_{2g}$ ($1\varphi_u{}^1 4\pi_u{}^1$) + 15% ${}^1\Delta_{2g}$ ($2\delta_g{}^1 5\sigma_g{}^1$). Gagliardi *et al.* [84] obtained a high oscillator strength of 0.1816 for the $2_u \rightarrow 2_g$ parallel transition, because they didn't include states from the $2\delta_g{}^1 5\sigma_g{}^1$ configuration in their reference space, which has resulted in some loss of intensity due to ${}^3\Phi_{2g} \leftrightarrow {}^1\Delta_{2g}$ spin-orbit coupling.

According to our results, there is an optically accessible state from the ground and first excited state at 39532 and 39093 cm^{-1} with the wave function character of 43% $^1\Phi_{3g}$ $(1\delta_u^1 4\pi_u^1)$ + 18% $^1\Phi_{3g}$ $(1\delta_u^1 3\pi_u^1)$. The parallel $3_u \rightarrow 3_g$ transition is far more intense than the $2_u \rightarrow 3_g$ perpendicular transition from the ground state. This 3_g upper state might be the candidate for the experimentally observed emission band with a slow decay rate observed for UO_2 in an Ar matrix at 37594 cm^{-1} [79].

2.3.2 Coupling Scheme

In this work the coupling scheme for the ground and excited states for UO_2 are studied. As with the electronic states of actinyl ions [76-78], the weak field approximation is only valid only among the four $5f\delta_u$ and $5f\varphi_u$ orbitals out of the seven 5f orbitals. On a larger energy scale, the splitting of $5f\pi$ and $5f\sigma$ away from $5f\delta_u$ and $5f\varphi_u$ is a strong-field effect due to their participation in the strong axial bonds.

In all the examples discussed below the coupling schemes are predicted based on analyzing the theoretical results that we have obtained using the MCSCF MO's and the reference space which attempts to treat the states arising from all the configuration on an equal footing. As a rule of thumb the ratio of the CI coefficients of the singlet and triplet terms is 0 and 1 for Λ-S and ω-ω coupling scheme respectively. In the case of ω-ω coupling scheme the spin-orbit interaction is a very large perturbation with respect to the exchange interaction, as a result the singlet and the triplet states arising from a particular configuration makes similar contribution to the total wave function. But the drawback in the approach lies in the fact for UO_2 most of the states are multireference in character, which can to an extent mask the nature of the exact coupling scheme.

In addition we have also used the semi-quantitative approach where the energy level pattern can give a good idea of the coupling scheme. For example as shown in Figure 2.1 the state arising from $\sigma^1\varphi^1$ type configuration under Λ-S coupling and ω-ω coupling will correspondingly follow a 3,1 or 2,2 pattern of energy levels based on the relative size of the exchange interaction and the spin-orbit interaction. Although the coulomb integral usually makes the largest contribution to the total energy but, as seen from Figure 2.1, it is the exchange and the spin-orbit integrals that determine the splitting of the states. Thus, the relative size of the spin-orbit coupling and the exchange interaction determines the coupling scheme.

The ground state of UO_2, $^3\Phi_u$ (2_u) stems from the $5f\varphi^17s\sigma^1$ electron configuration and then within few thousand cm^{-1} lie the states from the $5f\delta^17s\sigma^1$ electron configuration. For the states arising from both of these configurations the coupling scheme is closer to the ω-ω coupling rather than the Λ-S coupling. This can be seen from the wavefunction character of the 3_u and 2_u components of $^3\Phi_u$ and $^3\Delta_u$ states, which are 42% $^3\Phi_{3u}$ ($5f\varphi^17s\sigma^1$) + 26% $^1\Phi_{3u}$ ($5f\varphi^17s\sigma^1$) and 45% $^3\Delta_{2u}$ ($5f\delta^17s\sigma^1$) + 37% $^1\Delta_{2u}$ ($5f\delta^17s\sigma^1$) respectively. The $^1\Phi_{3u}/^3\Phi_{3u}$ and $^1\Delta_{2u}/^3\Delta_{2u}$ ratios are 0.63 and 0.88 in case of 3_u and 2_u states, where Λ-S coupling gives 0 and ω-ω coupling gives 1, so the coupling scheme is closer to the ω-ω than the Λ-S. For these states arising from the $5f\varphi^17s\sigma^1$ and $5f\delta^17s\sigma^1$ electron configurations, the electrons are in two shells with small radial overlap so the exchange integral is small, and in particular it is small in comparison to the spin-orbit effects, which are due to the electrons in the 5f orbitals. Since these 5f orbitals are non-bonding orbitals the $\zeta_\varphi \approx 1.5\ \zeta_{5f}$ and $\zeta_\delta \approx \zeta_{5f}$. For uranium, the value of ζ_{5f} is ~1640 cm^{-1}

[90] . The ${}^3\Delta_{3u}$ term is strongly mixed with the ${}^3\Phi_{3u}$ term with the contribution of 18%, which complicates our assignment of the ω-ω coupling scheme for the states corresponding to the $5f\varphi^1 7s\sigma^1$ configuration. But in the absence of the ${}^3\Phi_{3u}$ - ${}^3\Delta_{3u}$ mixing one would expect even higher mixing between the ${}^3\Phi_{3u}$ and ${}^1\Phi_{3u}$, moving the scheme even closer to the ω-ω limit.

According to our calculation the four states corresponding to the $5f\varphi^1 7s\sigma^1$ configuration occur at 0, 439 cm^{-1}, 5806 cm^{-1} and 6582 cm^{-1}, following the 2,2 energy pattern shown in Figure 2.1. Similarly the four states arising from $5f\delta^1 7s\sigma^1$ configuration follows the same energy pattern with the states lying at 1037 cm^{-1}, 1587 cm^{-1}, 5512 cm^{-1} and 6028 cm^{-1}.

The coupling scheme similar to that of the Φ_u and Δ_u states discussed above, is also observed in the states arising from the $5f\varphi^1 7p\sigma^1$ and $5f\delta^1 7p\sigma^1$ configurations, which contribute to the band in the UV-visible region of the spectrum. The 3_g and 2_g states are made up of 32% ${}^3\Phi_{3g}$ ($5f\varphi^1 7p\sigma^1$) + 26% ${}^1\Phi_{3g}$ ($5f\varphi^1 7p\sigma^1$) and 24% ${}^3\Delta_{2g}$ ($5f\delta^1 7p\sigma^1$) + 18% ${}^1\Delta_{2g}$ ($5f\delta^1 7p\sigma^1$), giving ratios of 0.81 and 0.75.

The lowest excited state of gerade symmetry arises predominantly from the f^2 ($5f\varphi^1 5f\delta^1$) configuration. This configuration generates the ${}^3H_{4g,5g,6g}$, ${}^1H_{5g}$, ${}^3\Pi_{0^+,0^-,1,2}$ and ${}^1\Pi_1$ Λ-S states. The 5_g state consists of 86% ${}^3H_{5g}$ ($5f\varphi^1 5f\delta^1$) + 0.9% ${}^1H_{5g}$ ($5f\varphi^1 5f\delta^1$) and the 1_g state consists of 34% ${}^3\Pi_{1g}$ ($5f\varphi_u^1 5f\delta_u^1$) + 10% ${}^1\Pi_{1g}$ ($5f\varphi_u^1 5f\delta_u^1$), giving ratios of 0.01 and 0.32. The H_g states follow the Λ-S coupling scheme, where the Π_g states are best described as having intermediate coupling. This is an example showing where within one electron configuration different states have different coupling schemes. The Π_g states have a smaller spin-orbit contribution to the total energy compared to the H_g. Also, for the Π_{1g} states the exchange integral is K_η, which is smaller than exchange integral of K_π for the H_{5g} states, where the subscript denoted the symmetry of the charge distributions in the exchange integral. As a result, the contributions from spin-orbit coupling and exchange electron repulsion result in intermediate coupling being the better approximation for this case. The excitation energies for $^3H_{4g}$, $^3H_{5g}$, $^3H_{6g}$ and $^1H_{5g}$ states are 3974 cm^{-1}, 8494 cm^{-1}, 12146 cm^{-1} and 25445 cm^{-1} respectively. The H_g energy states follows the 3:1 pattern, which further strengthens our analysis that these states should be described with a Λ-S coupling scheme.

The set of states from $5f\varphi^1 7p\pi^1$ and $5f\delta^1 7p\pi^1$ electron configurations contribute to the bands in the UV-visible region of the spectra. The pattern of coupling scheme for the states arising $5f\varphi^1 7p\pi^1$ and $5f\delta^1 7p\pi^1$ configurations is similar to the one obtained from the f^2 ($5f\varphi^1 5f\delta^1$) configuration, as described in the previous paragraph. The Γ_g and Φ_g states arising from $5f\varphi^1 7p\pi^1$ and $5f\delta^1 7p\pi^1$ respectively, have coupling closer to the Λ-S limit. The Δ_g and Π_g are best described as having intermediate coupling.

In the UV-visible region of the spectrum there also lie the states arising from $6d\delta^1 7s\sigma^1$ configuration. Analysis of the states arising from this configuration show that the coupling scheme followed by the states is very close to the Russell Saunders coupling. Thus the exchange interaction due to the substantial radial overlap of the 6d and 7s orbital outweighs the spin-orbit contribution from the 6d shell. For uranium, the value of the value of ζ_{6d} is ~1900 cm^{-1} [90].

2.2 Conclusions

In this work, the vertical transition energies and the wave function character of the experimentally observed vibronic states have been calculated below 36,000 cm^{-1}. In this energy range both metal-centered and charge-transfer excitations are observed. The multireference character of the states makes the transition energy and oscillator strength sensitive to correlation. The heavy spin-orbit mixing between the states strongly affects the transition energies and oscillator strengths. The spin-orbit interaction plays a very important role in increasing the transition moments of many states that are forbidden in the absence of spin-orbit. Excitations to the spin-forbidden states are even more pronounced from the $^3\Phi_u(3_u)$ first excited state, which has significant singlet-triplet mixing.

We have made assignments for the character of the observed bands and have also assigned the possible candidates for the structure observed with the UO_2 molecule observed in solid Ar. Among all the electric-dipole allowed transitions, the strongest transitions lie in the 27,000-30,000 cm^{-1} region. The excitations in this region involves excitation of an electron with mostly 7sσ character to states with predominantly 7pπ character. There are many optically accessible states outside the region 27,000-30,000 cm^{-1} with considerable oscillator strength. The calculated results are in good agreement with the experimentally observed absorption and emission structures.

From the coupling scheme analysis we can conclude in the 0-40,000 cm^{-1} region of the spectra there lie ~50 mostly multi-reference electronic states, and for all these states the excitation energies and transition moments for these states cannot be described well within the framework of one coupling scheme. Our multireference CI program, which follows the one-step approach to describe the spin-orbit interaction and correlation effects, is very effective in analyzing the electronic structure of the gaseous UO_2 molecule.

2.3 Future Work

In almost all the excited states, there is mixing between states with different 5f population, thus the 5s, 5p and 5d electrons also needs to be correlated as the change in the numbers of electrons in 5f will result in a change in the effective nuclear charge experienced by these orbitals. Hence, a significant change in correlation energy is expected on including these sets of orbitals as the part of reference space. The calculations in this work were performed using a 68-electron core potential where the 5s and 5p orbitals were not treated explicitly. Therefore the above calculation can be performed by using the 60-electron size core potential and allowing single excitations of the 5s, 5p and 5d orbitals which are enough to account for the orbital relaxation which characterizes the polarization effects.

Theoretical study could also be performed to explore the electronic structure in the region above 36,000 cm^{-1}, where the charge-transfer states arising from $5f\varphi^1 5f\sigma^1$ and $5f\delta^1 5f\sigma^1$ will be observed in addition to the other possible states. The study of this region gains importance from the fact that Heaven *et al.* have observed an emission band at 266 nm for UO_2 isolated in an argon matrix.

Calculations can also be performed with argon or neon ligands, as this will provide an interesting insight into how the guest-host interactions affect the vibrational frequencies and electronic structure of the molecule. The fact that extensive experimental study has been performed on the vibrational and electronic structure of molecules isolated in rare gas matrices should facilitate such a study. We have not performed this calculation as part of this work. This is because most of the interaction with the rare gas elements will be dispersion interactions, which result from the instantaneous correlation in the motion of electrons. So, even though the configuration interaction technique is ideal to study these interactions in the systems, there is a need to correlate a significantly increased number of electrons in this case. With the current serial version of COLUMBUS suite of programs this calculation is prohibitive to perform.

Spin-orbit included or not	Basis Set Quality	RECP Core Size	Number of Correlated electrons	Bond length (Å)
No	cc-pVTZ	68	14	1.784
Yes	cc-pVTZ	68	14	1.777
No	cc-pVTZ	68	36	1.774
No	cc-pVDZ	68	14	1.809
Yes	cc-pVDZ	68	14	1.803
No	cc-pVDZ	68	36	1.773
No	cc-pVDZ	60	14	1.810
No	cc-pVDZ	60	44	1.778

Table 2.1: Bond lengths R_e (Å) for UO_2 in the gas phase

	Orbital	Uranium AO’s				Oxygen AO’s		
	Energy	s (6s,7s)	p (6p, 7p)	d (5d,6d)	f (5f)	s (2s)	p (2p)	d (3d)
$1\sigma_u$	-2.994	--	45.42	--	1.97	46.34	6.05	0.21
$2\sigma_u$	-1.905	--	40.41	--	2.09	47.50	9.89	0.10
$2\pi_g$	-1.074	--	--	20.46	--	--	79.30	0.22
$4\sigma_g$	-1.054	2.34	--	18.97	--	5.84	72.61	0.18
$2\pi_u$	-0.992	--	3.70	--	14.58	--	81.59	0.13
$3\sigma_u$	-0.919	--	11.18	--	47.65	0.12	40.94	0.11

Table 2.2: Partial Gross Population Analysis for selected MOs of the average of wave functions of $^3\Phi_u$ ($5f^1 7s^1$) and the $^3\Delta_u$ ($5f^1 7s^1$) states at R_e = 1.803 Å

	Orbital	Uranium AO’s				Oxygen AO’s		
	Energy	s (6s,7s)	p (6p, 7p)	d (5d,6d)	f (5f)	s (2s)	p (2p)	d (3d)
$1\sigma_u$	-2.809	--	40.99	--	1.84	50.80	6.17	0.20
$2\sigma_u$	-1.722	--	41.72	--	1.47	43.30	13.38	0.14
$2\pi_g$	-0.941	--	--	20.52	--	--	79.29	0.18
$4\sigma_g$	-0.921	3.16	--	18.38	--	5.24	73.02	0.15
$2\pi_u$	-0.840	--	4.60	--	11.26	--	84.05	0.09
$3\sigma_u$	-0.688	--	17.42	--	37.83	-0.78	45.49	0.04

Table 2.3: Partial Gross Population Analysis for selected MOs of the MCSCF wave functions from the average of ^{3}Hg (5f^2) and $^3\Pi_g$ (5f^2) states at R_e = 1.803 Å

	Gross Atomic Populations					
Atom	s	p	d	f	g	Total
U	2.858	6.014	11.542	2.617	0.002	23.036
O	3.774	9.158	0.0303	0.000	0.000	12.963

Table 2.4: Mulliken Population Analysis for the average of wave functions of $^3\Phi_u$ and the $^3\Delta_u$ states at R_e = 1.803 Å using the 68-electron RECP

	Gross Atomic Populations					
Atom	s	p	d	f	g	Total
U	2.073	6.097	11.357	3.271	0.002	22.802
O	3.749	9.422	0.025	0.000	0.000	13.198

Table 2.5: Mulliken Population Analysis for the MCSCF wave functions from the ^3H_g (5f^2) and $^3\Pi_g$ (5f^2) states at R_e = 1.803 Å using the 68-electron RECP

	Gross Atomic Populations					
Atom	s	p	d	f	g	Total
U	4.813	12.037	11.549	2.591	0.003	30.995
O	3.744	9.230	0.029	0.000	0.000	13.005

Table 2.6: Mulliken Population Analysis for the average of wave functions of $^3\Phi_u$ and the $^3\Delta_u$ states at R_e = 1.809 Å using the 60-electron RECP

	Gross Atomic Populations					
Atom	s	p	d	f	g	Total
U	4.069	12.096	11.310	3.277	0.002	30.757
O	3.715	9.501	0.0251	0.000	0.000	3.243

Table 2.7: Mulliken Population Analysis for the MCSCF wave functions from the average of ^3H_g ($5f^2$) and $^3\Pi_g$ ($5f^2$) states at R_e = 1.809 Å using the 60-electron RECP

Transitions	Calculated Result (cm^{-1})	Experimental data for UO_2 gas (cm^{-1})
$2_u \leftrightarrow 1_g$	16542	17499
$3_u \leftrightarrow 4_g$	17328	18159
$2_u \leftrightarrow 3_g$	18935	18423
$2_u \leftrightarrow 1_g$	19613	18587
$2_u \leftrightarrow 3_g$	27259	27661
$3_u \leftrightarrow 2_g$	28885	28667 - 28805
$3_u \leftrightarrow 4_g$	29623	29654
$2_u \leftrightarrow 1_g$	29670	29700
$3_u \leftrightarrow 3_g$	34245	31478
$2_u \leftrightarrow 2_g$	34625	31838

Table 2.8: Comparison of the calculated and the experimentally observed electronic structure for gaseous UO_2 in the UV-visible range

	cc-pVDZ		cc-pVTZ	
Leading Wave functions	T_e (cm^{-1})	f (υ)[a]	T_e (cm^{-1})	f (υ)[a]
$^3\Phi_u\ (1\varphi_u^1 5\sigma_g^1)$	0	-	0	-
$^3H_g\ (1\varphi_u^1 1\delta_u^1)$	4989	0.0000	5304	0.0000
$^3\Sigma_g^-\ (1\delta_u^2) + {}^3\Sigma_g^-\ (1\varphi_u^2)$	6912	0.0000	7178	0.0000
$^3\Pi_g\ (1\varphi_u^1 1\delta_u^1)$	8568	0.0000	8944	0.0000
$^3\Gamma_g\ (1\varphi_u^1 3\pi_u^1) + {}^3\Gamma_g\ (1\varphi_u^1 4\pi_u^1)$	13693	0.0760	14333	0.0879
$^3\Delta_g\ (1\varphi_u^1 3\pi_u^1) + {}^3\Delta_g\ (1\varphi_u^1 4\pi_u^1)$	13919	0.0864	14861	0.1152
$^3\Phi_g\ (1\delta_u^1 3\pi_u^1) + {}^3\Phi_g\ (1\delta_u^1 4\pi_u^1)$	14450	0.0002	15324	0.0001
$^3\Pi_g\ (1\delta_u^1 3\pi_u^1) + {}^3\Pi_g\ (1\delta_u^1 4\pi_u^1)$	18740	0.0000	18912	0.0000
$^3\Sigma_g^-\ (1\varphi_u^2) + {}^3\Sigma_g^-\ (1\delta_u^2)$	19794	0.0000	19647	0.0000
$^3\Delta_g\ (2\delta_g^1 5\sigma_g^1)$	22230	0.0126	22622	0.0414
$^3\Gamma_g\ (1\varphi_u^1 4\pi_u^1) + {}^3\Gamma_g\ (1\varphi_u^1 3\pi_u^1)$	27220	0.2577	27420	0.2077
$^3\Delta_g\ (1\varphi_u^1 4\pi_u^1) + {}^3\Delta_g\ (1\varphi_u^1 3\pi_u^1)$	28234	0.2888	28370	0.2340
$^3\Phi_g\ (1\delta_u^1 4\pi_u^1) + {}^3\Phi_g\ (1\delta_u^1 3\pi_u^1)$	28080	0.0001	28436	0.0000
$^3\Pi_g\ (1\delta_u^1 4\pi_u^1) + {}^3\Pi_g\ (1\delta_u^1 3\pi_u^1)$	29550	0.0000	30276	0.0000
$^3\Phi_g\ (1\varphi_u^1 4\sigma_u^1)$	33816	0.0499	32292	0.0503
$^3\Delta_g\ (1\delta_u^1 4\sigma_u^1)$	34401	0.0016	32807	0.0018

Table 2.9: Non spin-orbit results for the low and high-lying states of UO_2 for the triplet states (U68-electron RECP)

[a] Oscillator Strength with perpendicular polarization

State	Wave function Character	Initial State = 2_u		Initial State = 3_u	
		T_e (cm^{-1})	f	T_e (cm^{-1})	f
2_u	$71\%\ {}^{3}\Phi_{2u}\ (1\varphi_u^{1}5\sigma_g^{1}) + 13\%\ {}^{3}\Delta_{2u}\ (1\delta_u^{1}5\sigma_g^{1}) + 2\%\ {}^{1}\Delta_{2u}\ (1\delta_u^{1}5\sigma_g^{1})$	0	-	-	-
3_u	$42\%\ {}^{3}\Phi_{3u}\ (1\varphi_u^{1}5\sigma_g^{1}) + 26\%\ {}^{1}\Phi_{3u}\ (1\varphi_u^{1}5\sigma_g^{1}) + 18\%\ {}^{3}\Delta_{3u}\ (1\delta_u^{1}5\sigma_g^{1})$	439		0	
1_u	$85\%\ {}^{3}\Delta_{1u}\ (1\delta_u^{1}5\sigma_g^{1})$	1037	0.0000	598	0.0000
2_u	$45\%\ {}^{3}\Delta_{2u}\ (1\delta_u^{1}5\sigma_g^{1}) + 37\%\ {}^{1}\Delta_{2u}\ (1\delta_u^{1}5\sigma_g^{1}) + 3\%\ {}^{3}\Phi_{2u}\ (1\varphi_u^{1}5\sigma_g^{1})$	1587	0.0000	1148	0.0000
4_g	$81\%\ {}^{3}H_{4g}\ (1\varphi_u^{1}1\delta_u^{1}) + 4\%\ {}^{1}\Gamma_{4g}\ (1\delta_u^{2})$	3974	0.0000	3535	0.0003
1_g	$34\%\ {}^{3}\Pi_{1g}\ (1\varphi_u^{1}1\delta_u^{1}) + 26\%\ {}^{3}\Sigma_{1g}^{-}\ (1\delta_u^{2}) + 7\%\ {}^{3}\Sigma_{1g}^{-}\ (1\varphi_u^{2}) +$ $10\%\ {}^{1}\Pi_{1g}\ (1\varphi_u^{1}1\delta_u^{1})$	7823	0.0015	7384	0.0000
1_g	$35\%\ {}^{1}\Sigma_{1g}^{-}\ (1\delta_u^{2}) + 14\%\ {}^{3}\Pi_{1g}\ (1\varphi_u^{1}1\delta_u^{1}) + 19\%\ {}^{3}\Sigma_{1g}^{-}\ (1\varphi_u^{2}) +$ $14\%\ {}^{1}\Pi_{1g}\ (1\varphi_u^{1}1\delta_u^{1})$	11791	0.0021	11352	0.0000
2_g	$33\%\ {}^{3}\Pi_{2g}\ (1\varphi_u^{1}1\delta_u^{1}) + 13\%\ {}^{3}\Delta_{2g}\ (1\varphi_u^{1}3\pi_u^{1}) + 13\%\ {}^{3}\Phi_{2g}\ (1\delta_u^{1}3\pi_u^{1})$	12042	0.0000	11603	0.0282
3_g	$72\%\ {}^{3}\Gamma_{3g}\ (1\varphi_u^{1}3\pi_u^{1}) + 6\%\ {}^{3}\Gamma_{3g}\ (1\varphi_u^{1}4\pi_u^{1})$	13411	0.1047	12972	0.0001
4_g	$43\%\ {}^{1}\Gamma_{4g}\ (1\delta_u^{2}) + 28\%\ {}^{1}\Gamma_{4g}\ (1\varphi_u^{1}3\pi_u^{1}) + 6\%\ {}^{3}\Phi_{4g}\ (1\delta_u^{1}3\pi_u^{1}) + 6\%\ {}^{3}H_{4g}\ (1\varphi_u^{1}1\delta_u^{1})$	13836	0.0000	13397	0.0275
2_g	$30\%\ {}^{3}\Delta_{2g}\ (1\varphi_u^{1}3\pi_u^{1}) + 27\%\ {}^{1}\Delta_{2g}\ (1\varphi_u^{1}3\pi_u^{1}) + 21\%\ {}^{3}\Pi_{2g}\ (1\varphi_u^{1}1\delta_u^{1})$	14365	0.0001	13926	0.0650
2_g	$81\%\ {}^{3}\Phi_{2g}\ (1\delta_u^{1}3\pi_u^{1}) + 5\%\ {}^{3}\Phi_{2g}\ (1\varphi_u^{1}4\pi_u^{1})$	15174	0.0001	14735	0.0004
1_g	$58\%\ {}^{3}\Delta_{1g}\ (1\varphi_u^{1}3\pi_u^{1}) + 12\%\ {}^{3}\Delta_{1g}\ (2\delta_g^{1}5\sigma_g^{1})$	16542	0.0856	16103	0.0000
4_g	$72\%\ {}^{3}\Gamma_{4g}\ (1\varphi_u^{1}3\pi_u^{1}) + 6\%\ {}^{3}\Gamma_{4g}\ (1\varphi_u^{1}4\pi_u^{1})$	17767	0.0000	17328	0.0841
1_g	$39\%\ {}^{1}\Pi_{1g}\ (1\varphi_u^{1}1\delta_u^{1}) + 27\%\ {}^{3}\Pi_{1g}\ (1\varphi_u^{1}1\delta_u^{1})$	18132	0.0022	17693	0.0000
3_g	$74\%\ {}^{3}\Delta_{3g}\ (1\varphi_u^{1}3\pi_u^{1}) + 8\%\ {}^{3}\Delta_{3g}\ (2\delta_g^{1}5\sigma_g^{1})$	18312	0.0000	17873	0.0002
3_g	$76\%\ {}^{3}\Phi_{3g}\ (1\delta_u^{1}3\pi_u^{1}) + 4\%\ {}^{3}\Gamma_{3g}\ (1\varphi_u^{1}3\pi_u^{1})$	18935	0.0044	18496	0.0000
1_g	$51\%\ {}^{3}\Pi_{1g}\ (1\delta_u^{1}3\pi_u^{1}) + 21\%\ {}^{1}\Pi_{1g}\ (1\delta_u^{1}3\pi_u^{1})$	19613	0.0184	19174	0.0000
1_g	$35\%\ {}^{1}\Pi_{1g}\ (1\delta_u^{1}3\pi_u^{1}) + 18\%\ {}^{3}\Pi_{1g}\ (1\delta_u^{1}3\pi_u^{1})$	26999	0.0382	26560	0.0000
3_g	$67\%\ {}^{3}\Gamma_{3g}\ (1\varphi_u^{1}4\pi_u^{1})$	27661	0.1843	27222	0.0004

Continued

Table 2.10: Electronic Spectrum Results for the low and high-lying states of UO_2 using the cc-pVTZ basis set and 68-electron core potential

Table 2.10 continued

3_g	69% $^3\Delta_{3g}$ $(2\delta_g^1 5\sigma_g^1)$	27813	0.0012	27374	0.0003
2_g	36% $^3\Delta_{2g}$ $(1\varphi_u^1 4\pi_u^1)$ + 26% $^1\Delta_{2g}$ $(1\varphi_u^1 4\pi_u^1)$ + 5% $^3\Delta_{2g}$ $(2\delta_g^1 5\sigma_g^1)$	29324	0.0007	28885	0.1885
1_g	64% $^3\Delta_{1g}$ $(1\varphi_u^1 4\pi_u^1)$ + 7% $^3\Delta_{1g}$ $(1\varphi_u^1 3\pi_u^1)$	29670	0.1566	29231	0.0000
2_g	80% $^3\Phi_{2g}$ $(1\delta_u^1 4\pi_u^1)$	29922	0.0000	29483	0.0014
4_g	59% $^3\Gamma_{4g}$ $(1\varphi_u^1 4\pi_u^1)$ + 5% $^1\Gamma_{4g}$ $(1\delta_u^2)$	30062	0.0000	29623	0.1061
1_g	54% $^3\Pi_{1g}$ $(1\delta_u^1 4\pi_u^1)$ + 25% $^1\Pi_{1g}$ $(1\delta_u^1 4\pi_u^1)$	32369	0.0005	31930	0.0000
2_g	20% $^3\Phi_{2g}$ $(1\varphi_u^1 4\sigma_u^1)$ + 41% $^1\Delta_{2g}$ $(1\varphi_u^1 4\pi_u^1)$	34126	0.02491	33687	0.0068
2_g	56% $^3\Phi_{2g}$ $(1\varphi_u^1 4\sigma_u^1)$ + 5% $^1\Delta_{2g}$ $(1\varphi_u^1 4\pi_u^1)$ + 15% $^1\Delta_{2g}$ $(2\delta_g^1 5\sigma_g^1)$	34625	0.0885	34186	0.0005
3_g	32% $^3\Phi_{3g}$ $(1\varphi_u^1 4\sigma_u^1)$ + 26% $^1\Phi_{3g}$ $(1\varphi_u^1 4\sigma_u^1)$ + 9% $^3\Delta_{3g}$ $(1\delta_u^1 4\sigma_u^1)$	34684	0.0001	34245	0.0882
3_g	43% $^1\Phi_{3g}$ $(1\delta_u^1 4\pi_u^1)$ + 18% $^1\Phi_{3g}$ $(1\delta_u^1 3\pi_u^1)$	39532	0.0007	39093	0.0162

State	Wave function Character	Initial State = 2_u T_e (cm^{-1})	f	Initial State = 3_u T_e (cm^{-1})	f
2_u	71% $^3\Phi_{2u}$ $(1\varphi_u^1 5\sigma_g^1)$ + 13% $^3\Delta_{2u}$ $(1\delta_u^1 5\sigma_g^1)$ + 2% $^1\Delta_{2u}$ $(1\delta_u^1 5\sigma_g^1)$	0	-	-	-
3_u	42% $^3\Phi_{3u}$ $(1\varphi_u^1 5\sigma_g^1)$ + 26% $^1\Phi_{3u}$ $(1\varphi_u^1 5\sigma_g^1)$ + 18% $^3\Delta_{3u}$ $(1\delta_u^1 5\sigma_g^1)$	412	0.0000	0	-
1_u	85% $^3\Delta_{1u}$ $(1\delta_u^1 5\sigma_g^1)$	892	0.0000	480	0.0000
2_u	45% $^3\Delta_{2u}$ $(1\delta_u^1 5\sigma_g^1)$ + 37% $^1\Delta_{2u}$ $(1\delta_u^1 5\sigma_g^1)$ + 3% $^3\Phi_{2u}$ $(1\varphi_u^1 5\sigma_g^1)$	1431	0.0000	1019	0.0000
4_g	83% $^3H_{4g}$ $(1\varphi_u^1 1\delta_u^1)$ + 3% $^1\Gamma_{4g}$ $(1\delta_u^2)$	3578	0.0000	3166	0.0003
1_g	34% $^3\Pi_{1g}$ $(1\varphi_u^1 1\delta_u^1)$ + 26% $^3\Sigma_{1g}^-$ $(1\delta_u^2)$ + 7% $^3\Sigma_{1g}^-$ $(1\varphi_u^2)$ + 9% $^1\Pi_{1g}$ $(1\varphi_u^1 1\delta_u^1)$	7401	0.0016	6989	0.0000
1_g	37% $^1\Sigma_{1g}^-$ $(1\delta_u^2)$ + 13% $^3\Pi_{1g}$ $(1\varphi_u^1 1\delta_u^1)$ + 16% $^3\Sigma_{1g}^-$ $(1\varphi_u^2)$ + 12% $^1\Pi_{1g}$ $(1\varphi_u^1 1\delta_u^1)$	11272	0.0023	10860	0.0000
2_g	46% $^3\Pi_{2g}$ $(1\varphi_u^1 1\delta_u^1)$ + 14% $^3\Delta_{2g}$ $(1\varphi_u^1 3\pi_u^1)$ + 13% $^3\Phi_{2g}$ $(1\delta_u^1 3\pi_u^1)$	11282	0.0002	10870	0.0290
3_g	58% $^3\Gamma_{3g}$ $(1\varphi_u^1 3\pi_u^1)$ + 22% $^3\Gamma_{3g}$ $(1\varphi_u^1 4\pi_u^1)$	12187	0.0764	11775	0.0004
4_g	41% $^1\Gamma_{4g}$ $(1\delta_u^2)$ + 22% $^1\Gamma_{4g}$ $(1\varphi_u^1 3\pi_u^1)$ + 7% $^3\Phi_{4g}$ $(1\delta_u^1 3\pi_u^1)$ + 6% $^3H_{4g}$ $(1\varphi_u^1 1\delta_u^1)$	13221	0.0000	12809	0.0246
11	19% $^3\Delta_{2g}$ $(1\varphi_u^1 3\pi_u^1)$ + 16% $^1\Delta_{2g}$ $(1\varphi_u^1 3\pi_u^1)$ + 12% $^3\Delta_{2g}$ $(1\varphi_u^1 4\pi_u^1)$ + 10% $^1\Delta_{2g}$ $(1\varphi_u^1 4\pi_u^1)$ + 26% $^3\Pi_{2g}$ $(1\varphi_u^1 1\delta_u^1)$	13684	0.0005	13272	0.0500
12	59% $^3\Phi_{2g}$ $(1\delta_u^1 3\pi_u^1)$ + 27% $^3\Phi_{2g}$ $(1\varphi_u^1 4\pi_u^1)$	13973	0.0001	13561	0.0000
13	40% $^3\Delta_{1g}$ $(1\varphi_u^1 3\pi_u^1)$ + 25% $^3\Delta_{1g}$ $(1\varphi_u^1 4\pi_u^1)$ + 9% $^3\Delta_{1g}$ $(2\delta_g^1 5\sigma_g^1)$	16052	0.0738	15640	0.0000
14	58% $^3\Gamma_{4g}$ $(1\varphi_u^1 3\pi_u^1)$ + 21% $^3\Gamma_{4g}$ $(1\varphi_u^1 4\pi_u^1)$ + 3% $^1\Gamma_{4g}$ $(1\delta_u^2)$	16694	0.0000	16282	0.0550
15	55% $^3\Delta_{3g}$ $(1\varphi_u^1 3\pi_u^1)$ + 25% $^3\Delta_{3g}$ $(1\varphi_u^1 4\pi_u^1)$ + 5% $^3\Delta_{3g}$ $(2\delta_g^1 5\sigma_g^1)$	17263	0.0000	16851	0.0002
16	55% $^3\Phi_{3g}$ $(1\delta_u^1 3\pi_u^1)$ + 26% $^3\Phi_{3g}$ $(1\delta_u^1 4\pi_u^1)$ + 3% $^3\Gamma_{3g}$ $(1\varphi_u^1 3\pi_u^1)$	17743	0.0038	17331	0.0002
17	41% $^1\Pi_{1g}$ $(1\varphi_u^1 1\delta_u^1)$ + 26% $^3\Pi_{1g}$ $(1\varphi_u^1 1\delta_u^1)$ + 3% $^3\Pi_{1g}$ $(1\delta_u^1 3\pi_u^1)$ + 4% $^3\Pi_{1g}$ $(1\delta_u^1 4\pi_u^1)$	17853	0.0003	17441	0.0000

Continued

Table 2.11: Electronic Spectrum Results for the low and high-lying states of UO_2 using the cc-pVDZ basis and 68-electron core potential

Table 2.11 continued

18	23% $^{3}\Pi_{1g}$ $(1\delta_u^{1}3\pi_u^{1})$ + 27% $^{3}\Pi_{1g}$ $(1\delta_u^{1}4\pi_u^{1})$ + 7% $^{1}\Pi_{1g}$ $(1\delta_u^{1}3\pi_u^{1})$ + 12% $^{1}\Pi_{1g}$ $(1\delta_u^{1}4\pi_u^{1})$	19426	0.0182	19014	0.0000
19	19% $^{1}\Delta_{2g}$ $(1\varphi_u^{1}3\pi_u^{1})$ + 16% $^{3}\Delta_{2g}$ $(1\varphi_u^{1}3\pi_u^{1})$ + 11% $^{1}\Delta_{2g}$ $(1\varphi_u^{1}4\pi_u^{1})$ + 25% $^{3}\Pi_{2g}$ $(1\varphi_u^{1}1\delta_u^{1})$	21089	0.0000	20677	0.0169
20	51% $^{3}\Phi_{4g}$ $(1\delta_u^{1}3\pi_u^{1})$ + 25% $^{3}\Phi_{4g}$ $(1\delta_u^{1}4\pi_u^{1})$ + 4% $^{3}\Gamma_{4g}$ $(1\varphi_u^{1}3\pi_u^{1})$ + 3% $^{1}\Gamma_{4g}$ $(1\delta_u^{2})$	21810	0.0000	21398	0.0037
21	23% $^{3}\Pi_{2g}$ $(1\delta_u^{1}3\pi_u^{1})$ + 15% $^{3}\Pi_{2g}$ $(1\delta_u^{1}4\pi_u^{1})$ + 14% $^{1}\Delta_{2g}$ $(1\varphi_u^{1}3\pi_u^{1})$ + 13% $^{3}\Pi_{2g}$ $(1\varphi_u^{1}1\delta_u^{1})$ + 4% $^{3}\Delta_{2g}$ $(1\varphi_u^{1}3\pi_u^{1})$	22795	0.0001	22383	0.0079
22	56% $^{3}\Sigma_{1g}^{-}$ $(1\varphi_u^{2})$ + 16% $^{1}\Sigma_{1g}^{-}$ $(1\delta_u^{2})$ + 4% $^{1}\Pi_{1g}$ $(1\varphi_u^{1}1\delta_u^{1})$ + 3% $^{3}\Pi_{1g}$ $(1\delta_u^{1}3\pi_u^{1})$ + 4% $^{1}\Pi_{1g}$ $(1\delta_u^{1}3\pi_u^{1})$	22799	0.0027	22387	0.0000
23	63% $^{3}\Delta_{1g}$ $(2\delta_g^{1}5\sigma_g^{1})$ + 14% $^{3}\Delta_{1g}$ $(1\varphi_u^{1}3\pi_u^{1})$	23634	0.0143	23222	0.0000
24	65% $^{1}\Phi_{3g}$ $(1\delta_u^{1}3\pi_u^{1})$ + 15% $^{1}\Phi_{3g}$ $(1\delta_u^{1}4\pi_u^{1})$	24380	0.0194	23968	0.0006
25	43% $^{1}\Gamma_{4g}$ $(1\varphi_u^{1}3\pi_u^{1})$ + 8% $^{1}\Gamma_{4g}$ $(1\varphi_u^{1}4\pi_u^{1})$ + 29% $^{1}\Gamma_{4g}$ $(1\delta_u^{2})$	24530	0.0000	24118	0.1203
26	56% $^{3}\Delta_{2g}$ $(2\delta_g^{1}5\sigma_g^{1})$ + 4% $^{1}\Delta_{2g}$ $(2\delta_g^{1}5\sigma_g^{1})$ + 16% $^{3}\Delta_{2g}$ $(1\varphi_u^{1}3\pi_u^{1})$	24952	0.0002	24540	0.0000
27	34% $^{1}\Pi_{1g}$ $(1\delta_u^{1}3\pi_u^{1})$ + 12% $^{1}\Pi_{1g}$ $(1\delta_u^{1}4\pi_u^{1})$ + 12% $^{3}\Pi_{1g}$ $(1\delta_u^{1}3\pi_u^{1})$ + 5% $^{3}\Pi_{1g}$ $(1\delta_u^{1}4\pi_u^{1})$	26981	0.0620	26569	0.0000
28	51% $^{3}\Gamma_{3g}$ $(1\varphi_u^{1}4\pi_u^{1})$ + 19% $^{3}\Gamma_{g}$ $(1\varphi_u^{1}3\pi_u^{1})$ + 5% $^{3}\Delta_{3g}$ $(2\delta_g^{1}5\sigma_g^{1})$	27350	0.2154	26938	0.0004
29	63% $^{3}\Delta_{3g}$ $(2\delta_g^{1}5\sigma_g^{1})$ + 11% $^{3}\Gamma_{3g}$ $(1\varphi_u^{1}3\pi_u^{1})$	27488	0.0127	27076	0.0003
30	32% $^{3}\Delta_{2g}$ $(1\varphi_u^{1}4\pi_u^{1})$ + 6% $^{3}\Delta_{2g}$ $(1\varphi_u^{1}3\pi_u^{1})$ + 8% $^{3}\Delta_{2g}$ $(2\delta_g^{1}5\sigma_g^{1})$ + 13% $^{1}\Delta_{2g}$ $(1\varphi_u^{1}3\pi_u^{1})$	29077	0.0002	28665	0.2270
31	51% $^{3}\Delta_{1g}$ $(1\varphi_u^{1}4\pi_u^{1})$ + 15% $^{3}\Delta_{1g}$ $(1\varphi_u^{1}3\pi_u^{1})$	29382	0.2039	28970	0.0000
32	57% $^{3}\Phi_{2g}$ $(1\delta_u^{1}4\pi_u^{1})$ + 27% $^{3}\Phi_{2g}$ $(1\delta_u^{1}3\pi_u^{1})$	29404	0.0001	28992	0.0061
33	46% $^{3}\Gamma_{4g}$ $(1\varphi_u^{1}4\pi_u^{1})$ + 17% $^{3}\Gamma_{4g}$ $(1\varphi_u^{1}3\pi_u^{1})$ + 5% $^{3}\Phi_{4g}$ $(1\delta_u^{1}4\pi_u^{1})$ + 8% $^{1}\Gamma_{4g}$ $(1\delta_u^{2})$	29690	0.0000	29278	0.1399
34	25% $^{3}\Phi_{2g}$ $(1\varphi_u^{1}4\sigma_u^{1})$ + 17% $^{3}\Phi_{2g}$ $(2\delta_g^{1}5\sigma_g^{1})$ + 11% $^{3}\Delta_{2g}$ $(1\varphi_u^{1}4\pi_u^{1})$ + 3% $^{1}\Delta_{2g}$ $(1\varphi_u^{1}4\pi_u^{1})$ + 8% $^{3}\Delta_{2g}$ $(1\varphi_u^{1}3\pi_u^{1})$ + 7% $^{1}\Delta_{2g}$ $(1\varphi_u^{1}3\pi_u^{1})$	33980	0.0170	33568	0.0074

Continued

Table 2.11 continued

35	47% $^3\Phi_{4g}$ ($1\delta_u^1 4\pi_u^1$) + 23% $^3\Phi_{4g}$ ($1\delta_u^1 3\pi_u^1$) + 10% $^3\Gamma_{4g}$ ($1\varphi_u^1 4\pi_u^1$) + 4% $^3\Gamma_{4g}$ ($1\varphi_u^1 3\pi_u^1$)	34110	0.0000	33698	0.0038
36	27% $^3\Phi_{3g}$ ($1\varphi_u^1 4\sigma_u^1$) + 31% $^1\Phi_{3g}$ ($1\varphi_u^1 4\sigma_u^1$) + 9% $^3\Delta_{3g}$ ($1\delta_u^1 4\sigma_u^1$) + 7% $^3\Delta_{3g}$ ($1\varphi_u^1 4\pi_u^1$) + 2% $^3\Phi_{3g}$ ($1\varphi_u^1 5\sigma_u^1$) + 2% $^1\Phi_{3g}$ ($1\varphi_u^1 5\sigma_u^1$)	34141	0.0000	33729	0.0458
37	44% $^3\Phi_{2g}$ ($1\varphi_u^1 4\sigma_u^1$) + 6% $^3\Delta_{2g}$ ($1\varphi_u^1 4\pi_u^1$) + 3% $^1\Delta_{2g}$ ($1\varphi_u^1 4\pi_u^1$) + 5% $^1\Delta_{2g}$ ($2\delta_g^1 5\sigma_g^1$) + 2% $^3\Phi_{2g}$ ($1\varphi_u^1 5\sigma_u^1$) + 5% $^3\Delta_{2g}$ ($1\delta_u^1 4\sigma_u^1$)	34156	0.0344	33744	0.0001
38	33% $^3\Pi_{2g}$ ($1\delta_u^1 4\pi_u^1$) + 26% $^3\Pi_{2g}$ ($1\delta_u^1 3\pi_u^1$) + 9% $^1\Delta_{2g}$ ($2\delta_g^1 5\sigma_g^1$)	34769	0.0013	34357	0.0051
39	24% $^3\Delta_{2g}$ ($1\delta_u^1 4\sigma_u^1$) + 18% $^1\Delta_{2g}$ ($1\delta_u^1 4\sigma_u^1$) + 12% $^1\Delta_{2g}$ ($2\delta_g^1 5\sigma_g^1$) + 13% $^1\Delta_{2g}$ ($1\varphi_u^1 4\pi_u^1$)	36287	0.0013	35875	0.0003
40	41%$^1\Gamma_{4g}$ ($1\varphi_u^1 4\pi_u^1$) + 30% $^1\Gamma_{4g}$ ($1\varphi_u^1 3\pi_u^1$) + 4% $^1\Gamma_{4g}$ ($1\delta_u^2$)	36287	0.0000	35875	0.0020
41	49% $^1\Phi_{3g}$ ($1\delta_u^1 4\pi_u^1$) + 16% $^1\Phi_{3g}$ ($1\delta_u^1 3\pi_u^1$)	37156	0.0018	36744	0.0149

Molecular Orbital	Atomic Character
$1\sigma_g$	U5dσ
$2\sigma_g$	U6sσ
$3\sigma_g$	O2sσ
$4\sigma_g$	O2pσ, U6dσ
$5\sigma_g$	U7sσ
$1\pi_g$	U5dπ
$2\pi_g$	O2pπ, U6dπ
$1\delta_g$	U5dδ
$2\delta_g$	U6dδ
$1\sigma_u$	U6pσ, O2sσ
$2\sigma_u$	U6pσ, O2sσ
$3\sigma_u$	U5fσ, O2pσ
$4\sigma_u$	U7pσ
$1\pi_u$	U6pπ
$2\pi_u$	O2pπ, U5fπ
$3\pi_u$	U5fπ, U7pπ
$4\pi_u$	U7pπ, U5fπ
$1\delta_u$	U5fδ
$1\varphi_u$	U5fφ

Table 2.12: Atomic character for the MOs listed in the Tables 2.9-2.11

ω-ω Coupling Scheme (Energy Level Pattern 2,2)

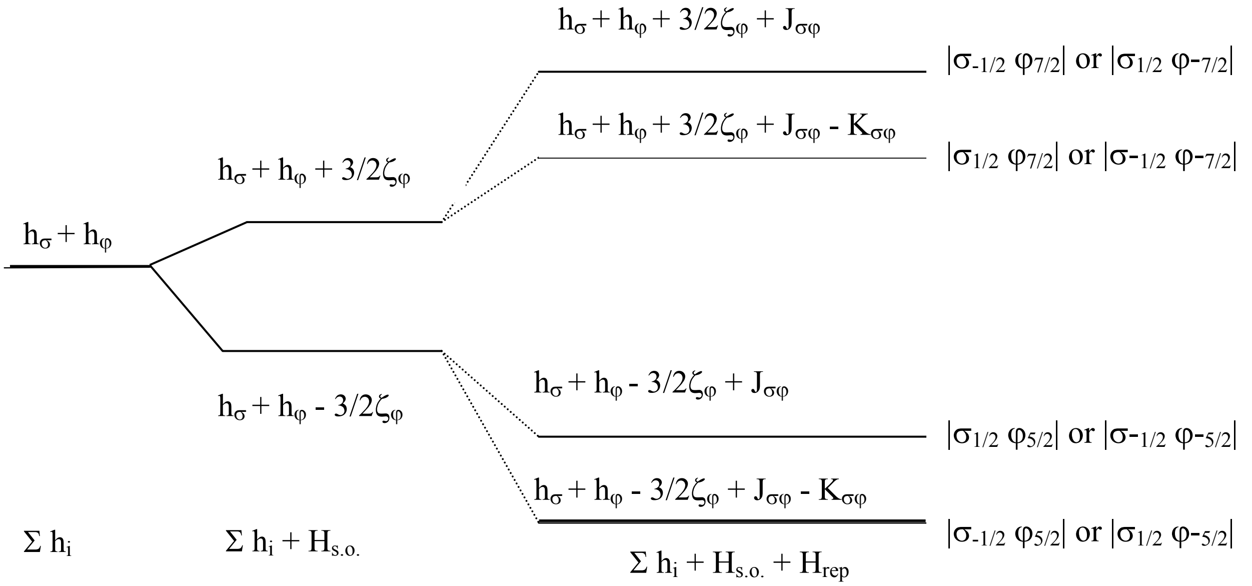

Λ-S Coupling Scheme (Energy Level Pattern 3,1)

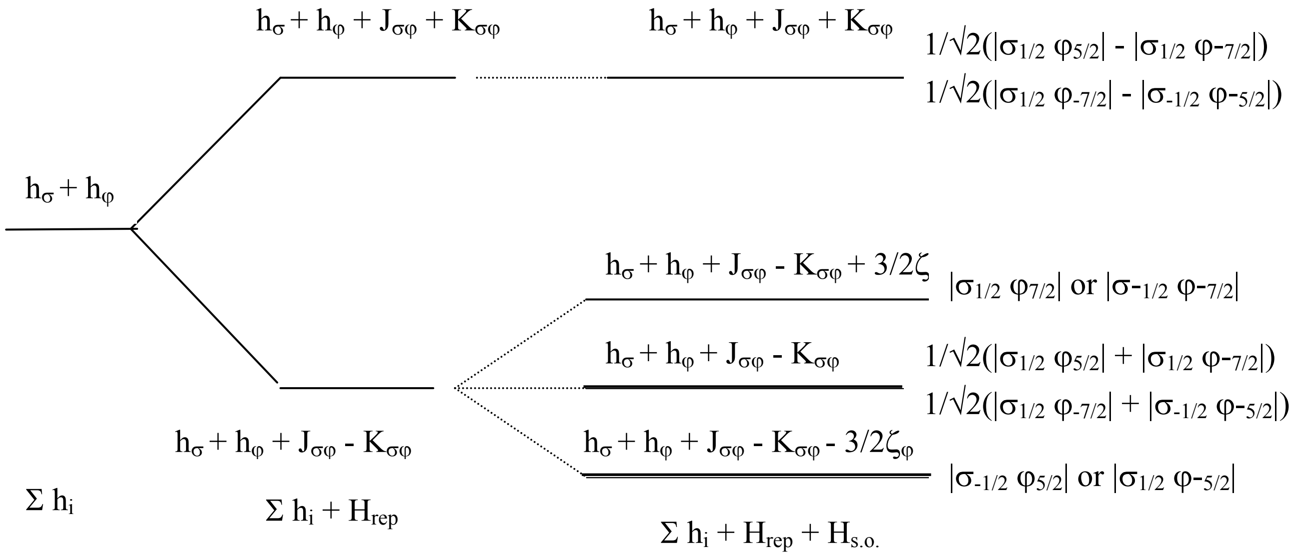

Figure 2.1: Energy level diagram of the (ω-ω) and (Λ-S) coupling schemes for the $\sigma^1\varphi^1$ electron configuration

CHAPTER 3

ELECTRONIC SPECTRUM OF THE UO AND UO^+ MOLECULES

3.1 Introduction

Uranium is a highly reactive metal even at low temperatures and it reacts very strongly with H_2, O_2, CO_2, etc., [91], resulting in the formation of UO, UO^+, UO_2, UO_2^+, UO_2^{2+}, UO_3, UH, UH_2, UH_3 among many other products. In addition to the obvious practical perspective, theoretical interest in studying these systems is high due to the fact that in UO and UO^+, relativistic effects and correlation effects play a very important role. The study of UO using absorption, emission and laser-induced fluorescence techniques [92-100] has provided a large amount of experimental data, making this system even more attractive as a candidate for theoretical study. For UO^+, there are no experimental data available in the current literature, but Heaven *et al.* [101] are in the process of obtaining such spectroscopic data. The work performed in this dissertation can be valuable for experimental studies as it will provide experimentalists with an appropriate frequency region to scan. According to our calculations, for UO^+, there are intense electronic transitions in the near IR region of the spectrum.

The $U^{16}O$ and $U^{18}O$ molecules have been studied spectroscopically in the gas phase [92-98] and also in low temperature rare-gas matrices [99-100] using absorption, emission and laser fluorescence techniques. Kaledin *et al.* [93] first obtained the electronic emission and absorption spectra of the UO molecule in the gas phase, revealing energies and molecular constants of five electronic states below 15,000 cm^{-1}. Heaven *et al.* [97-98] have experimentally observed a number of bands ranging from the near IR to the visible region. Vibrational and rotational analyses have been performed to obtain information on the spectroscopic constants of these states. Since the states belonging to the same electron configuration have similar constants, and the potential energy curves for these states are quite similar, this information aids greatly in the assignment of the transitions. Further facilitating the assignments is the fact that in the region lower than 10,000 cm^{-1} the states arise only from 5f^{3}7s^1, 5f^{2}7s^2 and 5f^{2}7s^{1}6d^1 type configurations and the rotational constants for the states arising from these configurations differ considerably. For example, the states arising from the 5f^{3}7s^1 and 5f^{2}7s^2 type configurations have rotational constant around 0.330 cm^{-1} and 0.346 cm^{-1} respectively.

Experimental data are available for the following isotopes: ^{238}U^{16}O, ^{235}U^{16}O and ^{238}U^{18}O [96,98]. Performing experiments using these different isotopes offers significant insight into the electronic structure of UO. This is especially helpful in this case since the ground and first excited state arising from the 5f^{3}7s^1 and 5f^{2}7s^2 type configurations, respectively, are separated by only ~ 300cm^{-1}. The low excited states with more 7s orbital occupancy than the ground state will experience more isotopic shifts since the 7s has a finite electron density at the nucleus [102].

The goal of this work is to study the low- and high-lying states of U^{16}O and U^{16}O$^+$ molecule using *ab initio* methods. The theoretical investigation of the electronic structure of UO and UO$^+$ is challenging due to the high density of electronic states arising from different configurations and different multiplicities. The active space consists of different distributions of valence electrons between the 5f, 6d and 7s open valence shells, making the computational size of the calculation quite large. For this reason, so far, the LFT approach has proved to be the method of choice in studying AcO and the analogous LnO molecules. Thus, a part of this work also deals with analyzing the success of LFT in studying these systems as it has proved to work quite well for LnO molecules.

For UO, experimental emission and absorption data are available at a low temperature of 130 K and a high temperature of ~2500 K. In the latter temperature range, the thermal excitations can cause significant populations of low-lying electronic energy levels up to ~1750 cm^{-1}. From our calculated results (refer to Table 3.14) and the LFT results [97-98] it can be seen that for UO in the gas phase, many low-lying states can be thermally populated at ~2500K. In the emission spectrum at 2400-2600 K, Kaledin *et al.* [93] observed 500 bands in the 4000-9000 Å region.

Currently we are not aware of any spin-orbit study that analyzes the wave function character of the low and high-lying states of UO observed experimentally. Further, for UO^+, there is a single-excitation spin-orbit study [105,106] that deals with only the states arising from $5f^3$ type configuration and our calculations predict the existence of states arising from several configurations in the region of study. Thus, our theoretical calculation can contribute valuable insight into the electronic spectra of the molecules under study.

3.2 Computational Details

The study of the electronic structures of UO and UO^+ was performed at the MCSCF and CI levels of theory. The calculation was performed with basis sets of cc-pVDZ and cc-pVTZ quality. Natural orbitals generated from MCSCF calculations were used for subsequent CISD calculations.

Our spin-orbit configuration interaction calculations were carried out with a 68-electron core potential for uranium and a 2-electron core potential for oxygen thus leaving 30 and 29 electrons for UO and UO^+ that need to be treated explicitly. The reference space for UO and UO^+ consists of the 5σ and 2π bonding MOs as part of the inactive space, where the MOs are doubly occupied in all the references but then single and double excitations are allowed out of them. The active space where changes in occupancy were allowed to generate the required references consisted of the 1φ, 2δ, 3δ, 4π, 6σ and 7σ orbitals, where 1φ, 2δ are non-bonding 5f orbitals; 3δ is the non-bonding 6d orbital; 4π and 6σ are the antibonding combination of 5f(π,σ) and O2p(π,σ) and 7σ MO has mainly 7sσ character with small contributions from the 6dσ and 7pσ orbitals. In the CI calculation, a few high energy virtuals were included in the frozen virtual space as they were meant for molecular SCF use only.

A more accurate calculation of the electronic spectrum of UO and UO^+ would involve correlating the 3σ and 4σ orbitals, which are formed by the bonding-antibonding interaction between the U6pσ, O2pσ and a small amount of U5fσ. With the change in the occupation number of 5f, there is a change in the extent of interaction between the MOs (due to the change in the effective nuclear charge experienced by the electrons in the 6p orbitals). This effect is evident from the atomic character for the MOs shown in Tables 3.10-3.13.

The multireference character of the ground and the excited states has made the calculation computationally intensive for UO and UO^+. For example, for UO^+ the number of CSFs before correlating the electrons in the 3σ and 4σ MOs was already 33 million. If these electrons are also included in the reference space, the number of CSFs rises sharply to 96 million. This mixing between the states from different configurations in case of UO and UO^+ is, however not as extensive as in case of the UO_2 results discussed in Chapter 2. The focus of this work is computing vertical transition energies at the equilibrium bond length of the ground state, and only a small amount of exploring potential curves is done. At this distance the mixing between the states arising from different type of configurations is quite small. Thus, the reference space without the electrons in 3σ and 4σ MOs will have little effect on the relative spacing of the states generated from a particular configuration for UO and UO^+ respectively. The oscillator strengths are calculated under the electric-dipole approximation not only from the ground state but also from the lower-lying excited states.

3.3 Results and Discussion

The ground state of the U^{+2} ion is $^5H_{4,}$ arising from the $5f^4$ configuration, and the lowest state energy that stems from the $5f^36d^1$ configuration lies only 210 cm^{-1} higher. The levels of $5f^37s^1$ start at 3744 cm^{-1} [102]. In the presence of oxide ion, the ground state of UO arises from the U^{2+} $(5f^37s^1)$ O^{2-} configuration. Similar behavior has been observed in the case of lanthanide oxides where the low-lying electronic states are derived from $4f^{N-1}6s^1$ configurations with the exception of EuO and YbO due to the stability associated with the half-filled and filled 4f shell. According to the oft-cited work by Field [103], in LnO systems the $f^{n-1}s$ lies below f^n and $f^{n-1}d$ due to the ligand field, which destabilizes the compact d and f orbitals more than the diffuse s and p orbitals.

The active space of both the LnO and AcO systems requires at a minimum, the valence ns, np, (n-1)d and (n-2)f metal-centered AOs in addition to the oxygen σ and π orbitals. With a valence space of this size, the number of low-lying electronic states becomes very large. As a result, at present, the simple LFT approach has been used widely in the literature for lanthanide oxides. A few researchers have used the method for some actinide oxides as well. LFT, including spin-orbit parameters, exploits the correspondence between the ordering of the electronic states of LnO with that of the free atomic ion, Ln^{+n}. This is due to the poor overlap of metal centered 4f and 5d orbitals with the orbitals of the ligand. Thus, irrespective of the coupling scheme, the states arising from a particular configuration will have similar values of spectroscopic constants.

For LnO, the 5d atomic orbital is involved more in bonding with oxygen AOs than with the electrons is the 4f shell. Similar behavior is observed for AnO, such as UO, where the bonding is mostly between the U6d and O2p and a relatively smaller contribution comes from the U5f orbital components, as is evident from the population analysis in Tables 3.7-3.13. The validity of applying the LFT to study the AnO systems stems from the relative participation of the U6d and U5f AOs in the bonding. For LnO molecules, the 4f electrons are localized and are chemically inactive [103] in molecular bonding but for AnO molecules the relativistic expansion of the 5f and 6d orbitals is enough larger that they play a more important role in bonding [104]. As can be seen from Tables 3.7-3.13, the contribution of 5f orbitals is higher for the bonding 5σ sigma MO than for the bonding 3π MO, which can easily be explained based on the amount of 6p character in the 5σ and 3π MOs. In UO and UO^+, there is a strong interaction between the O2sσ and U6pσ, which causes the higher destabilization of the antibonding $\sigma^*_{o2p\text{-}U6s}$ orbital. Further mixing with the 5fσ and 6dσ AOs results in a bonding 5σ MO with higher metal 5f, 6p and 6d character.

From Tables 3.10-3.13, we see that in UO, the participation of U5f and U6d in bonding is more significant for states derived from the $5f^27s^2$ and $5f^27s^16d^1$ type configurations than in the states derived from the $5f^37s^1$ type configuration. Similar behavior is observed for UO^+ between the states arising from the $5f^3$, $5f^27s^1$ and $5f^26d^1$ type configurations respectively. For UO^+, the extent of participation of the U5f and U6d shell in bonding is higher than that for UO, thereby reducing the atomic nature of 5f and 6d orbitals for UO^+.

For uranium monoxides, the bonding-antibonding interaction between the U5f AOs and the oxygen σ and π orbitals is not as strong as for the corresponding dioxides. As a result, the ground- and excited-state character is very different in the two systems. The point to note here is that, for actinyls, the weak-field approximation is good only among the $5f\delta_u$ and $5f\varphi_u$ orbitals. A strong-field approximation holds among the $5f\pi_u$ and $5f\sigma_u$ orbitals. For UO and UO^+, however, the weak-field approximation prevails among all the seven 5f orbitals. Consequently, the antibonding 5fπ and 5fσ contribute to the ground-state configuration of UO and UO^+, whereas for UO_2 and its ions, the antibonding

5fπ and 5fσ contribute to excited states. Further, the 5fφ - 5fδ separation due to the oxygen ligand field is also small in UO and its ions in comparison to that in UO_2 and its ions.

For UO and UO^+, analogous to UO_2 and its ions, spin-orbit effects are quite significant and in both cases the contribution of spin-orbit to the low-lying states comes exclusively from the 5f orbitals. The difference in size of the 5f shell for UO and UO^+ can result in a small difference in their spin-orbit coupling constant (ζ_{5f}) values. In the case of UO, analyzing the mixing between different Λ-S wave functions for example: ${}^5I_5 \leftrightarrow {}^3I_5$, ${}^5I_6 \leftrightarrow {}^3I_6$, ${}^5H_4 \leftrightarrow {}^3H_4$, ${}^5H_5 \leftrightarrow {}^3H_5$, ${}^5K_6 \leftrightarrow {}^3K_6$ states, shows that often neither ω-ω nor Λ-S coupling provides a good description, so the coupling should be described as intermediate. For example, for UO the contribution of the quintet and triplet term to the total wave function of (3)4, 1(5) and 2(6) states is 24% ${}^5H$ ($1\varphi^1 2\delta^1 7\sigma^1 6\sigma^1$) + 15% ${}^3H$ ($1\varphi^1 2\delta^1 7\sigma^1 6\sigma^1$), 37% ${}^5I$ ($1\varphi^1 2\delta^1 4\pi^1 6\sigma^1$) + 18% ${}^3I$ ($1\varphi^1 2\delta^1 4\pi^1 6\sigma^1$) and 52% ${}^5K_6$ ($1\varphi^1 2\delta^1 3\delta^1 6\sigma^1$) + 12% ${}^3K_6$ ($1\varphi^1 2\delta^1 3\delta^1 6\sigma^1$). The ratio of the quintet to triplet term for (3)4, 1(5) and 2(6) states is 0.62, 0.49 and 0.23 respectively.

3.3.1 Electronic Spectrum of UO

The ground state of UO is a Ω = 4 state with the leading contribution from the ${}^5I_4$ ($1\varphi^1 1\delta^1 4\pi^1 6\sigma^1$) wave function. In addition to the ground state with omega Ω = 4, there are two more states with Ω = 4 within 1500 cm^{-1} from the ground state. In this work the three low-lying Ω = 4 states are represented as X(1)4, (2)4 and (3)4, using the scheme (i)Ω used by Heaven *et al.* [97,98]. The principal terms for the X(1)4, (2)4 and (3)4 states arise from the $1\varphi^1 1\delta^1 4\pi^1 6\sigma^1$ ($5f^3 7s^1$), $1\varphi^1 1\delta^1 6\sigma^2$ ($5f^2 7s^2$) and $1\varphi^1 1\delta^1 7\sigma^1 6\sigma^1$ ($5f^3 7s^1$)

configurations respectively, where 1φ, 2δ are non-bonding 5f orbitals; 4π and 7σ are the antibonding combination of 5f(π,σ) and O2p(π,σ) and 6σ is the MO with mainly 7sσ character with small contributions from 7pσ and 6dσ AOs. The calculated bond lengths for the X(1)4, (2)4 and (3)4 states are summarized in Table 3.1 and 3.2 using the cc-pVTZ and cc-pVDZ basis sets. The values obtained for the X(1)4 and (3)4 states are 1.849 Å and 1.851 Å respectively using the cc-pVTZ basis set, and are in good agreement with the experimental bond length of 1.8383 Å. The X(1)4 and (3)4 states are multi-reference in character but still they have almost the same bond length due to the maximum contribution to the total wave function being from the $5f^3s^1$ configuration in both cases. The small difference of ~0.01 Å between the calculated and experimental value for these states might be due to the truncation of correlation in CISD or to the use of an effective core potential. Malli *et. al.* [107] using the relativistic density functional self-consistent-field method obtained a bond length of 1.88 Å, which is 0.04 Å higher than the experimental bond length.

The calculated bond length for the 2(4) first excited state, which arises predominantly from the $5f^27s^2$ configuration, is 1.792 Å. Our calculated bond length differs from the experimental value of 1.7932 Å by just 0.001 Å. In the event the mixing is not strong between the states arising from different configurations the spectroscopic constants for the states arising from a particular configuration will be almost identical. This is a feature that facilitates the analysis of the wave function character of the states [92,97,98].

For the ground state, with the inclusion of spin-orbit, the bond length changes by the order of 0.006 Å. The small effect is because of the spin-orbit mixing of the $^5I_4$

($1\varphi^1 1\delta^1 4\pi^1 6\sigma^1$) main term of the ground state mainly with the $^5H_4$ ($1\varphi^1 1\delta^1 7\sigma^1 6\sigma^1$) state, where both the $^5I_4$ and $^5H_4$ stem from the same $5f^3 7s^1$ configuration. Similarly spin-orbit reduces the bond length of the (3)4 state by the small amount of 0.005 Å because of the spin-orbit (SO) mixing of the $^5H_4$ ($1\varphi^1 1\delta^1 7\sigma^1 6\sigma^1$) main term with the $^5I_4$ ($1\varphi^1 1\delta^1 4\pi^1 6\sigma^1$) and $^5\Gamma_4$ ($1\varphi^1 4\pi^1 7\sigma^1 6\sigma^1$), where $^5H_{4,}$ $^5I_4$ and $^5\Gamma_4$ stem from the same $5f^3 7s^1$ configuration

According to the our calculation, the low-lying states of UO arise from the following three configurations U^{+2} ($5f^3\ 7s^1$)O^{2-}, U^{+2} ($5f^2 7s^2$)O^{2-} and U^{+2} ($5f^2 6d^1 7s^1$)O^{2-}.

Analysis of three omega = 4 states:

The first objective of this work is to analyze the wave function character of the three low-lying states all with $\Omega = 4$. The potential energy curves of these three states in the presence of SO are shown in Figure 3.1. As can be seen, the spin-orbit coupling changes the shape of the curves quite significantly for both the X(1)4 ground and the (2)4 first excited state.

At 1.835 Å, there is an avoided crossing between the X(1)4 ground state and the (2)4 first excited state. The amount of avoided crossing depends on the extent of spin-orbit mixing between the two states. The principal terms for the X(1)4 and the (2)4 states wave functions can be represented by (choosing Ω = - 4) the Slater determinants as $|1\varphi_{-3}\alpha\ 2\delta_{-2}\alpha\ 4\pi_{-1}\alpha\ 6\sigma\alpha|$ and $|1\varphi_{-3}\alpha\ 2\delta_{-2}\alpha\ 6\sigma\beta\ 6\sigma\alpha|$ respectively. The mixing between the two determinants comes from the spin-orbit matrix element between the $4\pi_{-1}\alpha$ and $6\sigma\beta$ spin-orbitals. The magnitude of the integral will be governed by the radial overlap of the 4π and 6σ MOs where the 4π MO is a $5f\pi$ orbital with some antibonding $O2p\pi$ character and the 6σ is made up of is 84% $7s\sigma$, 8% $7p\sigma$ and 6% $6d\sigma$. The spin-orbit matrix elements will have non-zero contributions only from the $7p\sigma$ and $6d\sigma$ part of the 6σ MO. Thus, small spin-orbit mixing is expected between the principal terms of X(1)4 and (2)4 states due to the difference in radial extent of the MOs involved and due to the small $7p\sigma$ and $6d\sigma$ contribution to total 6σ MO. In addition to the spin-orbit mixing between the principal terms, some amount of mixing will also arise from smaller wave functions terms that mix with the main terms of the respective states.

Next the amount of spin-orbit mixing between the X(1)4 and (3)4 is analyzed. The Slater determinant of the principal term of the (3)4 state is 1/2 ($|1\varphi_{-3}\alpha\ 2\delta_{-2}\alpha\ 7\sigma\alpha\ 6\sigma\beta| + |1\varphi_{-3}\alpha\ 2\delta_{-2}\alpha\ 7\sigma\beta\ 6\sigma\alpha| + |1\varphi_{-3}\alpha\ 2\delta_{-2}\beta\ 7\sigma\alpha\ 6\sigma\alpha| + |1\varphi_{-3}\beta\ 2\delta_{-2}\alpha\ 7\sigma\alpha\ 6\sigma\alpha|$). Between the main terms of X(1)4 and (3)4, the spin-orbit mixing involves evaluating the non-zero integral between $4\pi_{-1}\alpha$ and $6\sigma\beta$. Since there is strong radial overlap between the 3π ($5f\pi$) and 7σ($5f\sigma$) MOs, significant SO coupling will occur between the X(1)4 and (3)4 states. Similarly the spin-orbit mixing between the principal terms of the 2(4) and 3(4) states will come from the SO matrix elements between $6\sigma\alpha$ and $7\sigma\alpha$ MOs, which, however, is zero.

According to our calculation the adiabatic excitation energy for the 2(4) first excited state is at 140 cm^{-1}. The experimental [97,98] T_v (0-0) and T_e value for X(1)4 → (2)4 transition is 294.11 and 175.7 cm^{-1} respectively. The zero point energy (ZPE) correction between the two X(1)4 and (2)4 states is of the order of 50 cm^{-1}. After taking the ZPE correction into account, the small difference left between the calculated and the experimental value can easily be attributed to higher order correlation effects. The oscillator strength associated with X(1)4 → (2)4 transition is 1.63×10^{-6}. The transitions between the principal terms are forbidden in the absence of spin-orbit coupling. The small transition moment is from the small terms that mix with the principal terms of X(1)4 and (2)4 states through spin-orbit coupling.

The calculated T_e for the (3)4 state is 1740 cm^{-1}, which is bit higher than the experimental value of 1574 cm^{-1}. In our first attempt to perform the calculation we did a three-reference calculation with the states generated from the $1\varphi^1 1\delta^1 5f\pi^1 6\sigma^1$, $1\varphi^1 1\delta^1 6\sigma^2$ and $1\varphi^1 1\delta^1 7\sigma^1 6\sigma^1$ configurations. A transition energy of 2800 cm^{-1} was obtained with the wave function character of 3(4) state being 43% $^5H_4$ ($1\varphi^1 2\delta^1 7\sigma^1 6\sigma^1$) + 27% $^3H_4$ ($1\varphi^1 2\delta^1 7\sigma^1 6\sigma^1$) + 5% $^5I_4$ ($1\varphi^1 2\delta^1 4\pi^1 6\sigma^1$). But then with inclusion of states arising from the $1\varphi^1 1\pi^1 7\sigma^1 6\sigma^1$ and $1\varphi^1 4\pi^2 6\sigma^1$ in addition to many other configurations in the reference space, the transition energy was lowered to 1740 cm^{-1}, now just 166 cm^{-1} different from the experimental value. The final wave function character of the 3(4) state is listed in Table 3.14. Since our calculated value for this transition is still overestimated, our calculation may still be lacking some important references that contribute to the differential correlation energy. The zero-point energy correction is negligible between the X(1) and the (3)4 states.

Low-Lying states for UO:

The calculated and the experimental values for the low-lying states, along with their wave function characters and oscillator strengths are listed in Tables 3.14-3.15. In Table 3.15, the adiabatic energy is given for Ω=4, which stems from $5f^2 7s^2$ type configuration, but for the rest of the states, values are vertical transition energies since they all are states of $5f^3 7s^1$ type configuration. The difference is not expected to be significant between the vertical and adiabatic values for the states arising from $5f^3 7s^1$, because these states do not show any substantial mixing with the states arising from the $5f^2 7s^2$ and $5f^2 6d^1 7s^1$ type configurations.

As in the calculations for the 3(4) state, for the first Ω=3 state we first performed a three-reference calculation with the states generating from the $1\varphi^1 1\delta^1 4\pi^1 6\sigma^1$, $1\varphi^1 1\delta^1 6\sigma^2$ and $1\varphi^1 1\delta^1 7\sigma^1 6\sigma^1$ configurations and obtained a T_e value of 1231 cm^{-1} where the Ω=3 state consisted of 83% $^5H_3$ ($1\varphi^1 2\delta^1 7\sigma^1 6\sigma^1$). But then a larger reference space consisting of states arising from the $5f\varphi^1 5f\pi^1 5f\sigma^1 7s\sigma^1$ and $5f\varphi^1 5f\pi^2 7s\sigma^1$ type configurations resulted in a T_e value of 608 cm^{-1}, very close to the experimentally obtained value of 651 cm^{-1}. Experimentally there lies another Ω=3 state at 1941.48 cm^{-1}. Based on our calculation, this state is assigned to a highly multireference 13% $^5\Phi_3$ ($1\varphi^1 4\pi^2 6\sigma^1$) + 12% $^5H_3$ ($1\varphi^1 2\delta^1 7\sigma^1 6\sigma^1$) + 8% $^5\Gamma_3$ ($1\varphi^1 2\delta^1 4\pi^1 6\sigma^1$) + 6% $^5\Gamma_3$ ($1\varphi^1 7\sigma^1 4\pi^1 6\sigma^1$) state with a calculated transition energy of 2117 cm^{-1}. The rotational constants for these two Ω=3 states are 0.328 cm^{-1} and 0.327 cm^{-1} respectively, indicating that they are states from the $5f^3 7s^1$ type configuration, as shown by our calculations.

The experimental results predict a state with $\Omega = 5$ at 1043 cm^{-1}. According to our calculation, this state has the wave function character of 37% $^5I_5$ ($1\varphi^1 2\delta^1 4\pi^1 6\sigma^1$) + 18% $^3I_5$ ($1\varphi^1 2\delta^1 4\pi^1 6\sigma^1$) + 13% $^5H_5$ ($1\varphi^1 2\delta^1 7\sigma^1 6\sigma^1$). Thus, both the $\Omega' = 5$ and $\Omega'' = 4$ states have the leading terms from the same $5f\varphi^1 5f\delta^1 5f\sigma^1 7s\sigma^1$ electron configuration, which is further supported by their similar rotational constant of 0.3333 cm^{-1} and 0.3297 cm^{-1}. The small change in the rotational constants between the two states, according to our calculation, results from the high multireference character of the $\Omega' = 5$ final state. The strong mixing between $^5I_5$ - $^3I_5$ shows that the spin-orbit interaction is not a small perturbation with respect to the exchange interaction.

According to our calculations, the second low-lying state with $\Omega = 5$ has the maximum oscillator strength in the IR region of the spectrum. This state has not been categorized by Kaledin *et al.* [96,97]. The principal term of this state arises from the $5f^26d^17s^1$ type configuration and is the lowest state of this type. According to the LFT calculation (1994), the state with minimum energy from the $5f^26d^17s^1$ type configuration lies at 9300 cm^{-1}. From our calculation, this state lies at 3928 cm^{-1} and the principal contribution is 80% ^5K ($1\varphi^1 2\delta^1 3\delta^1 6\sigma^1$). The main term in the transition moment is the matrix element between 4π and 3δ. The next state that arises from the $5f^26d^17s^1$ type configuration also has the same 5f components and is an $\Omega = 6$ state, lying at 5805 cm^{-1} and containing 52% $^5K_6$ ($1\varphi^1 2\delta^1 3\delta^1 6\sigma^1$) + 12% $^3K_6$ ($1\varphi^1 2\delta^1 3\delta^1 6\sigma^1$). As can be seem from the extent of quintet-triplet mixing, the spin-orbit coupling is significant with respect to the exchange electron repulsion interaction. The spin-orbit effects are due to both the electrons in the 5f and 6d shell. The spin-orbit coupling constant for 5f and 6d is ~1640 cm^{-1} and ~1900 cm^{-1} respectively [98]. The next state from the $5f^26d^17s^1$ type configuration has different 5f components and is an $\Omega = 4$ state with $^5I_4$ ($1\varphi^1 4\pi^1 3\delta^1 6\sigma^1$) as the main term.

There is an experimentally observed transition at 4469 cm^{-1} with a final state of Ω=6. According to our calculation this final state has the same principal electron configuration as that of the ground state, which is further corroborated by fact that $\Omega' = 6$ and $\Omega'' = 4$ states have the same experimentally observed rotational constant of 0.333 cm^{-}

^{1}. The $\Omega' = 6$ state contains 52% $^5I_6$ ($1\varphi^1 2\delta^1 4\pi^1 6\sigma^1$) + 18% $^5H_6$ ($1\varphi^1 2\delta^1 7\sigma^1 6\sigma^1$) + 11% $^3I_6$ ($1\varphi^1 2\delta^1 4\pi^1 6\sigma^1$).

The experimental results show two features with $\Omega = 2$ at 958 cm^{-1} and 2118 cm^{-1} respectively. Our calculated results predict these two states to be at 916 cm^{-1} and 2294 cm^{-1}. The 916 cm^{-1} state is a highly multireference state containing 23% $^5\Gamma_2$ ($1\varphi^1 2\delta^1 4\pi^1 6\sigma^1$), 21% $^5\Phi_2$ ($1\varphi^1 4\pi^2 6\sigma^1$) and 14% $^5\Gamma_2$ ($1\varphi^1 7\sigma^1 4\pi^1 6\sigma^1$). Our assignment for the transition at 916 cm^{-1} is in agreement with its rotational constant of 0.3245 cm^{-1}, which shows that it is a state from the $5f^3 7s^1$ type configuration. The 2118 cm^{-1} state has components $^5\Gamma_2$ ($1\varphi^1 7\sigma^1 4\pi^1 6\sigma^1$) and $^5\Pi_2$ ($1\varphi^1 2\delta^1 7\sigma^1 6\sigma^1$).

According to the experimental results [94], there are seven states with $\Omega = 0, 1, 2$ or 3 below 4000 cm^{-1} arising from the $5f^3 7s^1$ type configurations. Our calculation predicts seven such states at 608 cm^{-1} ($\Omega = 3$), 916 cm^{-1} ($\Omega = 1$), 1100 cm^{-1} ($\Omega = 1$), 2117 cm^{-1} ($\Omega = 3$), 2294 cm^{-1} ($\Omega = 2$), 2347 cm^{-1} ($\Omega = 1$) and 2354 cm^{-1} ($\Omega = 0$).

High-lying excited states:

Preliminary excited-state calculation results are available for high-lying states. The possible assignments and the oscillator strength associated with these states are listed in Tables 3.16-3.18.

Per the experimental result, the electronic transition at 14016 cm^{-1} has $\Omega' = 4$ and $\Omega'' = 4$, with the rotational constant of Ω' and Ω'' being 0.3409 cm^{-1} and 0.3333 cm^{-1}. Our calculation predicts an $\Omega' = 4$ to $\Omega'' = 4$ excitation at 13359 cm^{-1}, where the main term of $\Omega' = 4$ stems from the $5f^2 7s^1 7p^1$ type configuration. The rotational constant for the states with the $5f^2 7s^2$ type configuration fall close to 0.3461 cm^{-1}, and as 7s and 7p have almost the same shielding properties, the rotational constant of the state from the $5f^27s^17p^1$ type configuration will also be close to 0.34 cm^{-1}. Thus our assignment for observed state at 14016 cm^{-1} as the $\Omega = 4$ state from the $5f^27s^17p^1$ type configuration with a leading contribution from the $^5I_4$ ($1\varphi^12\delta^15\pi^16\sigma^1$) wave function is also supported by the rotational constant of the final state. The LFT theory calculation [97] predicts the minimum energy state arising from the $5f^27s^17p^1$ type configuration to lie at 23300 cm^{-1} with respect to the X(1) ground state, which differs by ~10,000 cm^{-1} from our calculated result. Also, based on LFT theory, the state at 14016 cm^{-1} has been tentatively assigned to the $5f^27s^2$ type configuration by Heaven *et al*. [97].

There is also a state calculated at 14310 cm^{-1} arising from the $5f^26d^17s^1$ type configuration. This is an ideal candidate for the experimentally observed peak at 14016 cm^{-1} as its rotational constant might fall close to the experimentally observed value of 0.3409 cm^{-1} but its intensity is six times smaller than that of the $^5I_4$ ($1\varphi^12\delta^15\pi^16\sigma^1$) state at 13359 cm^{-1}.

According to the experimental results, the strongest transition is at 16845 cm^{-1} (8), which has $\Omega' = 5$. According to our calculation, there is a very strong transition from the ground state to the $\Omega' = 5$ state at 15532 cm^{-1}. The principal term for $\Omega' = 5$ state is ^5K ($1\varphi^12\delta^15\pi^14\pi^1$). Based on the leading terms in the wave functions, the $\Omega'' = 4 \rightarrow \Omega' = 5$ excitation can be categorized as a 7s → 7p excitation. This is the strongest electric-dipole transition among the states up to 16,000 cm^{-1}. The strong oscillator strength is due to the strong 7s-7p overlap due to their similar radial extents. The LFT calculation [97] predicted the lowest state arising from the $5f^37p^1$ type configuration to lie at 21300 cm^{-1}.

The next state arising from the $5f^37p^1$ type configuration is a $\Omega' = 4$ state with $^5I_4$ ($1\varphi^1 2\delta^1 5\pi^1 7\sigma^1$) as the main term. It is a double excitation from the main wave function term of the ground state. From the X(1)4 state, the transition energy and oscillator strength to this state are 15911 cm^{-1} and 0.00272 respectively. But, again, since the $\Omega'' = 3$ state can be significantly populated at 2500 K, hot bands are possible from this state. This $\Omega''= 3 \rightarrow \Omega' = 4$ transition has an oscillator strength of 0.04667 that is almost 17 times more intense than the transition from the X(1)4 state since from the $\Omega''= 3$ state it is a single 7s → 7p excitation.

3.3.2 Electronic Spectrum of UO^+

In this work we have studied the transitions lower than 8500 cm^{-1} in the presence of spin-orbit. As there are no experimental data available, the calculation is compared only with the calculated result using the LFT [97] and the valence configuration interaction technique [105, 106].

The ground state of UO^+ is a ^4I state arising primarily from the $5f^3$ type configuration predicted by the LFT calculation [97], the valence configuration interaction study, and our work [105,106]. Based on the bonding picture, the list of molecular orbitals that will contribute to the low-lying excited states are: 1φ, 2δ, 3δ, 4π, 6σ and 7σ orbitals, where 1φ, 2δ are non-bonding 5f orbitals; 3δ is the non-bonding 6d orbital; 4π and 6σ are the antibonding combination of $5f(\pi,\sigma)$ and $O2p(\pi,\sigma)$; and 7σ is the MO with mainly $7s\sigma$ character.

The equilibrium bond length for the ^4I ground state of UO^+ is 1.814 Å using the cc-pVTZ basis set. Currently there are no experimental values for R_e, but since for UO at a similar level of correlation, our calculated result differs from the experimental result by just 0.01 Å, a similar or even lower magnitude of error is expected in case of UO^+. Krauss *et al.* [105] obtained the bond length of 1.841 Å for the ground state at the SCF level of theory.

For UO^+, the states studied in this work arise from the $U^{3+}(5f^3)O^{2-}$, $U^{3+}(5f^27s^1)O^{2-}$ and $U^{3+}(5f^26d^1)O^{2-}$ type configurations. As can be seen from the bond-length values for the low-lying non-SO states in Table 3.4, the equilibrium bond lengths for the states arising from the three configurations are in the following order: $U^{3+}(5f^27s^1)O^{2-} < U^{3+}(5f^26d^1)O^{2-} < U^{3+}(5f^3)O^{2-}$. Accordingly, the order for the vibrational frequencies and the rotational constant follows: $U^{3+}(5f^27s^1)O^{2-} > U^{3+}(5f^26d^1)O^{2-} > U^{3+}(5f^3)O^{2-}$. The order is consistent with the ability of the last orbital to screen the nuclear charge of the atom and also the amount of bonding/non-bonding/anti-bonding character of the wave function. As seen from the values in Table 3.4, the bond length for states arising from the $5f^3$ configuration lie in the 1.845-1.842 range. Due to the ineffective shielding of the uranium nuclear charge by electrons in the 6d and 7s shells, the excitation of electrons from the 5f shell to 6d and 7s shells results in shorter bond lengths. Both the ^4K $(1\varphi^12\delta^13\delta^1)$ and ^4I $(1\varphi^14\pi^13\delta^1)$ states arise from the same configuration, but then the bond length for the former is 0.11 Å smaller than the latter due to higher anti-bonding character of the latter wave function.

Study of States in the Absence of Spin-Orbit:

In order to get a rough idea of the configurations that contribute to the lower energy states, a simple spin-free calculation was performed. Table 3.5 lists the transition energy and the oscillator strength from the ^4I ground state to the electronic states of UO at the equilibrium geometry of the ground state.

In the absence of spin-orbit coupling, the UO^+ molecule has a ground state of ^4I arising from the $1\varphi^1 2\delta^1 4\pi^1$ configuration. The ground state is almost single reference in character with 89% contribution from the principal term.

The first excited state, ^4H, stems from the $5f^3$ electron configuration. In the atomic picture, the transition from the ground state to the first excited state will result in an f-f parity-forbidden transition, but this selection rule is relaxed due to the oxygen ligand field. As a result, the ^4I - ^4H transition in the absence of spin-orbit coupling is a weak transition visible in the infrared absorption spectrum with an oscillator strength of 0.0017×10^{-2}. As can be seen from Table 3.6, the energy region below ~3,000 cm^{-1} contains the excited states derived from the $5f^3$ electronic configuration.

The lowest state arising from the $7s^1 5f^2$ type configuration lies 3391 cm^{-1} above the ground state and has 88% ^4H ($1\varphi^1 2\delta^1 7\sigma^1$) wavefunction character. The oscillator strength for the $^4I \rightarrow {}^4H$ transition is 3×10^{-5}. In this transition, the transition probability has maximum contribution from the principal terms of both the initial and final states. Thus, based on the leading term approximation, a small value of oscillator strength can easily be attributed to the small 7s and 5f radial overlap.

The states arising from the $6d^1 5f^2$ type configuration that contribute to the low-lying excited states have the following wave function characters: $1\varphi^1 2\delta^1 3\delta^1$ ($5f\varphi^1 5f\delta^1 6d\delta^1$) and $1\varphi^1 4\pi^1 3\delta^1$ ($5f\varphi^1 5f\pi^1 6d\delta^1$). The ^4K excited state that stems from the $1\varphi^1 2\delta^1 3\delta^1$ electron configuration lies at 5878 cm^{-1}. In spite of the strong f-d allowed transition in the atomic system, the oscillator strength for this transition is 0.0432. In the

^{4}I - ^{4}K transition the only difference between the main wave function terms is the spatial part of the third electron, 4π(5fπ) ↔ 3δ(6dδ). The antibonding character of the 4π orbital and the highly metal-centered character of the 3δ orbital decreases the spatial overlap between the two MOs.

Among all the states below ~8500 cm^{-1}, the strongest electric-dipole allowed transitions from the ^{4}I ground state occurs to the ^{4}I state arising from the $1\varphi^1 4\pi^1 3\delta^1$ configuration with an oscillator strength of 0.2611, which is six times higher than the next most intense transition. In this metal-centered transition, an electron from the non-bonding U5fδ orbital is excited to the orbital with non-bonding U6dδ character. As both the initial and the final state wave functions have their amplitude mostly centered on the uranium atom, the strong 5f-6d radial overlap is responsible for such a high value of oscillator strength. This is an atomic transition to a very good approximation.

Study of States in the Presence of Spin-Orbit Coupling:

The ground state of UO$^+$ is ^{4}I$_{9/2,}$ arising from the$1\varphi^1 2\delta^1 3\pi^1$ electron configuration. The ground state is multi-reference in character with the following wave-function character 66% ^{4}I$_{9/2}$ ($1\varphi^1 1\delta^1 4\pi^1$) + 8% ^{4}H$_{9/2}$ ($1\varphi^1 1\delta^1$ $6\sigma^1$). In the single-excitation calculation of Krauss and Stevens [105], the leading term contributes 88% to the total wave function.

In the presence of spin-orbit, the ground state has an equilibrium bond length of 1.812 Å using the cc-pVTZ basis set, which differs by 0.002 Å from the value obtained in the non-SO calculation. The effect of spin-orbit coupling on the bond length is very small because the principal $^4I_{9/2}$ ($1\varphi^1 1\delta^1 4\pi^1$) term of the ground state mainly mixes with the $^4H_{9/2}$ ($1\varphi^1 1\delta^1\ 6\sigma^1$) term arising from the same $5f^3$ configuration.

The low-lying states and the wave-function character of the calculated states in the presence of spin-orbit are listed in Table 3.6. The first excited state arises from the same configuration as that of the ground state and the $^4H_{7/2}$ ($1\varphi^1 2\delta^1 6\sigma^1$) leading term contributes less than 50% to the total wave function, whereas Krauss and Stevens [105-106] obtained this contribution as 69%. The high multireference character of the first excited state makes it more sensitive to correlation. Earlier, when the reference space consisted of states arising from $5f\varphi^1 5f\delta^1 5f\pi$, $5f\varphi^1 5f\delta^1 5f\sigma^1$ and $5f\varphi^1 5f\delta^1 7s\sigma^1$, we obtained a value of 1336 cm^{-1} for the $^4I_{9/2}$ – $^4H_{7/2}$ transition. When the reference space was augmented with additional $5f^3$ functions that mixed substantially with the leading term, however, the difference between the ground and the first excited state went down by more than half to 582 cm^{-1}. Thus, we can conclude that the value of 1319 cm^{-1} for $^4I_{9/2}$ – $^4H_{7/2}$ computed by Krauss and Stevens [105] using single excitations from the reference configurations lacks some important differential dynamical correlation contributions. The $^4I_{7/2}$ – $^4H_{9/2}$ cannot be compared with the results from LFT since only the minimum energy from different electron configurations have been computed using LFT [107].

The first low-lying state that arises from a configuration different from the $5f^3$ configuration arises when the $4\pi(5f\pi)$ electron is excited to the orbital with predominantly $7s\sigma$ character accompanied by small amount of charge transfer. In the Λ-S coupling scheme the $1\varphi^1 2\delta^1 7\sigma^1$ configuration gives rise to ^4H, $^4\Pi$, ^2H and $^2\Pi$ states. The calculated transition energy to these states cannot be compared to results obtained by Krauss and Stevens [105,106] since their spin-orbit study did not include the $5f^2 7s^1$

states. Based on center of gravity data, the LFT result predicts the state with minimum energy from the $5f^27s$ type configuration to lie at 8600 cm^{-1} above the $^4I_{9/2}$ ground state. The result obtained from LFT [97] is at least 5000 cm^{-1} more than our calculated result because our calculated results are the vertical transition energy numbers. The discrepancy in the result might be due to the fact that there is significant change in the composition of bonding MOs between the $5f^3$ and $5f^2s^1$ configurations as shown in Tables 3.7 and 3.8. As can be seen from Table 3.8, the contribution of O2p to the total 5σ wave function is 57.85 % with the rest of the contribution coming from U5fσ, U6dσ and U6pσ at the equilibrium geometry of the ground state. The strong bonding/antibonding interactions between the oxygen and uranium AOs can result in inaccurate LFT results [97].

In contrast to the states arising from $7s^15f^2$, the minimum energy for the states arising from $6d^15f^2$ predicted by LFT data using the CG data is in better agreement with our calculated result. The LFT [97] predicts the levels of $6d^15f^2$ type configuration to start at 5600 cm^{-1} and our computed value is 4941 cm^{-1}.

3.4 Conclusions

In this work electronic structure calculations for $U^{16}O$ have been reported. Assignments are made for many low- and few high-lying excited states. Our assignments of the transitions are in line with the experimentally observed rotational constant values. The electronic states for UO are highly multireference in character and there is a strong spin-orbit mixing between them, resulting in the significant spreading of the intensity. Due to the multireference character of the states the calculated results are very sensitive to the choice of the reference space and the MOs used for the correlation calculation. The low-lying results (less than 5000 cm^{-1}) are in good agreement with the experimental values. The high-lying results (greater than 13,000 cm^{-1}) are somewhat lower than the experimental values but there are ~120 electronic states lower than these states based on our reference space, making it difficult to perform a higher order correlation calculation. This is the first work that has attempted to provide the wave function character of these transitions. According to our calculation the intense band at 16845 cm^{-1} is due to the $7s\sigma \rightarrow 7p\pi$ metal-centered transition. Thermally excited bands from the lower excited states are also studied in this work. The bond length values for the first three states with $\Omega = 4$ states agree well with experimental values and afford a higher degree of accuracy than previously calculated results.

In this work, low-lying states arising from $U^{3+}(5f^3)O^{2-}$, $U^{3+}(5f^27s^1)O^{2-}$ and $U^{3+}(5f^26d^1)O^{2-}$ in the IR region for UO^+ have been characterized. Spin-orbit coupling makes a significant contribution to all electronic states. The ground state for UO^+ is found to be 66% $^4I_{9/2}$ $(1\varphi^12\delta^14\pi^1)$ + 8% $^4H_{9/2}$ $(1\varphi^12\delta^16\sigma^1)$ at its equilibrium geometry. The transition energy and the oscillator strength for the transitions below 9000 cm^{-1} have been calculated. According to our calculation there are intense metal-centered electronic transitions in the IR region of the spectrum. Our calculation provides the wave-function character for these states in addition to other states with lesser intensity. The expected availability of experimental data for the UO^+ will provide insight into the quality of our results. For both the UO and UO^+ molecules, substantial differences are observed between our results and the results obtained from the LFT model.

State	Principal Term	Re(Å) (MCSCF)	Re(Å) (CISD – without SO)	Re(Å) (CISD - SO)	Re(Å) Exp.[a]
X(1)4	$^5I_4$ ($6\sigma^1 1\varphi^1 1\delta^1 4\pi^1$)	1.842	1.854	1.849	1.8383
2(4)	$^3H_4$ ($6\sigma^2 1\varphi^1 1\delta^1$)	1.779	1.796	1.792	1.7932
3(4)	$^5H_4$ ($6\sigma^1 1\varphi^1 1\delta^1 7\sigma^1$)	1.843	1.856	1.851	1.8383

[a]ref [97]-[98]

Table 3.1: Bond lengths of the UO molecule for the three low-lying states with Ω = 4 using the cc-pVTZ Basis Set

State	Principal Term	Re(Å) (MCSCF)	Re(Å) (CISD -SO)	Re(Å) Exp[a]
X(1)4	$^5I_4$ ($6\sigma^1 1\varphi^1 1\delta^1 4\pi^1$)	1.867	1.879	1.8383
2(4)	$^3H_4$ ($6\sigma^2 1\varphi^1 1\delta^1$)	1.793	1.826	1.7932
3(4)	$^5H_4$ ($6\sigma^1 1\varphi^1 1\delta^1 7\sigma^1$)	1.869	1.876	1.8383

[a]ref [97]-[98]

Table 3.2: Bond lengths of the UO molecule for the three low-lying states with Ω = 4 using the cc-pVDZ Basis Set

State	Principal Term	Re(Å) (without SO)	Re(Å) (with SO)
$^4I_{9/2}$	$1\varphi^1 1\delta^1 4\pi^1$	1.821	1.812
$^4H_{7/2}$	$1\varphi^1 1\delta^1 6\sigma^1$	1.822	1.814
$^4H_{7/2}$	$1\varphi^1 1\delta^1 7\sigma^1$	1.772	1.764

Table 3.3: Bond length of the UO^+ molecule for the ground state and two excited states using the cc-pVTZ basis set

	Leading Λ-S term	R_e(Å)
1	89% ^4I ($1\varphi^1 2\delta^1 4\pi^1$)	1.845
2	92% ^4H ($1\varphi^1 2\delta^1 6\sigma^1$)	1.844
3	51% $^4\Gamma$ ($1\varphi^1 2\delta^1 4\pi^1$) + 39% $^4\Gamma$ ($1\varphi^1 4\pi^1 6\sigma^1$)	1.845
4	66% $^4\Phi$ ($1\varphi^1 4\pi^2$) + 16% $^4\Phi$ ($1\varphi^1 2\delta^2$)	1.842
5	42% $^4\Gamma$ ($1\varphi^1 2\delta^1 4\pi^1$) + 21% ($1\varphi^1 4\pi^1 6\sigma^1$)	1.842
6	88% ^4H ($1\varphi^1 2\delta^1 7\sigma^1$)	1.794
7	91% ^4K ($1\varphi^1 2\delta^1 3\delta^1$)	1.809
8	81% $^4\Gamma$ ($1\varphi^1 4\pi^1 7\sigma^1$)	1.804
9	89% ^4I ($1\varphi^1 4\pi^1 3\delta^1$)	1.820

Table 3.4: Bond length of the UO^+ molecule for the ground state and the excited states in the absence of spin-orbit using the cc-pVDZ basis set

	Leading Λ-S term	T_e (cm^{-1})	Oscillator Strength x 10^2
1	$89\%\ {}^4\mathrm{I}\ (1\varphi^1 2\delta^1 4\pi^1)$	0	-
2	$92\%\ {}^4\mathrm{H}\ (1\varphi^1 2\delta^1 6\sigma^1)$	781	0.0017
3	$51\%\ {}^4\Gamma\ (1\varphi^1 2\delta^1 4\pi^1) + 39\%\ {}^4\Gamma\ (1\varphi^1 4\pi^1 6\sigma^1)$	796	0.0000
4	$66\%\ {}^4\Phi\ (1\varphi^1 4\pi^2) + 16\%\ {}^4\Phi\ (1\varphi^1 2\delta^2)$	893	0.0000
5	$42\%\ {}^4\Gamma\ (1\varphi^1 2\delta^1 4\pi^1) + 21\%\ (1\varphi^1 4\pi^1 6\sigma^1)$	1081	0.0000
6	$88\%\ {}^4\mathrm{H}\ (1\varphi^1 2\delta^1 7\sigma^1)$	3391	0.0030
7	$91\%\ {}^4\mathrm{K}\ (1\varphi^1 2\delta^1 3\delta^1)$	5878	0.0432
8	$81\%\ {}^4\Gamma\ (1\varphi^1 4\pi^1 7\sigma^1)$	6428	0.0000
9	$89\%\ {}^4\mathrm{I}\ (1\varphi^1 4\pi^1 3\delta^1)$	8683	0.2611

Table 3.5: Electronic states of the UO^+ molecule without spin-orbit using the cc-pVDZ basis set at R_e = 1.845 Å

State	Leading Λ-S terms	$T_e(cm^{-1})$
9/2	$66\%\ {}^4\mathrm{I}_{9/2}\ (1\varphi^1 2\delta^1 4\pi^1) + 8\%\ {}^4\mathrm{H}_{9/2}\ (1\varphi^1 2\delta^1 6\sigma^1)$	0
7/2	$47\%\ {}^4\mathrm{H}_{7/2}\ (1\varphi^1 2\delta^1 6\sigma^1) + 15\%\ {}^4\mathrm{I}_{7/2}\ (1\varphi^1 2\delta^1 4\pi^1) + 10\%\ {}^4\Gamma_{7/2}\ (1\varphi^1 4\pi^1 6\sigma^1) + 4\%\ {}^4\Phi_{7/2}(1\varphi^1 4\pi^2)$	582
5/2	$20\%\ {}^4\Gamma_{5/2}\ (1\varphi^1 1\delta^1 4\pi^1) + 17\%\ {}^4\Phi_{5/2}\ (1\varphi^1 4\pi^2) + 16\%\ {}^4\Gamma_{5/2}\ (1\varphi^1 4\pi^1 6\sigma^1)$	856
3/2	$17\%\ {}^4\Phi_{3/2}\ (1\varphi^1 4\pi^2) + 8\%\ {}^4\Delta_{3/2}\ (2\delta^1 4\pi^2) + 7\%\ {}^4\Delta_{3/2}\ (1\varphi^1 4\pi^1 6\sigma^1)$	1076
11/2	$69\%\ {}^4\mathrm{I}_{11/2}\ (1\varphi^1 2\delta^1 4\pi^1) + 11\%\ {}^4\mathrm{H}_{11/2}\ (1\varphi^1 2\delta^1 6\sigma^1)$	3744
9/2	$36\%\ {}^4\mathrm{H}_{9/2}\ (1\varphi^1 2\delta^1 6\sigma^1) + 15\%\ {}^4\mathrm{I}_{9/2}\ (1\varphi^1 2\delta^1 4\pi^1) +13\%\ {}^4\Gamma_{9/2}\ (1\varphi^1 4\pi^1 6\sigma^1)$	4180
7/2	$58\%\ {}^4\mathrm{H}_{7/2}\ (1\varphi^1 2\delta^1 7\sigma^1) + 6\%\ {}^4\mathrm{H}_{7/2}\ (1\varphi^1 2\delta^1 6\sigma^1)$	4287
5/2	$35\%\ {}^4\Gamma_{5/2}\ (1\varphi^1 1\delta^1 4\pi^1) + 22\%\ {}^4\Gamma_{5/2}\ (1\varphi^1 4\pi^1 6\sigma^1) + 12\%\ {}^4\Delta_{3/2}\ (2\delta^1 4\pi^2)$	4549
11/2	$83\%\ {}^4\mathrm{K}_{11/2}\ (1\varphi^1 2\delta^1 3\delta^1)$	4941
9/2	$47\%\ {}^4\mathrm{H}_{9/2}\ (1\varphi^1 2\delta^1 7\sigma^1) + 25\%\ {}^2\mathrm{H}_{9/2}\ (1\varphi^1 2\delta^1 7\sigma^1)$	5522
13/2	$77\%\ {}^4\mathrm{I}_{13/2}\ (1\varphi^1 2\delta^1 4\pi^1) + 8\%\ {}^4\mathrm{H}_{13/2}\ (1\varphi^1 2\delta^1 6\sigma^1)$	7021
11/2	$48\%\ {}^4\mathrm{H}_{11/2}\ (1\varphi^1 2\delta^1 6\sigma^1) + 15\%\ {}^4\mathrm{I}_{11/2}\ (1\varphi^1 2\delta^1 4\pi^1)$	7453
9/2	$75\%\ {}^4\mathrm{I}_{9/2}\ (1\varphi^1 3\delta^1 4\pi^1)$	8801

Table 3.6: Electronic states of the UO^+ molecule with the cc-pVDZ basis set

	Uranium AO's				Oxygen AO's		
	s (6s,7s)	p (6p, 7p)	d (5d,6d)	f (5f)	s (2s)	p (2p)	d (3d)
5σ	1.31	6.32	17.05	8.22	3.31	61.65	0.08
3π	--	1.33	15.18	5.99	--	75.30	0.15

Table 3.7: Partial Gross Population Analysis for the bonding MOs for the ^{4}I + $^4\Gamma$ + $^4\Delta$ + $^4\Sigma$ (5f$\varphi^1$5f$\delta^1$5fπ^1) states for UO^+ at R_e = 1.845 Å

	Uranium AO's				Oxygen AO's		
	s (6s,7s)	p (6p, 7p)	d (5d,6d)	f (5f)	s (2s)	p (2p)	d (3d)
5σ	1.32	5.61	16.38	10.95	3.38	59.91	0.10
3π	--	1.25	14.82	7.82	--	73.50	0.16

Table 3.8: Partial Gross Population Analysis for the bonding MOs for the ^{4}H + $^4\Pi$ (5f $\varphi^1$5f$\delta^1$7sσ^1) states for UO^+ at R_e = 1.845 Å

	Uranium AO's				Oxygen AO's		
	s (6s,7s)	p (6p, 7p)	d (5d,6d)	f (5f)	s (2s)	p (2p)	d (3d)
5σ	1.24	6.38	16.99	11.55	3.70	57.85	0.10
3π	--	1.35	14.66	8.03	--	73.50	0.18

Table 3.9: Partial Gross Population Analysis for the bonding MOs for the ^{4}H + $^4\Pi$ (5f $\varphi^1$5f$\delta^1$7sσ^1) states for UO^+ at R_e = 1.803 Å

	Uranium AO’s				Oxygen AO’s		
	s (6s,7s)	p (6p, 7p)	d (5d,6d)	f (5f)	s (2s)	p (2p)	d (3d)
3σ	0.91	39.55	1.90	0.96	53.45	3.14	0.08
4σ	1.41	54.51	2.88	0.58	37.10	3.49	0.03
5σ	1.63	7.77	16.12	6.34	2.25	65.81	0.27
3π	--	1.75	13.27	4.22	--	80.63	0.12

Table 3.10: Partial Gross Population Analysis for selected MOs for the ${}^5I + {}^5\Gamma + {}^5\Delta + {}^5\Sigma$ ($5f\varphi^1 5f\delta^1 5f\pi^1 7s\sigma^1$) state for UO at R_e = 1.879 Å

	Uranium AO’s				Oxygen AO’s		
	s (6s,7s)	p (6p, 7p)	d (5d,6d)	f (5f)	s (2s)	p (2p)	d (3d)
3σ	0.55	49.74	1.41	1.05	43.69	3.45	0.10
4σ	1.45	45.90	3.55	0.65	46.69	1,74	0.02
5σ	1.47	5.65	16.72	8.08	2.92	65.04	0.10
3π	--	1.48	13.52	5.37	--	79.48	0.15

Table 3.11: Partial Gross Population Analysis for selected MOs for ${}^3H + {}^3\Pi$ ($5f\varphi^1 5f\delta^1 7s\sigma^2$) states for UO at R_e = 1.879 Å

	Uranium AO’s				Oxygen AO’s		
	s (6s,7s)	p (6p, 7p)	d (5d,6d)	f (5f)	s (2s)	p (2p)	d (3d)
3σ	0.46	48.49	1.33	1.15	45.10	3.37	0.10
4σ	1.72	46.72	3.68	0.44	45.36	2.06	0.02
5σ	1.85	6.38	16.53	6.89	2.69	65.55	0.09
3π	--	1.46	13.38	4.72	--	80.29	0.13

Table 3.12: Partial Gross Population Analysis for selected MOs for the ${}^5K + {}^5\Phi + {}^5\Pi$ ($5f\varphi^1 5f\delta^1 7s\sigma^1 6d\delta^1$) states for UO at R_e = 1.879 Å

	Uranium AO's				Oxygen AO's		
	s (6s,7s)	p (6p, 7p)	d (5d,6d)	f (5f)	s (2s)	p (2p)	d (3d)
3σ	1.35	46.39	2.03	1.44	45.01	3.65	0.12
4σ	0.76	47.56	4.17	0.72	43.05	3.70	0.04
5σ	1.49	7.19	18.13	9.83	3.70	59.55	0.10
3π	--	1.60	13.28	6.15	--	78.78	0.18

Table 3.13: Partial Gross Population Analysis for selected MOs for the ^{3}H + $^3\Pi$ (5f $\varphi^1$5f$\delta^1$7sσ^2) states for UO at R_e = 1.826 Å

	Leading Λ-S terms	T_e (cm^{-1})	Dipole length (e bohr)	Oscillator Strength (10^{-6})
4	63% ^{5}I $(1\varphi^1 2\delta^1 4\pi^1 6\sigma^1)$ + 14% ^{5}H $(1\varphi^1 2\delta^1 7\sigma^1 6\sigma^1)$	-	-	-
3	46% ^{5}H $(1\varphi^1 2\delta^1 7\sigma^1 6\sigma^1)$ + 15% $^5\Gamma$ $(1\varphi^1 2\delta^1 4\pi^1 6\sigma^1)$ + 11% $^5\Gamma$ $(1\varphi^1 7\sigma^1 4\pi^1 6\sigma^1)$	608	0.01764	0.541
2	23% $^5\Gamma$ $(1\varphi^1 2\delta^1 4\pi^1 6\sigma^1)$ + 21% $^5\Phi$ $(1\varphi^1 4\pi^2 6\sigma^1)$ + 14% $^5\Gamma$ $(1\varphi^1 7\sigma^1 4\pi^1 6\sigma^1)$	916	0.00000	0.000
5	37% ^{5}I $(1\varphi^1 2\delta^1 4\pi^1 6\sigma^1)$ + 18% ^{3}I $(1\varphi^1 2\delta^1 4\pi^1 6\sigma^1)$ + 13% ^{5}H $(1\varphi^1 2\delta^1 7\sigma^1 6\sigma^1)$	1325	0.03193	4.102
4	74% ^{3}H $(1\varphi^1 2\delta^1 6\sigma^2)$	1581	0.00522	0.195
4	24% ^{5}H $(1\varphi^1 2\delta^1 7\sigma^1 6\sigma^1)$ + 17% ^{5}I $(1\varphi^1 2\delta^1 4\pi^1 6\sigma^1)$ + 15% ^{3}H $(1\varphi^1 2\delta^1 7\sigma^1 6\sigma^1)$ + 8% $^5\Gamma$$(1\varphi^1 7\sigma^1 4\pi^1 6\sigma^1)$ + 6% $^5\Phi$ $(1\varphi^1 4\pi^2 6\sigma^1)$	1770	0.05898	18.71
3	13% $^5\Phi$ $(1\varphi^1 4\pi^2 6\sigma^1)$ + 12% ^{5}H $(1\varphi^1 2\delta^1 7\sigma^1 6\sigma^1)$ + 8% $^5\Gamma$$(1\varphi^1 2\delta^1 4\pi^1 6\sigma^1)$ + 6% $^5\Gamma$ $(1\varphi^1 7\sigma^1 4\pi^1 6\sigma^1)$	2117	0.02352	3.577
2	17% $^5\Gamma$ $(1\varphi^1 7\sigma^1 4\pi^1 6\sigma^1)$ + 14% $^5\Gamma$ $(1\varphi^1 2\delta^1 4\pi^1 6\sigma^1)$ + 11% $^5\Gamma$ $(1\varphi^1 7\sigma^1 4\pi^1 6\sigma^1)$ + 8% $^5\Pi$ $(1\varphi^1 2\delta^1 7\sigma^1 6\sigma^1)$	2294	0.00000	0.000
5	80% ^{5}K $(1\varphi^1 2\delta^1 3\delta^1 6\sigma^1)$	3928	0.13407	219.5
6	52% ^{5}I $(1\varphi^1 2\delta^1 4\pi^1 6\sigma^1)$ + 18% ^{5}H $(1\varphi^1 2\delta^1 7\sigma^1 6\sigma^1)$ +11% ^{3}I $(1\varphi^1 2\delta^1 4\pi^1 6\sigma^1)$	4641	0.00000	0.000
6	52% ^{5}K $(1\varphi^1 2\delta^1 3\delta^1 6\sigma^1)$ + 12% ^{3}K $(1\varphi^1 2\delta^1 3\delta^1 6\sigma^1)$	5805	0.0000	0.00
4	61% ^{5}I $(1\varphi^1 3\delta^1 4\pi^1 6\sigma^1)$	6540	0.02288	10.40

Table 3.14: Vertical Transition Energies and Intensities for UO from the $\Omega'' = 4$ ground state

	Leading Λ-S terms	T_e (cm^{-1})	Expt. (cm^{-1})^a
4	63% ^{5}I ($1\varphi^1 2\delta^1 4\pi^1 6\sigma^1$) + ^{5}H 14% ($1\varphi^1 2\delta^1 7\sigma^1 6\sigma^1$)	-	-
4	64% ^{3}H ($1\varphi^1 2\delta^1 6\sigma^2$) + 12% ^{5}I ($1\varphi^1 2\delta^1 4\pi^1 6\sigma^1$)	140	294
3	46% ^{5}H ($1\varphi^1 2\delta^1 7\sigma^1 6\sigma^1$) + 15% $^5\Gamma$ ($1\varphi^1 2\delta^1 4\pi^1 6\sigma^1$) + 11% $^5\Gamma$ ($1\varphi^1 7\sigma^1 4\pi^1 6\sigma^1$)	608	651
2	23% $^5\Gamma$ ($1\varphi^1 2\delta^1 4\pi^1 6\sigma^1$) + 21% $^5\Phi$ ($1\varphi^1 4\pi^2 6\sigma^1$) + 14% $^5\Gamma$ ($1\varphi^1 7\sigma^1 4\pi^1 6\sigma^1$)	916	958
5	37% ^{5}I ($1\varphi^1 2\delta^1 4\pi^1 6\sigma^1$) + 18% ^{3}I ($1\varphi^1 2\delta^1 4\pi^1 6\sigma^1$) + 13% ^{5}H ($1\varphi^1 2\delta^1 7\sigma^1 6\sigma^1$)	1325	1043
4	24% ^{5}H ($1\varphi^1 2\delta^1 7\sigma^1 6\sigma^1$) + 17% ^{5}I ($1\varphi^1 2\delta^1 4\pi^1 6\sigma^1$) + 15% ^{3}H ($1\varphi^1 2\delta^1 7\sigma^1 6\sigma^1$) + 8% $^5\Gamma$($1\varphi^1 7\sigma^1 4\pi^1 6\sigma^1$) + 6% $^5\Phi$ ($1\varphi^1 4\pi^2 6\sigma^1$)	1770	1574
3	13% $^5\Phi$ ($1\varphi^1 4\pi^2 6\sigma^1$) + 12% ^{5}H ($1\varphi^1 2\delta^1 7\sigma^1 6\sigma^1$) + 8% $^5\Gamma$($1\varphi^1 2\delta^1 4\pi^1 6\sigma^1$) + 6% $^5\Gamma$ ($1\varphi^1 7\sigma^1 4\pi^1 6\sigma^1$)	2117	1941
2	17% $^5\Gamma$ ($1\varphi^1 7\sigma^1 4\pi^1 6\sigma^1$) + 14% $^5\Gamma$ ($1\varphi^1 2\delta^1 4\pi^1 6\sigma^1$) + 11% $^5\Gamma$ ($1\varphi^1 7\sigma^1 4\pi^1 6\sigma^1$) + 8% $^5\Pi$ ($1\varphi^1 2\delta^1 7\sigma^1 6\sigma^1$)	2294	2118
6	52% ^{5}I ($1\varphi^1 2\delta^1 4\pi^1 6\sigma^1$) + 18% ^{5}H ($1\varphi^1 2\delta^1 7\sigma^1 6\sigma^1$) +11% ^{3}I ($1\varphi^1 2\delta^1 4\pi^1 6\sigma^1$)	4641	4469

^{a}ref [97]-[98]

Table 3.15: Adiabatic Transition Energies for the UO molecule

	Leading Configuration	Leading Λ-S term	T_e (cm^{-1})	Oscillator Strength
4	$5f^37s^1$	^5I ($1\varphi^12\delta^14\pi^16\sigma^1$)	0	-
4	$5f^27s^17p^1$	^5I ($1\varphi^12\delta^15\pi^16\sigma^1$)	13359	0.00110
4	$5f^27s^16d^1$	$^5\Phi$ ($1\varphi^12\delta^13\delta^16\sigma^1$)	14310	0.00019
5	$5f^37p^1$	^5K ($1\varphi^12\delta^15\pi^14\pi^1$)	15532	0.2008
4	$5f^37p^1$	^5I ($1\varphi^12\delta^15\pi^17\sigma^1$)	15911	0.00272

Table 3.16: High-lying excited state calculations with intensities from the $\Omega'' = 4$ ground state at its equilibrium geometry

	Configuration	Leading Λ-S term	T_e (cm^{-1})	Oscillator Strength
4	$5f^37s^1$	^5I ($1\varphi^12\delta^14\pi^16\sigma^1$)	0	-
3	$5f^37s^1$	^5H ($1\varphi^12\delta^17\sigma^16\sigma^1$)	608	-
4	$5f^27s^17p^1$	^5I ($1\varphi^12\delta^15\pi^16\sigma^1$)	13359	0.00536
5	$5f^37p^1$	^5K ($1\varphi^12\delta^15\pi^14\pi^1$)	15532	0.0000
4	$5f^37p^1$	^5I ($1\varphi^12\delta^15\pi^17\sigma^1$)	15911	0.04667

Table 3.17: High-lying excited state calculations from the $\Omega'' = 3$ first excited state at the equilibrium geometry of the ground state

	Configuration	Leading Λ-S term	T_e (cm^{-1})	Exp.	Rotational Constant (cm^{-1})	Oscillator Strength
4	$5f^37s^1$	^5I ($1\varphi^12\delta^14\pi^16\sigma^1$)	0	-	0.3330	-
4	$5f^27s^17p^1$	^5I ($1\varphi^12\delta^15\pi^16\sigma^1$)	13359	14016	0.3409	0.00110
5	$5f^37p^1$	^5K ($1\varphi^12\delta^15\pi^14\pi^1$)	15532	16845	0.330	0.2008

Table 3.18: Tentative Assignments

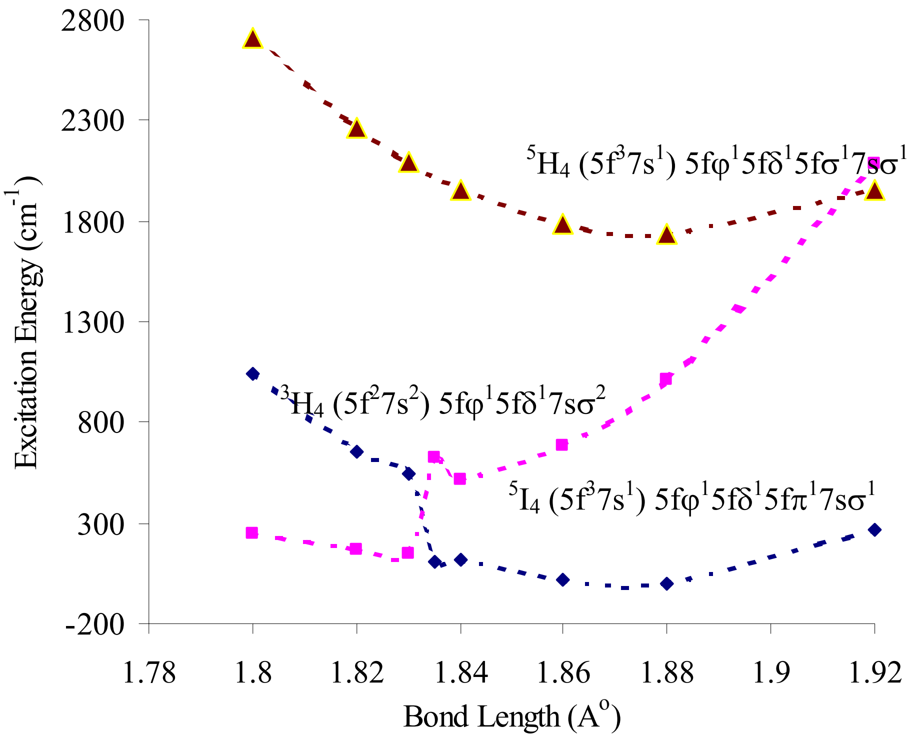

Figure 3.1: Potential energy curves for three low-lying Ω = 4 states of UO using the cc-pVDZ quality basis set

CHAPTER 4

ELECTRONIC SPECTRUM OF THE ThO AND ThO$^+$ MOLECULES

4.1 Introduction

Relativistic *ab initio* calculations have been carried out in this work to explore the electronic structure of the ThO and ThO$^+$ systems. Large amounts of experimental data [112-114] in the IR and visible regions and the corresponding theoretical results [108-111] are available for ThO. This calculation serves primarily as a benchmark calculation to check the effectiveness of our method to treat important correlation and relativistic effects. This work also reports the wave functions for the few high-lying electronic states, which have been observed experimentally, and haven't been assigned in previous sets of calculations. The transition-moment results under the electric-dipole mechanism are also presented in this work, which is also absent in the previous calculations. The theoretical analysis of ThO is available for both the one-step [108,109 and this work] and the two-step approach [110] to include correlation and spin-orbit effects in the calculation. The one-step approach involves simultaneous consideration of electron repulsion and spin-orbit effects but in a two-step approach the computational effort is reduced by first introducing correlation and second adding the spin-orbit interaction. Thus our electronic structure study of ThO provides a good framework to study the effectiveness of either approach to predict the transition energy results in the framework of the coupling scheme that prevails in ThO.

For ThO^+ currently there are no spectroscopic data published, but Heaven *et al.* [115] are in the process of acquiring such data. Thus this work can provide them with information on what frequency regions to scan. In this work we have analyzed both the metal-centered and charge-transfer states from the IR to the visible region of the spectra. In ThO^+, low-lying states are one-electron states where the coupling scheme is indeterminate due to the absence of electron-repulsion splittings and the only important splitting interaction is the spin-orbit interaction. Above 30,000 cm^{-1} lie the charge-transfer states with excitations from the lower bonding MOs where both spin-orbit and electron-repulsion interactions are present and their relative size will decide the applicable coupling scheme.

4.2 Computational Details

In the present study the calculations for ThO and ThO^+ were carried out using the shape-consistent Christiansen 68-e core potential for uranium and 2-e core potential for oxygen. The atomic set for Th was obtained by optimizing the (5sd,4p,4f) exponents in Hartree-Fock calculations on the $5d^{10}6s^26p^67s^17p^15f^16d^1$ average of configurations. The optimization can also be performed for the high-spin states for which the orbitals were less diffuse because the additional exchange interactions decreases the repulsion between the electrons. For oxygen the cc-pVDZ the atomic set was obtained by optimizing the (s,p)-exponents in Hartree-Fock calculations on the ground, ^3P state. We also performed the calculation using the basis set optimized for O^-, but a higher SCF energy was obtained. Thus all the results listed in this chapter used the basis set generated for neutral oxygen. The calculations for ThO and ThO^+ were carried out in C_{2v} symmetry. The MOs for the excited-state calculations were obtained using the MCSCF and SCF techniques.

The reference space for ThO and ThO^+ consisted of 12 electrons and 11 electrons, respectively. For ThO the 3σ, 4σ, 5σ and 3π MOs are doubly occupied in all the references but then single and double excitations were allowed out of them. The reference space also had two electrons distributed among the 6σ(7sσ), 2δ(6dδ), 4π(6dπ), 7σ(6dσ), 5π(7pπ), 8σ(7pσ), 1φ(5fφ) and 3δ(5fδ) MOs. Even though the states arising from $5\pi^2$ (7pπ) and $8\sigma^2$ (7pσ) are very high in energy, there were incorporated to take into account $7s^2 \rightarrow 7p^2$ near degeneracy excitations. No additional constraints were imposed on the calculation.

For ThO^+, two sets of calculations were performed. In the first calculation the 3σ, 4σ, 5σ and 3π MOs were part of the inactive space while in the second calculation, where we interested in analyzing the charge-transfer states, the bonding 5σ and 2π MOs were placed in the active space.

In this work the vertical transition energies and the oscillator strengths under the electric-dipole approximation were calculated for the low- and high-lying electronic states of ThO and ThO^+.

4.3 Electronic Spectrum of ThO^+

To a first approximation the bonding in ThO^+, can be described by a $Th^{3+}O^{2-}$ ionic bond. The ground state of ThO^+ is an $\Omega = ½$ state arising from $3\pi^4 5\sigma^2 6\sigma^1$ configuration, where the 6σ MO is predominantly 7sσ in character. The listed 3π and 5σ MOs are mostly bonding MOs formed by mixing of O2p(π,σ) with U6d (π,σ) and U5f (π,σ). The ground state has also been established experimentally as $\Omega = ½$ by Heaven *et al.* [115] with a bond length of 1.807 Å. Our multireference bond length was calculated with $6\sigma^1$ (7sσ), $8\sigma^1$ (7pσ), $4\pi^1$ (7pπ) and $2\delta^1$ (6dδ) in the reference space. We obtained a bond length of 1.825 Å using the cc-pVDZ quality basis set, which is high by 0.018 Å; with added correlation using a better quality basis set it is expected to move closer to the experimental value.

The bonding in ThO^+ is mostly between the O2p and Th6d AO's with a lesser contribution from Th5f. The population analysis is shown in Tables 4.4-4.5. As in the UO and UO^+ systems discussed in the chapter 3, the 6p is also significantly involved in bonding for ThO^+, where its contribution to the 5σ highest occupied bonding MO is 8%. The overall population analysis shown in Tables 4.7-4.8 shows that thorium and oxygen have charge distribution of +1.272 and –0.272 respectively.

In this work the electronic structure of ThO^+ is studied from the IR to the UV regions of the spectra. In this region there are two type of transitions, metal-centered transitions and charge-transfer transitions. There are two types of charge-transfer excitations. The first type involves excitation of an electron from 7sσ orbital to an antibonding orbital with mostly Th6dπ^*, Th5fπ^*, or Th6dσ^* character and the second type involves excitation of an electron from the bonding 3π or 5σ MOs to the thorium-centered 6σ or 2δ MOs.

The first 11 excited states for ThO^+ form a one-electron spectrum analogous to alkali atom spectra where the single unpaired electron is excited to higher levels and where important influence on the electronic structure comes from the spin-orbit interaction. In the presence of spin-orbit the first five low-lying states of ThO^+ were found to be 6d orbtials. The first pair of states are $^2\Delta$ states arising from the $6\sigma \rightarrow 1\delta$ configuration, where the 1δ orbital is the nonbonding U6dδ orbital which does not get perturbed by the oxygen field. This is a metal-centered excitation. The $^2\Delta_{5/2}$ - $^2\Delta_{3/2}$ splitting was found to be ~3249 cm^{-1}, which is close to the 3230 cm^{-1} (0.4eV) $d_{5/2}$- $d_{3/2}$ spin-orbit splitting for the thorium atom [115]. In the atomic-ion limit, $\zeta_\delta = \zeta_{6d}$. The very small deviation from the atomic picture is due to the fact that $^2\Delta_{5/2}$ is 90% of the total Ω =5/2 wave function and similarly $^2\Delta_{3/2}$ contributes 89% to the respective Ω=3/2 wave function. The Ω = 3/2 and Ω = 5/2 states lie at 2602 and 5852 cm^{-1} from the Ω = 1/2 ground state. The calculated T_e values for the 3/2 and 5/2 states are in good agreement with the experimental values of 2933 cm^{-1} and 5814 cm^{-1} respectively [115]. Our preliminary results were used to guide the search for the 2933 cm^{-1} transition.

The next sets of transitions are the charge-transfer transitions arising from excitation from the 6σ MO to the antibonding 4π and 7σ MOs. In the absence of SO the oscillator strength to 4π and 7σ are 0.01710 and 0.02037 respectively as a result of $^2\Sigma^+$ ($7s\sigma$) $\rightarrow$ $^2\Pi$ ($6d\pi$) perpendicular and $^2\Sigma^+$ ($7s\sigma$) $\rightarrow$ $^2\Sigma^+$ ($6d\sigma$) parallel transitions. There is a strong spin-orbit mixing between the $^2\Pi_{1/2}$ ($4\pi^1$) and $^2\Sigma_{1/2}^+$ (7σ) states. The two resulting Ω = ½ wave functions are 75% $^2\Pi$ ($4\pi^1$) + 12% $^2\Sigma^+$ ($7\sigma^1$) and 73% $^2\Sigma^+$ ($7\sigma^1$) + 11% $^2\Pi$ ($4\pi^1$) respectively.

The next set of excited states arise from excitation from the 6σ MO to the 1φ and 3δ MOs, where 1φ and 3δ are the non-bonding components of the 5f orbital. The state arising from the non-bonding 5fφ lies higher than the antibonding 6dπ and 6dσ MO's, further showing the extent of the higher energy of the 5f with respect to 6d and 7s for the thorium atom. The first state, $\Omega = 5/2$, with an electron in 5f shell occurs in the visible at $T_e = 23718$ cm^{-1}. The $^2\Phi_{7/2}$ - $^2\Phi_{5/2}$ difference was found to be ~3249 cm^{-1}. There is a spin-orbit mixing between $^2\Delta_{5/2}$ and $^2\Phi_{5/2}$ states. The resultant $\Omega = 5/2$ wave functions are 81% $^2\Phi_{5/2}$ + 8% $^2\Delta_{5/2}$ and 81% $^2\Delta_{5/2}$ + 8% $^2\Phi_{5/2}$ respectively. In the atomic ion limit the ratio of the coefficients of the $^2\Phi_{5/2}$ and $^2\Delta_{5/2}$ terms are 1:6 and 6:1 for the two wave functions respectively. In our calculation the ratio is close to 10:1 for the lowest energy $\Omega = 5/2$ state and vice versa, which is due to lifting of the degeneracy of the 5fφ and 5fδ in the presence of the oxygen field. The smaller spin-orbit mixing is because 5fφ is lower in energy than 5fδ; in the absence of spin-orbit the $^2\Delta$ lies 1227 cm^{-1} above $^2\Phi$. In addition, the splitting of $^2\Phi$ ($^2\Phi_{7/2}$ - $^2\Phi_{5/2}$) is 1.25 times the splitting of $^2\Delta$ ($^2\Delta_{5/2}$ - $^2\Delta_{3/2}$), which is close to atomic ion limit of 1.5.

Due to the high single-reference character of the initial and the final states the next set of transitions (6σ to 5π or 8σ) can be categorized as 7sσ → 7pπ and 7sσ → 7pσ. As expected these are the transitions which have the strongest oscillator strength from the ground state due to the high radial overlap between the 7s and 7p orbitals. In the absence of spin-orbit the perpendicular $^2\Sigma_0^+$ (7sσ) → $^2\Pi$ (7pπ) transition has transition energy and oscillator strength of 27469 and 0.8125 cm^{-1} respectively. Similarly the parallel $^2\Sigma_0^+$

(7sσ) → $^2\Sigma_0^+$ (7pσ) transition has transition energy and oscillator strength of 39668 and 0.3111 cm^{-1}.

The excitation from the 6σ MO to the 6π MO formed by the antibonding mixing between 5f and O2p lies around 53,000cm^{-1}. In the absence of spin-orbit the oscillator strength to the 6π state is 0.1100 which is quite significant due to the following reasons; firstly in thorium the 5f orbital has a large <r> value, so the radial overlap with 6σ MO, which has mostly 7sσ character, is higher than in the case of the monooxides of U, Np, Pu etc. and secondly due to the fact that in addition to U5fπ and O2pπ it has some U7pσ and U6dσ character mixed in. The excitation from 6σ to 9σ (5fσ) lies higher in energy, and was not studied in detail.

A preliminary SO calculation was performed to study the region in which many charge-transfer states lie based on the excitation out of the bonding 3π and 5σ MOs. The atomic character of the 3π and 5σ MOs are 7.7% Th(5f) + 18.6% Th(6d) + 62.4% O(2p) and 7.6% Th(5f) + 15.8% Th(6d) + 74% O(2p) respectively. With the bonding MO being mostly O2p in character, the amount of charge transfer associated with these transitions is quite significant as all the low-lying unoccupied MOs are mostly localized on the thorium atom. The charge-transfer states have higher equilibrium bond lengths and lower vibrational frequencies. Both quartet and doublet charge-transfer states are possible, and due to the high-spin character of the quartet states their equilibrium bond length will be larger than that of the doublet states.

The quartet and doublet charge-transfer states arising from excitation of an electron out of the 3π and 5σ bonding MOs are listed in Table 4.4. The 5σ and 3π are the bonding MOs and have orbital energies of -0.6750 and -0.6946 H respectively. The first set of charge-transfer states arises from the 5σ MO, followed by the excited states with the excitation out of the 3π MO. The excitation energy at the Hartree-Fock level from the 5σ and 3π MO is given by $\varepsilon_a - \varepsilon_i - J_{ai}$ [89] where a is the virtual orbital and i is the closed-shell orbital and J_{ai} is the coulomb integral between the two. Thus in addition to the differences in the orbital energies of 5σ and 3π MO with the virtual MO, the coulomb integral between the 5σ or 3π MO and the virtual MO will contribute to the charge-transfer excitation energies.

The first charge-transfer state occurs at 39706 cm^{-1} above the $^2\Sigma^+$ ground state. This is a $^4\Delta$ state arising from the excitation of an electron to the unoccupied 2δ MO rather than the $^2\Sigma^+$ state arising from the excitation of an electron to the lower singly occupied 6σ MO. This is due to following reasons: 1) The $^4\Delta$ state arising from $3\pi^4 5\sigma^1 6\sigma^1 2\delta^1$ configuration, having high spin, is favored due to the additional exchange interactions; 2) The spin-orbit stabilization is higher for the $^4\Delta$ state than for the $^2\Sigma^+$ doublet state from the $3\pi^4 5\sigma^1 6\sigma^2$ configuration and finally 3) The 5σ bonding MO has ~ 18% U6d character with its maximum amplitude centered on oxygen atom, thus the $J_{5\sigma,2\delta}$ coulomb integral will be a bit larger than the $J_{5\sigma,6\sigma}$ coulomb integral. At the SCF level the $^4\Delta$ ($3\pi^4 5\sigma^1 6\sigma^1 2\delta^1$) state lies 7600 cm^{-1} lower than the $^2\Sigma^+$ ($3\pi^4 5\sigma^1 6\sigma^2$) at the equilibrium geometry of the ground state. The spin-orbit contribution will further lower the $^4\Delta$ ($3\pi^4 5\sigma^1 6\sigma^1 2\delta^1$) state by an approximate value of 1615 cm^{-1} ($\zeta_\delta = \zeta_{6d} = 1615$ cm^{-1}). Although with the effect of electron correlation treatment the energy of $^2\Sigma^+$ ($3\pi^4 5\sigma^1 6\sigma^2$)

will be lowered more than that of the $^4\Delta$ ($3\pi^4 5\sigma^1 6\sigma^1 2\delta^1$) state since the former has more doubly occupied MOs.

The Ω = 3/2 and Ω = 5/2 states from $3\pi^4 5\sigma^1 6\sigma^1 2\delta^1$ configuration undergo significant $^4\Delta$ - $^2\Delta$ spin-orbit mixing with the wavefunction character of 70% $^4\Delta$ + 14% $^2\Delta$ and 66% $^4\Delta$ + 13% $^2\Delta$ respectively. The first doublet $^2\Delta_{3/2}$ state lies at 41762 cm^{-1} and arises from this $3\pi^4 5\sigma^1 6\sigma^1 2\delta^1$ configuration rather than the $^2\Sigma^+$ from the $3\pi^4 5\sigma^1 6\sigma^2$ configuration, which lies at 42047 cm^{-1}.

The charge-transfer states from excitation out of the bonding 3π MO start at 48705 cm^{-1}. Since the atomic composition of the 3π and the 5σ MOs is almost the same, the relative ordering of the states arising from $3\pi^3 5\sigma^2 6\sigma^1 2\delta^1$ and $3\pi^3 5\sigma^2 6\sigma^2$ follow a trend similar to that of $3\pi^4 5\sigma^1 6\sigma^1 2\delta^1$ and $3\pi^4 5\sigma^1 6\sigma^2$ configurations as discussed above. The state at 48705 cm^{-1} is a $^4\Phi_{3/2}$ state, the lowest state from the $3\pi^3 5\sigma^2 6\sigma^1 2\delta^1$ based on Hunds's rule. The charge-transfer states calculated in this work are listed in Table 4.2.

4.4 Electronic Spectrum of ThO

The ground state for ThO is well known experimentally and theoretically as a $^1\Sigma^+{}_0$ state arising from the $3\pi^4 5\sigma^2 6\sigma^2$ electronic configuration. It has calculated and experimental bond lengths of 1.861 Å and 1.840 Å [69] respectively. The reference space for calculating the equilibrium bond length consisted of $6\sigma^2$ ($7s\sigma$), $3\delta^2$($6d\delta$), $5\pi^2$($7p\pi$) and $8\sigma^2$ ($7p\sigma$) to account for the near-degeneracy effects associated with the $7s^2 \rightarrow 7p^2$ and $7s^2 \rightarrow 6d^2$ excitations. With higher quality basis sets the added correlation will result in the decrease in the value closer to the experimental value as seen in case of UO, UO_2 and its ions in chapters 2 and 3.

The excited-state calculations were formed with MOs obtained using the SCF IVO technique. The results for the excited-state calculations along with the transition moments at the equilibrium geometry of the ground state are summarized in Table 4.5. Zero-point energy corrections are not included.

The lowest set of excited states arise from the $3\pi^4 5\sigma^2 6\sigma^1 2\delta^1$ configuration. This configuration generates the $^3\Delta_{1,2,3}$ and $^1\Delta_2$ Λ-S states. The coupling scheme is close to the Λ-S limit. The lower $\Omega = 2$ state is made up of 81% $^3\Delta_2$ + 6% $^1\Delta_2$. Based on the extent of singlet-triplet mixing we can say the electron-repulsion interaction due to the similar radial extent of 7s and 6d shells is a larger effect than the spin-orbit interaction arising from the electron in the 6dδ orbital. Also, at the equilibrium geometry of the ground state, the $^3\Delta_3 - {}^3\Delta_1$ separation is 2856 cm^{-1}. For Λ-S coupling in the absence of mixing with other states, the $^3\Delta_3$ - $^3\Delta_1 \approx 2\zeta_\delta$. The $^3\Delta_3$ - $^3\Delta_1$ value is 88% of the $d_{5/2}$- $d_{3/2}$ spin-orbit splitting of 3230 cm^{-1} for the thorium atom. As can be seen from Table 4.6, the transition energies from the ground state to the $^3\Delta_{1,2,3}$ obtained theoretically and experimentally are in good agreement.

The first discrepancy between the numbers obtained using the one step and two-step methods is associated with the $0^+(^1\Sigma_0^+)$ - 2 ($^1\Delta_2$) transition. In the Λ-S limit and also in the absence of mixing with other states, the $^3\Delta - {}^1\Delta$ and $^3\Delta_2 - {}^1\Delta_2$ differences are equal to $2K_{\sigma\delta}$. According to our calculation the $^3\Delta - {}^1\Delta$ and $^3\Delta_2 - {}^1\Delta_2$ differences are 5191 and 5696 respectively. The difference in the due the fact that states arising from the

$7s\sigma^1 6d\delta^1$ configuration show a small deviation from the Λ-S coupling scheme. The point in doing this exercise is to obtain an estimate for the value of $^1\Delta_2$ as there is no dispute associated with the transition energy for the $^3\Delta_2$ state. Based on the $2K_{\sigma\delta} = 5191$ cm^{-1} relationship and the experimentally obtained value of T_e ($^3\Delta_2$) = 6128 cm^{-1} the approximate value of T_e ($^1\Delta_2$) = 11319 cm^{-1}. Thus within the framework of the Λ-S coupling scheme our T_e ($^1\Delta_2$) = 11319 cm^{-1} seems reasonable but then the discrepancy in the number may also be due to the omission of some unrecognized shortening in our list of references.

The next sets of transitions are the charge-transfer transitions arising from the excitation to the $6\sigma^1 4\pi^1$ and $6\sigma^1 7\sigma^1$ configurations. These configurations generate $^3\Pi_{0^+,0^-,1,2}$, $^1\Pi_1$, $^3\Sigma^+_{0,1}$ and $^1\Sigma^+_0$ Λ-S states respectively. As can seen from the results in Table 4.6, the $^3\Pi_{0^+}$, $^3\Pi_1$ and $^3\Pi_2$ obtained theoretically and experimentally are in good agreement. Again there is a discrepancy associated with the transition energy value for $^1\Pi_1$ not only between the results obtained from one- and two-step approaches but also from the experimentally obtained value. Again, we may have omitted some important references in our calculation, but this is not clear at this point.

The 0^+ ($^1\Sigma_0^+$) → $1(^1\Pi_1)$ transition at the calculated value of 17443 is the strongest electric-dipole transition with the oscillator strength of 0.1413. There is a significant mixing between $^3\Pi_1$ and $^1\Pi_1$ and between $^3\Sigma_1^+$ and $^1\Pi_1$ terms which results in the spreading of intensity to the 0^+ ($^1\Sigma_0^+$) → $1(^3\Pi_1)$ and 0^+ ($^1\Sigma_0^+$) → $1(^3\Sigma_1^+)$ transitions at 11866 and 20331 cm^{-1}, which are forbidden in the absence of spin-orbit.

The next set of states arise from the $3\delta^2$, $3\delta^1 4\pi^1$ and $6\sigma^1 5\pi^1$ configurations, which were not studied in detail in previous calculations. But in the region 20,000 cm^{-1} – 25,000 cm^{-1} our calculated result matches very well with the experimentally observed transitions, as can be seen from Table 4.6.

4.5 Conclusions

In this work, electronic-structure calculations for ThO and ThO$^+$ have been reported. The vertical transition energies are calculated for the low- and high-lying states for ThO and ThO$^+$ in addition to their wave-function character and intensities. The bond lengths for ThO and ThO$^+$ match very well with the experimental values, having a maximum deviation of 0.02 Å. For ThO the electronic-structure calculations are in agreement with the experimental value except for few transitions for which further work is needed. For ThO$^+$, the three low-lying states are in good agreement with the experimental data and the expected availability of the experimental data for the higher states will provide insight into the quality of the results.

State	Λ-S terms	$T_e(cm^{-1})$
½	$90\%\ ^2\Sigma^+ (6\sigma^1)$	-
3/2	$89\%\ ^2\Delta (2\delta^1)$	2602
5/2	$90\%\ ^2\Delta (2\delta^1)$	5852
1/2	$75\%\ ^2\Pi (4\pi^1) + 12\%\ ^2\Sigma^+ (7\sigma^1)$	9167
3/2	$83\%\ ^2\Pi (4\pi^1)$	11846
1/2	$73\%\ ^2\Sigma^+ (7\sigma^1) + 11\%\ ^2\Pi (4\pi^1)$	14815
5/2	$81\%\ ^2\Phi (1\varphi^1) + 8\%\ ^2\Delta (3\delta^1)$	23718
1/2	$77\%\ ^2\Pi (5\pi^1) + 6\%\ ^2\Pi (6\pi^1) + 3\%\ ^2\Pi (3\pi^1)$	25504
3/2	$86\%\ ^2\Delta (3\delta^1)$	25652
7/2	$89\%\ ^2\Phi (1\varphi^1)$	26796
5/2	$81\%\ ^2\Delta (3\delta^1) + 8\%\ ^2\Phi (1\varphi^1)$	27969
3/2	$79\%\ ^2\Pi (5\pi^1) +6\%\ ^2\Pi (4\pi^1) + 3\%\ ^2\Pi (6\pi^1)$	29321
½	$79\%\ ^2\Sigma^+ (8\sigma^1)$	39904
½	$78\%\ ^2\Pi (6\pi^1)$	52734
3/2	$80\%\ ^2\Pi (6\pi^1)$	53929

Table 4.1: Electronic States of the ThO^+ molecule at the equilibrium geometry of the ground state using the cc-pVDZ basis set and based on excitation from the 6σ MO

State	Leading Λ-S term	$T_e(cm^{-1})$
½	$^2\Sigma^+ (3\pi^4 5\sigma^2 6\sigma^1)$	-
½	$^4\Delta (3\pi^4 5\sigma^1 6\sigma^1 2\delta^1)$	39706
3/2	$^4\Delta (3\pi^4 5\sigma^1 6\sigma^1 2\delta^1)$	40263
5/2	$^4\Delta (3\pi^4 5\sigma^1 6\sigma^1 2\delta^1)$	41296
3/2	$^2\Delta (3\pi^4 5\sigma^1 6\sigma^1 2\delta^1)$	41762
½	$^2\Sigma^+ (3\pi^4 5\sigma^1 6\sigma^2)$	42047
7/2	$^4\Delta (3\pi^4 5\sigma^1 6\sigma^1 2\delta^1)$	43217
5/2	$^2\Delta (3\pi^4 5\sigma^1 6\sigma^1 2\delta^1)$	44245
3/2	$^4\Phi (3\pi^3 5\sigma^2 6\sigma^1 2\delta^1)$	48705

Table 4.2: Charge-transfer transitions at the equilibrium geometry of the ground state based on the excitations from the 5σ or 3π bonding MOs

Leading Term	T_e(cm^{-1})	Oscillator Strength
90% $^2\Sigma_0^+$ ($6\sigma^1$)	-	-
89% $^2\Delta$ ($2\delta^1$)	4158	0
75% $^2\Pi$ ($4\pi^1$)	10807	0.0342
73% $^2\Sigma_0^-$ ($7\sigma^1$)	14102	0.0203
81% $^2\Phi$ ($1\varphi^1$)	25010	0.0000
86% $^2\Delta$ ($3\delta^1$)	26237	0.0000
79% $^2\Pi$ ($5\pi^1$)	27469	0.8125
79% $^2\Sigma_0^+$ ($8\sigma^1$)	39668	0.3111
78% $^2\Pi$ ($6\pi^1$)	53044	0.1100

Table 4.3: Transition Energies and Intensities for ThO^+ in the absence of spin-orbit

Molecular Orbital	Atomic Character
1σ	U5dσ
2σ	U6sσ
3σ	O2sσ, U6pσ
4σ	U6pσ, O2sσ
5σ	O2pσ, U6dσ, U5fσ, U6dσ
6σ	U7sσ
7σ	U6dσ, O2sσ
8σ	U7pσ
1π	U5dπ
2π	U6pπ
3π	O2pπ, U6dπ, U5fπ
4π	U6dπ, U5fπ, O2pπ
5π	U7pπ
6π	U5fπ
1δ	U5dδ
2δ	U6dδ
3δ	U5fδ
1φ	U5fφ

Table 4.4: Atomic character for the ThO and ThO^+ MOs listed in Tables 4.1-4.3 and 4.6-4.7

State	Λ-S terms	T_e(cm^{-1})	Oscillator Strength
0^+	90% $^1\Sigma^+$ ($6\sigma^2$)		0.0000
1	88% $^3\Delta$($6\sigma^1 3\delta^1$)	5732	0.0000
2	81% $^3\Delta$ ($6\sigma^1 3\delta^1$)+ 6% $^1\Delta$ ($6\sigma^1 3\delta^1$)	6726	0.0000
3	89% $^3\Delta$ ($6\sigma^1 3\delta^1$)	8587	0.0000
0^-	54% $^3\Pi$ ($6\sigma^1 4\pi^1$)+ 28% $^3\Pi$ ($6\sigma^1 5\pi^1$)	10530	0.0000
0^+	56% $^3\Pi$ ($6\sigma^1 4\pi^1$)+ 29% $^3\Pi$ ($6\sigma^1 5\pi^1$)	10839	0.0021
2	66% $^1\Delta$ ($6\sigma^1 3\delta^1$) + 7% $^3\Delta$ ($6\sigma^1 3\delta^1$)	12422	0.0000
1	57% $^3\Pi$ ($6\sigma^1 4\pi^1$) + 23% $^3\Pi$ ($6\sigma^1 5\pi^1$) + 4% $^1\Pi$ ($6\sigma^1 4\pi^1$)	11866	0.0147
2	50% $^3\Pi$ ($6\sigma^1 4\pi^1$) + 11% $^3\Pi$ ($6\sigma^1 5\pi^1$) + 5% $^1\Delta$ ($6\sigma^1 3\delta^1$)	14446	0.0000
1	42% $^1\Pi$ ($6\sigma^1 4\pi^1$) + 10% $^3\Pi$ ($6\sigma^1 4\pi^1$) + 7% $^3\Sigma^+$ ($6\sigma^1 7\sigma^1$)	17333	0.1413
2	41% $^3\Phi$ ($3\delta^1 4\pi^1$) + 36% $^3\Phi$ ($3\delta^1 5\pi^1$)	19275	0.0000
0^+	38% $^3\Sigma^-$ ($3\delta^2$) + 12% $^1\Sigma^+$ ($3\delta^2$) + 12% $^1\Sigma^+$($6\sigma^1 7\sigma^1$)	20213	0.0238
1	71% $^3\Sigma^+$ ($6\sigma^1 7\sigma^1$) + 5% $^1\Pi$ ($6\sigma^1 4\pi^1$)	20331	0.0215
0^-	54% $^3\Pi$ ($6\sigma^1 5\pi^1$) + 26% $^3\Pi$ ($6\sigma^1 4\pi^1$)	21682	0.0000
0^+	48% $^3\Pi$ ($6\sigma^1 5\pi^1$) + 30% $^3\Pi$ ($6\sigma^1 4\pi^1$)	21758	0.0018
1	35% $^3\Pi$ ($6\sigma^1 5\pi^1$) + 18% $^3\Pi$ ($6\sigma^1 4\pi^1$) + 8% $^1\Pi$ ($6\sigma^1 4\pi^1$) + 2% $^1\Pi$ ($6\sigma^1 5\pi^1$)	21962	0.0108
2	50% $^3\Pi$ ($6\sigma^1 5\pi^1$) + 20% $^3\Pi$ ($6\sigma^1 4\pi^1$)	22903	0.0000
1	72% $^3\Sigma^-$ ($3\delta^2$)	22579	0.0041
3	42% $^3\Phi$ ($3\delta^1 4\pi^1$) + 34% $^3\Phi$ ($3\delta^1 5\pi^1$)	22585	0.0000
0^+	39% $^1\Sigma^+$ ($6\sigma^1 7\sigma^1$) + 34% $^3\Sigma^-$ ($3\delta^2$) + 4% $^1\Sigma^+$ ($3\delta^2$)	23668	0.0411
1	20% $^3\Pi$ ($6\sigma^1 5\pi^1$) + 15% $^1\Pi$ ($6\sigma^1 4\pi^1$) + 9% $^1\Pi$ ($6\sigma^1 5\pi^1$) + 5% $^3\Pi$ ($6\sigma^1 4\pi^1$)	24491	0.0983

Table 4.5: Transition Energies and Intensities for ThO

	Λ-S terms	This work	MOLPRO (Ref 109)	DK3-AIMP (Ref 110)	Exp. (Ref 111 - 114)
0^+	90% $^1\Sigma^+$ $(6\sigma^2)$	-	-		-
1	88% $^3\Delta(6\sigma^13\delta^1)$	5732	5768	5600	5317
2	81% $^3\Delta$ $(6\sigma^13\delta^1)$+ 6% $^1\Delta$ $(6\sigma^13\delta^1)$	6726	6628	6778	6128
3	89% $^3\Delta$ $(6\sigma^13\delta^1)$	8587	8213	8609	8600
0^-	54% $^3\Pi$ $(6\sigma^14\pi^1)$+ 28% $^3\Pi$ $(6\sigma^15\pi^1)$	10530	11051	10181	
0^+	56% $^3\Pi$ $(6\sigma^14\pi^1)$+ 29% $^3\Pi$ $(6\sigma^15\pi^1)$	10839	11328	10216	10601
2	66% $^1\Delta$ $(6\sigma^13\delta^1)$ + 7% $^3\Delta$ $(6\sigma^13\delta^1)$	12422	12190	14508	
1	57% $^3\Pi$ $(6\sigma^14\pi^1)$ + 23% $^3\Pi$ $(6\sigma^15\pi^1)$ + 4% $^1\Pi$ $(6\sigma^14\pi^1)$	11866	12252	11045	11129
2	50% $^3\Pi$ $(6\sigma^14\pi^1)$ + 11% $^3\Pi$ $(6\sigma^15\pi^1)$ + 5% $^1\Delta$ $(6\sigma^13\delta^1)$	14446	14504	14508	
1	42% $^1\Pi$ $(6\sigma^14\pi^1)$ + 10% $^3\Pi$ $(6\sigma^14\pi^1)$ + 7% $^3\Sigma^+$ $(6\sigma^17\sigma^1)$	17333	17156	14132	14490
2	41% $^3\Phi$ $(3\delta^14\pi^1)$ + 36% $^3\Phi$ $(3\delta^15\pi^1)$	19275	19401	17221	18010
0^+	38% $^3\Sigma^-$ $(3\delta^2)$ + 12% $^1\Sigma^+$ $(3\delta^2)$ + 12% $^1\Sigma^+(6\sigma^17\sigma^1)$	20213	19084	17681	16320
1	71% $^3\Sigma^+$ $(6\sigma^17\sigma^1)$ + 5% $^1\Pi$ $(6\sigma^14\pi^1)$	20221	19040	19426	
0^-	54% $^3\Pi$ $(6\sigma^15\pi^1)$ + 26% $^3\Pi$ $(6\sigma^14\pi^1)$	21682			
0^+	48% $^3\Pi$ $(6\sigma^15\pi^1)$ + 30% $^3\Pi$ $(6\sigma^14\pi^1)$	21758			
1	35% $^3\Pi$ $(6\sigma^15\pi^1)$ + 18% $^3\Pi$ $(6\sigma^14\pi^1)$ + 8% $^1\Pi$ $(6\sigma^14\pi^1)$ + 2% $^1\Pi$ $(6\sigma^15\pi^1)$	21962			21734
2	50% $^3\Pi$ $(6\sigma^15\pi^1)$ + 20% $^3\Pi$ $(6\sigma^14\pi^1)$	22903			
1	72% $^3\Sigma^-$ $(3\delta^2)$	22579			22635
3	42% $^3\Phi$ $(3\delta^14\pi^1)$ + 34% $^3\Phi$ $(3\delta^15\pi^1)$	22585			
0^+	39% $^1\Sigma^+$ $(6\sigma^17\sigma^1)$ + 34% $^3\Sigma^-$ $(3\delta^2)$ + 4% $^1\Sigma^+$ $(3\delta^2)$	23668			23155
1	20% $^3\Pi$ $(6\sigma^15\pi^1)$ + 15% $^1\Pi$ $(6\sigma^14\pi^1)$ + 9% $^1\Pi$ $(6\sigma^15\pi^1)$ + 5% $^3\Pi$ $(6\sigma^14\pi^1)$	24491			24856

Table 4.6: Experimental and theoretical T_e (cm^{-1}) results for ThO using different methods

Atom	Gross Atomic Populations					
	s	p	d	f	g	Total
Th	2.859	6.114	11.203	0.4963	0.0554	20.728
O	1.846	4.412	0.0140	0.000	0.000	6.272

Table 4.7: Mulliken Population Analysis for the $^2\Sigma^+$ ($7s\sigma^1$) wavefunction of ThO^+ at R_e = 1.825 Å

Atom	Gross Atomic Populations					
	s	p	d	f	g	Total
Th	3.755	6.211	11.152	0.4432	0.0519	21.615
O	1.839	4.534	0.0114	0.000	0.000	6.385

Table 4.8: Mulliken Population Analysis for the $^1\Sigma^+$ ($7s\sigma^2$) wavefunction of ThO at R_e = 1.861 Å

CHAPTER 5

IONIZATION POTENTIAL STUDY OF OXIDES OF ACTINIDES

5.1 Introduction

The ionization potentials (IP) of AnO and AnO_2 in the gas phase have been measured using electron impact [116] and mass spectrometry techniques [117-119]. There is a large discrepancy in the value of IP from these two experimental techniques. The ionization IP of UO and UO_2 reported by the electron impact measurements is 0.5 eV higher than the ones obtained by the mass spectrometry technique. In fact, from an experimental standpoint, the mass spectrometric technique is liable to provide an underestimated value of the IP. This is because this technique is not free from thermal effects and hence the ionization can result from low-lying excited states rather than the ground state.

In this work the IPs for the Th and U atoms, monoxides and dioxides have been calculated. The IP calculations for atomic uranium and thorium was performed more as a benchmark calculation since there is no known discrepancy in the IP values for these systems. Atomic U and Th systems also serve as good examples since the core-valence, valence-valence and valence-virtual correlation effects are quite different among the two even though in both cases the 5f, 6d and 7s shells compose the valence shell. The systems

ThO, UO, ThO_2, UO_2 under study have the ground state configurations of $7s\sigma^{1-2}5f^{n-1}$. On ionization of an electron from an orbital with 7s character, the systems under study conserve their $7s^{0-1}5f^{n-1}$ configurations without any rearrangement. Since the electron comes out of the diffuse 7s shell, the effect of spin-orbit coupling and the difference between the vertical and the adiabatic ionization potential (IP) values are both quite small. If there are low-lying excited states arising from a configuration different from that of the ground state, then the difference between the adiabatic and vertical IP is dependent on the shielding properties of the electrons in the valence space. Experimental study of the ionization potential of these molecules is complicated by the fact that both the molecules and their ions have many low-lying states arising from configurations which are the same or different from that of the ground state. Due to the high-density of low-lying states of the Th, U, ThO, UO, ThO_2 and UO_2 systems and their ions, multi-reference *ab initio* methods are well-adapted for their study, though size consistency errors may arise. Where non-spin-orbit calculations apply well, the considerable decrease in the size of the computation allowed us to address electron-correlation to a higher-order.

For actinide atoms except Ac, Pa and U, the ionization involves removal of an electron from the state with 7s character [120-121]. In the cases of Ac, Pa and U, where the electrons come out of the 6d shell, the polarization of 6s, 6p, 5s, 5p or 5d orbitals and spin-orbit effects will make a significant contribution to the first IPs. The general electronic configuration for all the actinide atoms are $s^2d^{0-2}f^n$. Along the actinide series, even though there are changes in the number of electrons in the 5f shell, the energy required to remove the electron from the 7s shell falls in the 5.99-6.5 eV range. This also shows that the intershell correlation between the electrons in 5f and the 7s shell is small, as expected from their different radial extent. The IP calculation of actinide atoms is difficult to perform as the valence electrons are distributed among closely spaced 5f, 6d and 7s shells resulting in a high density of low-lying electronic states. Also along the series there is a change in the order of stability of the 5f, 6d, 7s and 7p thereby changing the relative importance of exchange interactions between various pairs.

Currently there is a discrepancy in the IP values for UO and UO_2, not only for different experimental techniques but also for the different theoretical methods that have been utilized so far. The theoretical adiabatic IP obtained for UO_2 is 6.1eV using the CASPT2 [122] method and 6.3 eV using DFT [123]. The *ab initio* calculation performed in this work gives a smaller value of 5.6 eV.

In order to study the reason behind the discrepancies in the value of IP between the different theoretical approaches, we have looked at several issues in this work: 1) quality of the basis set 2) spin-orbit effects 3) order of Correlation and 4) size of the core potential.

5.2 Methods

Calculations are performed using double-zeta (cc-pVDZ) and triple-zeta (cc-pVTZ) quality basis sets of the correlation consistent type developed by our group. The calculations utilized 68- and 60-electron RECP and SO operators for uranium and 68-electron RECP and SO operator for thorium. The IP calculations were also carried out with the RECPs generated using the methods employed by Christiansen (10) and by Preuss, Stoll and co-workers at Stuttgart [124-125]. Natural orbitals generated from

MCSCF calculations were used in the CI calculations. Both the vertical and adiabatic IP values were computed for the systems under study.

5.3 Results and Discussion

The low and high-lying electronic structure of UO_2 is studied in detail in Chapter 4. In the presence of spin-orbit, the ${}^3\Phi_u$ (2_u) ground state for UO_2 stems from the $1\varphi_u^1 5\sigma_g^1$ ($5f\varphi^1 7s\sigma^1$) electron configuration with the equilibrium bond length of 1.777 Å using the cc-pVTZ basis set. The ${}^2\Phi_u$ ($5/2_u$) ground state of UO_2^+ arises from the $1\varphi^1$ ($5f\varphi^1$) configuration which has an R_e value of 1.741 Å.

As can be seen from Table 5.4, there is not much difference between the vertical and adiabatic values of the IPs. This is due to the small change in the bond length upon ionization because the ionization involves the removal of electrons predominantly with the diffuse non-bonding 7s character and there is no subsequent change in the electron configuration upon ionization. A large change in vertical and adiabatic ionization energy, however, is observed in the event the electron is ionized from the lowest state with f^2 ground state, which lies 1250 cm^{-1} above the ground state. The adiabatic and vertical ionization from the ${}^3H_{4g}$ ($1\delta_u^1\ 1\varphi_u^1$) ground state of UO_2 to the ${}^2\Phi_{5/2u}$ ($1\varphi_u^1$) final state of UO_2^+ is 5.474 and 6.196 eV respectively, as shown in Table 5.5.

Results from Table 5.4 show that non-spin orbit and spin-orbit CI calculation give almost the same values for the IPs. This is because the ionization involves removal of an electron from the orbital with σ symmetry. With the small size core potential, a better value for spin-orbit energy is obtained due to the increase in the quality of the inner part of the orbital due to the $1/r^3$dependence of the spin-orbit operator. This aspect of the use of the small size core, however, will not result in a change in IP for UO_2. As the effect of spin-orbit coupling is not significant on the IP, higher order correlation effects can be included in the calculation because there is a sizable decrease in the computational cost in the absence of spin orbit.

Next we studied the effect of the quality of basis set on the IP of UO_2. With the improvement in the quality of the basis set, one can further expect the increase in IP, as the system with two unpaired electrons will benefit more from correlation than the one-electron system upon ionization. As can be seen from the values in Table 5.4 and 5.5, the basis set does not have much effect on the IP. Similar behavior was observed in the CASPT2 calculation performed by Gagliardi *et al.* [122].

The next important issue that needs to be considered is the intershell correlation energy between the 5s, 5p, 5d, 6s or 6p, with the valence 7s electron. Polarization of the 5d, 6s and 6p orbitals upon ionization can be studied using the 68-electron core potential, but this does not allow us to correlate the 5s and 5p since these orbitals are frozen in their atomic environment. Thus, in order to incorporate these effects, we performed the IP calculations using the 60-electron core RECP as well. The 5s, 5p, 5d and 6s orbitals are not involved in bonding; they merely polarize in molecular environments. Therefore, only single excitations are needed out of the orbitals because they are enough to account for the orbital relaxation that characterizes the polarization effects and for intershell correlation effects. As can be seen from the IP values in Table 5.3, with the 68-electron RECP, no change in the IP was obtained when the electrons in the 5d, 6s and 6p shells were allowed to correlate.

Even though 5s, 5p and 5d have similar radial extent in non-relativistic calculations, the relativistic effects result in the further contraction of 5s and 5p orbitals and the expansion of the 5d orbital. As a result, the exchange interaction between the 7s and 5d will be more than in the 7s-5p and 7s-5s pairs. As no effect on the IP was observed when the excitations were allowed out of the 5d orbitals, it is logical to conclude that the correlation of 5s and 5p electrons will not have any effect either. In the event the ionization would have involved a change in the 5f occupation number either by reorganization or removal of electron from the 5f shell, however, one can expect polarization effects to make a significant impact on the IP values because of the similar radial extent of 5s, 5p, 5d, 6s and 6p orbitals.

An important argument has been made in the literature [126] in favor of small size 60-electron RECP for uranium. Since a 7s electron is being ionized, it is possible that the 7s orbital needs to look like an orbital rather than a pseudo-orbital in the 5f radial region. Partially restoring the correct radial nodal structure will also improve the value of exchange integrals involving these orbitals. As can seen from the values in Table 5.2 this also did not result in any change in the value of the IP.

At the same time, an important argument can be made against the use of small size correlation potential considering the type of calculation performed in this work, wherein the relativistic effects are incorporated implicitly using a core potential rather than explicitly included as in the case of the Dirac Hamiltonian or the Briet-Pauli Hamiltonian. The 60-electron core allows us to incorporate higher order correlation effects, but then at the same time it removes from the calculation the relativistic terms associated with the electrons in the 5s and the 5p shell.

Finally, the effect of electron correlation on the IPs was explored. First we performed a 2-reference CI singles and doubles calculation with the MOs obtained from the MCSCF calculations. For the UO_2 molecule the references used to represent the ground state were $1\varphi_u^1 5\sigma_g^1$ and $1\delta_u^1 5\sigma_g^1$. Similarly for UO_2^+, the reference space consisted of the $1\varphi_u^1$ and $1\delta_u^1$ configurations. Using this reference space the adiabatic and vertical ionization energies of 5.629 and 5.682 eV was obtained using the cc-pVTZ basis set in the presence of spin-orbit.

The most important differential electron correlation that can affect the IP is the 5f-7s intershell correlation. This effect depends critically on the radial distance between the shells. Due to the small spatial overlap of the 5f and 7s shells, however, the 5f-7s intershell correlation effects are very small. Even though the calculation was performed at the MRCISD level, single and double excitations with significant coefficients were included in our calculation as references in order to include the important triple and quadruple excitations. This reduces the amount of correlation error inherent in the calculation due to the truncation of CI excitations at the SD (singles and doubles) level. Moreover, beyond quadruple excitations, the contributions to the IP are usually quite small.

Analysis of the coefficients of the configurations mixing with the reference configuration showed that most of the contributions were due to the cross-shell correlation involving the bonding MO's $4\sigma_g$, $3\pi_g$, $2\pi_u$ and $3\sigma_g$ and the corresponding antibonding MOs. This shows that MOs used in the CI calculation were not optimum for the correlated description of π and σ bonding. Refinement of MOs can be done by including these MOs in the MCSCF calculation, which will improve the contribution of the reference configuration and the single and double excitations out of these references. The distribution of 10-12 electrons among the $4\sigma_g$, $3\pi_g$, $2\pi_u$ and $3\sigma_g$ bonding MOs and 0-2 electrons in the antibonding MOs resulted in the wave function consisting of ~28,000 CSFs. Since in the MCSCF calculation both the MOs in the CSFs and the coefficients of the CSFs are simultaneously optimized variationally, calculations of this size are quite intensive to perform. Analysis of the coefficients of the CI vectors describing the intershell correlation effects discussed in this paragraph shows a quite similar contribution to the total wave function of the ground state for both UO_2 and UO_2^+ systems. This might be due to the small difference of 0.036 Å in their equilibrium bond lengths. The triple and quadruple excitations from these configurations were not included in this calculation as this effect is liable to make a very small contribution to the change in correlation energy upon ionization.

The electrons occupying the highest occupied bonding $3\sigma_u$ have substantial 5f character and they are highly correlated with electrons in the non-bonding $1\delta_u$ and $1\varphi_u$ uranium-centered orbitals [89]. Their contribution to the correlation energy was studied with the reference space consisting of states arising from $3\sigma_u^2 5\sigma_g^1 1\varphi_u^1$, $3\sigma_u^2 5\sigma_g^1 1\delta_u^1$, $5\sigma_g^1 3\sigma_u^0 1\delta_u^2 1\varphi_u^1$ configurations for UO_2 and the states arising from $3\sigma_u^2 1\varphi_u^1$, $3\sigma_u^2 1\delta_u^1$, $3\sigma_u^0 1\delta_u^2 1\varphi_u^1$configurations for UO_2^+ for the non-spin-orbit CI calculation. The first IP of 5.599 eV was obtained with this reference space. Incorporating this correlation effect did not affect the value of the IP for UO_2 since the number of electrons in the non-bonding 5fφ or 5fδ remained unchanged upon ionization even though there will be a small change in the effective nuclear charge experienced by the electrons in these orbitals.

As the ground state of UO_2 arises from the $5f^17s^1$ configuration, the 7p and 6d orbitals were included in the reference space to account for the non-dynamical correlation arising from the 7s-7p and 7s-6d near-degeneracy excitations. The inclusion of near-degeneracy correlation effects resulted in an increase in the ionization energy by only 0.05 eV.

Finally the technique by which the core potential was generated was also explored. In addition to using the shape-consistent RECP by Christiansen *et al.* [17-23] the IP calculation was also performed using the Stuttgart energy-fitted RECP [124-125]. The cc-pVDZ basis set that goes with the Stuttgart 60-electron small size core potential was generated. Using the Stuttgart core potential the first ionization energy of 5.36 eV and equilibrium bond lengths of 3.32 Å and 3.25 Å were obtained for UO_2 and UO_2^+ respectively. Using the same reference frozen and virtual space and the Christiansen RECP, the calculated value of the adiabatic IP and equilibrium bond lengths for UO_2 and UO_2^+ were 5.60 eV, 3.36 Å and 3.29 Å respectively. This discrepancy between the results from the core potentials obtained using different techniques opens up a new area of research as the techniques are expected to provide similar results. For our purpose of understanding the discrepancy involving the IP of UO_2, however, no insight was obtained.

The second ionization energy for UO_2 involves the following process, UO_2^+ $(3\sigma_u^2 1\varphi_u^1) \rightarrow UO_2^{2+}$ $(3\sigma_u^2)$. Unlike for the first IP, the spin-orbit contribution to the second IP will be quite significant. The ground state of UO_2^{2+} is the ${}^1\Sigma^+_{0g}$ term arising from the closed shell $3\sigma_u^2$ configurations with computed equilibrium bond lengths of 1.685 Å and 1.675 Å using cc-pVDZ and cc-pVTZ quality basis sets, respectively. In the absence of spin-orbit, the R_e of the ${}^1\Sigma_g^+$ state is 1.687 and 1.678 Å using cc-pVDZ and cc-pVTZ basis sets. MOs for use in the CI calculation were generated using an SCF calculation on the closed-shell configuration.

The second IP for UO_2 has been reported as 15.4 ± 2.6eV [127]. Such a large error in the IP does not allow us to benchmark our result with the experimental observed value. In this work, we have obtained an adiabatic IP value of 14.277 using the cc-pVDZ basis set and 14.299 using the basis set of cc-pVTZ quality. Unlike the first IP, which differs from the results obtained from the CASPT2 approach [122] by 0.5 eV, the second IP results are in agreement. *Gagliardi et al.* [122] obtained the second ionization energy values of 14.02 and 14.36 eV with their small and large basis sets respectively.

5.4 Ionization Potential Study of UO

The electronic structures of UO and UO^+ are studied in detail in Chapter 2. The ground state of UO is ${}^5I_4$ arising from the U^{+2} $(7s\sigma^1 5f\varphi^1 5f\delta^1 5f\pi^1)O^{2-}$ configuration with a calculated equilibrium bond length of 1.8423 Å. The calculated bond length differs from the experimental bond length of 1.8383 Å [15] by just 0.004 Å. The ground state of UO^+ is ${}^4I_{9/2}$ arising primarily from the $U^{+2}(5f\varphi^1 5f\delta^1 5f\pi^1)O^{2-}$ configuration also predicted by ligand field calculation [97] and the valence configuration interaction study [105].

Similar to the results obtained for UO_2, the effect of spin-orbit, 5f-7s intershell correlation energy and the polarization of inner 6s, 6p, 5d shell on the first IP are very small. In the presence of spin-orbit with the cc-pVTZ quality basis, the calculated adiabatic and vertical IPs for UO are 5.550 and 5.587 eV. The experimental value found for the IP of UO using the electron transfer [117-118] and photoionization techniques [116] is 5.6±0.1 and 6.0313eV respectively. Previous theoretical calculations have obtained values of 6.17 eV from an RDF-SCF [129] calculation and 5.71 eV using the semi empirical QR–SCMEH–MO (quasirelativistic–self-consistent modified extended Hückel–molecular orbital) method [128].

For UO, the first excited state lies just 300 cm^{-1} above the ground state arising from the U^{+2} $(7s\sigma^1 5f\varphi^1 5f\delta^1)O^{2-}$ configuration. The calculated and experimental values of R_e for this state are 1.795 Å and 1.7932 Å, very close to the R_e values for the ground state of UO^+. As a result, from the first excited state of UO, the adiabatic and vertical ionization energies differ by a mere 0.01 eV.

5.5 First Ionization Potential Study of Uranium

The IP calculation for the uranium atom was performed using the 60-electron core potential with the basis set of cc-pVDZ quality. The experimentally obtained first ionization energy of uranium atom is 6.15±0.05 eV [118], 6.194 [116] and 6.193± 0.002 eV [118] using mass spectrometric, REMPI and optical measurements respectively. Since the first IP of uranium values are in good agreement among different experimental techniques, it serves as a good test case to check the accuracy of the theoretical approach to handle the calculation of the IP of actinide atoms and its oxides.

The first ionization energy involves the removal of a 6d electron from the $^5K_6$ state arising from the $f^3d^1s^2$ configuration. The ground state of U^+ is $^4I_{9/2}$, which stems from the f^3s^2 electron configuration.

The first IP calculation of uranium gives a different result with or without spin-orbit. The IP using SOCI is ~0.25 eV (2018cm^{-1}) higher in comparison to the non-spin-orbit CI. This difference is comparable to the spin-orbit splitting associated with U6d. For uranium the 6d spin-orbit coupling constant is ~2000 cm^{-1}. This shows that most of the contribution to the first IP with SO is as a result of the 6d SO splitting and hence an insignificant contribution can be expected from the configurations which are allowed to mix with the reference state only after inclusion of spin-orbit effects.

First, spin-orbit calculations were performed with the reference space for U and U$^+$ consisting of all states arising from the $f^3d^1s^2$ and f^3s^2 configurations. In addition, the active space consisted of references incorporating $7s^2 \leftrightarrow 7p^2$ and $7s^2 \leftrightarrow 6d^2$ excitations. Even though there is no change in 7s occupation number between U and U$^+$, there is a change in the relative energy difference between 7s, 7p and 6d with the increase in ionic charge. With this reference space a first IP value of 5.77 eV was obtained.

Next SOCI correlation consisted of including 6s and 6p in the reference space. Unlike the cases where the electron comes out of 7s shell, the correlation of 6s and 6p is expected to have significant influence on the first IP of uranium due to strong 6s-6d and 6p-6d intershell correlation effects as a result of their same radial extent. Even though only single excitations from different shells are required to characterize the intershell correlation effects upon ionization, we included both singles and doubles from the 6s and 6p orbitals due to the inflexibility of the current GUGA version of COLUMBUS. Double excitations out of 6s and 6p will make a significant contribution to the total correlation energy for U and U$^+$, but their contribution to differential correlation energy will be very little. After allowing the singles and doubles out of 6s and 6p the first IP went up to 5.96 eV.

The ~0.23 eV difference between the calculated and the experimental value may be due to basis set truncation or the omission of some important triple and quadruple excitations that contributes to the differential correlation energy. The intershell correlation energy associated between the 5d, 5s and 5p core and 5f, 6d and 7s valence orbitals are also liable to make a small contribution to the first IP. The size of the computation as a result of correlating the electrons in the 5s, 5p and 5d orbitals is too large to handle based on the currently available computing resources and the nature of the current version of the COLUMBUS programs.

5.6 Ionization Potential Study of Thorium

The IP calculation of thorium was performed using the 68-electron core potential with a basis set of cc-pVDZ quality. The experimentally obtained first ionization energy of the Th atom is 6.3067 eV [129] obtained using Resonance Ionization Mass Spectroscopy (RIMS). Currently there is no discrepancy associated with the first IP value of thorium in the literature. Hence this is another test case where the efficacy of the theoretical approach can be tested in calculating the IP of actinide systems. Unlike the first IP calculation of the uranium atom, the IP calculation of the thorium atom is facilitated by the fact that the ionization involves removing an electron from the 7s shell. making the effect of spin-orbit on the IP very small. Therefore, we were able to perform a higher-level non-spin-orbit CI calculation incorporating intershell correlation effects and non-dynamical near degeneracy effects.

The first IP involves the excitation of an electron from the $^3F_2$ state arising from the d^2s^2 configuration to the $^4F_{3/2}$ state arising from the d^2s^1 configuration. A first IP value of 6.18 eV was obtained with the 7s, 5f, 6d and 7p orbitals included in the active space and only the four valence electrons in case of Th and three valence electrons in case of Th^+ were allowed to correlate. With the inclusion of 6s and 6p in the reference space, where these orbitals were doubly occupied in the reference space, but single and double excitations were then allowed out of these orbitals, the IP went up to 6.21 eV. The small change on IP with the 6s and 6p as a part the reference space is due to the fact that the ionization involved removal of the 7s electron with no change in the occupation number of the 6d and 5f shells, although the electrons in the 5f and 6d shell did become more stable with the increase in the effective nuclear charge. The calculated IP of thorium is in very good agreement with the existing experimental value of 6.3 eV.

5.7 Ionization Potential Study of ThO

The first IP of ThO has been reported as 6.1 and 6.6 eV using the electron transfer [130] and pulsed field ionization-zero kinetic energy (PFI-ZEKE) photoelectron [111] techniques respectively. The $^1\Sigma^+_0$ ground state of ThO stems from the $6\sigma^2$ ($7s\sigma^2$) electron configuration and has calculated and experimental bond lengths of 1.861 Å and 1.840 Å [69] respectively. Similarly, the $^2\Sigma^+_0$ ground stats of ThO^+ arises from the $6\sigma^1$ ($7s\sigma^1$) electronic configuration and has calculated and experimental bond length of 1.825 Å and 1.807 Å [101] respectively.

An IP value of 5.345 eV was obtained starting with single determinant wave functions of $3\pi^4 5\sigma^2 6\sigma^2$ for ThO and $3\pi^4 5\sigma^2 6\sigma^1$ and the ThO^+ ion in the Hartree-Fock method. The listed 3π and 5σ MOs are mostly bonding MOs formed by mixing of $O2p_{\pi,\sigma}$ with $U6d_{\pi,\sigma}$ and $U5f_{\pi,\sigma}$. Due to the large Th-O bond length and relativistic destabilization of 5f, the 6d atomic orbitals mix more with O2p orbitals than do the U5f atomic orbitals. The 6σ MO has mostly non-bonding $7s\sigma$ character.

Improvement of the Hartree-Fock SCF orbitals mainly arising from the non-dynamical correlation related to the 7s-7p and 7s-6d degeneracy effect were incorporated using the MCSCF method. Using this approach, an IP value of 6.05 eV, closer to the experimental value, was obtained. For ThO, the correlation, governed by the exchange integral, provided by the 7s-7p excitation is higher than that provided by the 7s-6d excitation, hence the contribution to the differential correlation energy was more from the 7s → 7p excitation than from the 7s → 6d excitation. For ThO^+, in the absence of spin-orbit there is no mixing between the $7s_\sigma^1$ ground state and the $7p_{\pi,\sigma}^1$ based on symmetry arguments. The MCSCF ground state wavefunction has 92% from the principal term for ThO and 100% for ThO^+.

Using the natural orbitals obtained from the MCSCF calculation, dynamical correlation effects were included in the calculation using the MRCISD method. The active space consisted of distributing two electrons among the 7s, 7p, 6d and 5f shells for ThO and one electron among the 7s, 7p, 6d and 5f shells for ThO^+. With the active space consisting of the 7s, 7p, 6d and 5f shells, adiabatic and vertical IP values of 6.42 eV and 6.45 eV were obtained.

5.8 Ionization Potential Study of ThO_2

The first IP for ThO_2 is 8.7±0.2 eV [130], larger than the values obtained for all the systems studied above and for the other AnO and AnO_2 molecules listed in Table 5.1. This is due to the fact that in case of the above molecules the electrons come out of non-bonding MOs mostly centered on the metal atom but in ThO_2 the ionization involves removal of a bonding electron. Thus an increase in bond length and decrease in vibrational frequency is expected upon ionization.

ThO_2 is isoelectronic with UO_2^{2+}, but unlike UO_2^{2+} which is linear, ThO_2 is bent, with an experimental O-Th-O angle of 122±2° [131]. In this work the vertical IP for ThO_2 is calculated using three geometries obtained from Gaussian using the B3LYP functional (Th-O = 1.906 Å, O-Th-O = 118.75°), ADF (Th-O = 1.9105 Å, O-Th-O = 117.863°) and Hartree-Fock (Th-O = 1.91 Å, O-Th-O = 118°) [132], the results are listed in Tables 5.13-5.14.

The ground-state ($^1A_1$) configuration for ThO_2 is $6a_1^2 4b_2^2 2a_2^2\ 3b_1^2 7a_1^2 5b_2^2$. The orbitals listed are bonding MOs with mostly O2p character and some mixing with Th6d, Th5f and Th6p. The atomic characters of these MOs are shown in Table 5.9. As can be seen from the orbital-energy values listed in these tables, there are several high-lying MOs very close in energy. The ground state for ThO_2^+ was obtained by removing, in turn, electrons from each of the bonding MOs. The lowest ionization energy was obtained with excitation out of $5b_2$ orbital, which is mostly localized on the oxygen atom. The ground state for ThO_2^+ is $^2B_2$ with electron configuration of $6a_1^2 4b_2^2 2a_2^2\ 3b_1^2 7a_1^2 5b_2^1$.

An important observation can be made in case of for ThO_2^+ system, even though Th has four valence electrons, the oxidation state of the Th atom is +5. As can be seen from the population analysis listed in Tables 5.9-5.12, the fifth electron comes out the $5b_2$ bonding MO where half the electron comes off of the oxygens. Thus, almost 70% of the atomic character of the $5b_2$ MO was oxygen O2p for ThO_2. The ionization of the electron from this MO results in a charge transfer from the metal to the oxygens as can be seen by comparing the contributions of O2p to the six bonding MO's in ThO_2 and ThO_2^+.

A vertical IP value of 8.40 eV was obtained from the Hartree-Fock calculation using the SCF wave functions for $6a_1^2 4b_2^2 2a_2^2$ $3b_1^2 7a_1^2 5b_2^2$ for ThO_2 and $6a_1^2 4b_2^2 2a_2^2$ $3b_1^2 7a_1^2 5b_2^1$ for ThO_2^+. The single-reference CISD calculation resulted in a vertical IP of 8.48 eV.

5.9 Conclusions

The calculated values of the first IPs of the thorium and uranium atoms and are in good agreement using experimental techniques like mass spectrometry, photoionization, and optical measurements. Our calculated results of 6.21 and 5.96 eV for the first IP of thorium and uranium match very well with the experimental result of 6.3 and 6.19 eV respectively. The calculation of IPs for actinide atoms needs a higher degree of correlation then their mono- and dioxides counterparts, due to the actinides atoms having valence electrons distributed among three valence orbitals (5f, 6d and 7s) with different principal quantum numbers. Since our MRCISD calculations predict the first IPs of U and Th to a good accuracy, the same method is likely to work favorably in IP calculations for the corresponding di and mono oxides.

The first calculated IP value of 6.42 eV for ThO is close to the experimentally obtained value of 6.6 eV obtained using the pulsed field ionization-zero kinetic energy (PFI-ZEKE) photoelectron technique. The large discrepancy in the calculated IPs is in the theoretical and calculated results for UO and UO_2. Although our calculated IPs matches well with the electron transfer technique, they are 0.5 eV lower than the ones obtained using with the most recent REMPI technique. Many issues associated with the accurate computation of these IPs have been examined but so far no success has been obtained in resolving the discrepancy.

Future work involves modification of the COLUMBUS code to allow only singles out of selected MOs in the reference space. This will not only decrease the size of the calculation but also more selectivity can be obtained by particularly including the configurations that make significant contributions to the differential correlation energy.

Systems	Electron Transfer	Photoionization
ThO2	8.7 ± 0.15	-
UO2	5.5± 0.1	6.128
NpO2	5.0± 0.1	-
PuO2	9.4± 0.5	-
	10.0± 0.1	
	7.3± 0.12	
AmO2		-
ThO	6.1 ± 0.1	6.6
UO	5.6± 0.1	6.031
NpO	5.7± 0.1	-
PuO	5.8± 0.2	-
	6.6± 0.2	
AmO	5.8± 0.2	-

Table 5.1: Ionization Energy of AnO and AnO_2 systems using different experimental techniques (Refs. 117-120, 131-132)

Spin-orbit included or not	Basis Set Quality	RECP Core size	Number of Correlated electrons	Ionization Energy (eV)
No	cc-pVTZ	68	14	5.628
Yes	cc-pVTZ	68	14	5.629
No	cc-pVDZ	68	14	5.652
Yes	cc-pVDZ	68	14	5.649
No	cc-pVDZ	68	36	5.599
No	cc-pVDZ	60	44	5.601

Table 5.2: Adiabatic Ionization energy (eV) for UO_2 (gas phase)

	Adiabatic Ionization Energy (eV)	Vertical Ionization Energy (eV)
6s, 6p and 5d electrons in the frozen space	5.652	5.735
6s, 6p electrons in the frozen space	5.651	5.748
5d electrons in the frozen space	5.593	5.684
No electrons in the frozen space	5.599	5.683

Table 5.3: Ionization energies (eV) for UO_2 (gas phase) with different levels of electron correlation

	Initial State		Final State		IE
	State	R_e	State	R_e	(eV)
Adiabatic IE	$^{3}\Phi_{2u}$	1.777	$^{2}\Phi_{5/2u}$	1.741	5.629
Vertical IE	$^{3}\Phi_{2u}$	1.777	$^{2}\Phi_{5/2u}$	---	5.682
Adiabatic IE	$^{3}\Phi_{u}$	1.784	$^{2}\Phi_{u}$	1.748	5.628
Vertical IE	$^{3}\Phi_{u}$	1.784	$^{2}\Phi_{u}$	---	5.695

Table 5.4: CISD (spin-orbit) and CISD (non-spin-orbit) equilibrium bond length and ionization energy results for the UO_2 molecule using the cc-pVTZ Basis Set

	Initial State		Final State		IE
	State	R_e	State	R_e	(eV)
Adiabatic IE	$^{3}\Phi_{2u}$	1.803	$^{2}\Phi_{5/2u}$	1.762	5.649
Vertical IE	$^{3}\Phi_{2u}$	1.803	$^{2}\Phi_{5/2u}$	---	5.733
Adiabatic IE	$^{3}\Phi_{u}$	1.809	$^{2}\Phi_{u}$	1.768	5.652
Vertical IE	$^{3}\Phi_{u}$	1.809	$^{2}\Phi_{u}$	---	5.735

Table 5.5: CISD (spin-orbit) and CISD (non-spin-orbit) equilibrium bond length and ionization energy results for the UO_2 molecule using the cc-pVDZ Basis Set

	Initial State		Final State		IE
	State	R_e	State	R_e	(eV)
Adiabatic IE	$^{3}H_{4g}$	1.852	$^{2}\Phi_{5/2u}$	1.741	5.474
Vertical IE	$^{3}H_{4g}$	1.852	$^{2}\Phi_{5/2u}$	---	6.196

Table 5.6: CISD (spin-orbit) result for the Ionization Energy (eV) of the UO_2 molecule from the f^2 electron configuration using the cc-pVTZ Basis Set

	Initial State		Final State		IE
	State	R_e	State	R_e	(eV)
Adiabatic IE	$^5I_4$	1.8423	$^4I_{9/2}$	1.8110	5.550
Vertical IE	$^5I_4$	1.8423	$^4I_{9/2}$	---	5.587
Adiabatic IE	^5I	1.8545	^4I	1.8143	5.552
Vertical IE	^5I	1.8545	^4I	---	5.590

Table 5.7: Ionization Energy (eV) for the UO molecule using the cc-pVTZ Basis Set

	Initial State		Final State		IE
	State	R_e	State	R_e	(eV)
Adiabatic IE	$^5I_4$	1.8729	$^4I_{9/2}$	1.835	5.507
Vertical IE	$^5I_4$	1.8729	$^4I_{9/2}$	---	5.534

Table 5.8: Ionization Energy (eV) for the UO molecule using the cc-pVDZ Basis Set

	Orbital	Thorium AO's				Oxygen AO's		
	Energy	s (6s,7s)	p (6p, 7p)	d (5d,6d)	f (5f)	s (2s)	p (2p)	d (3d)
$6a_1$	-0.4733	0.60	2.57	15.55	1.81	1.58	77.26	0.14
$4b_2$	-0.4618	-	4.25	14.13	6.11	1.01	74.20	0.14
$2a_2$	-0.4602	-	-	18.98	5.00	-	75.23	0.14
$3b_1$	-0.4210	-	3.90	9.78	7.88	-	77.34	0.09
$7a_1$	-0.4030	0.85	4.13	13.12	5.91	0.06	75.00	0.05
$5b_2$	-0.3795	-	8.17	8.82	12.83	0.39	68.99	0.03

Table 5.9: Partial Gross Population Analysis for selected MOs of the $^1A_1$ state of ThO_2 using the Gaussian geometry (Th-O = 1.906 Å, O-Th-O = 118.75°)

	Thorium AO's				Oxygen AO's		
	s (6s,7s)	p (6p, 7p)	d (5d,6d)	f (5f)	s (2s)	p (2p)	d (3d)
$6a_1$	0.37	3.42	13.77	2.79	0.00	78.27	0.07
$4b_2$	-	3.53	13.86	5.53	1.19	75.58	0.15
$2a_2$	-	-	14.71	4.65		79.72	0.16
$3b_1$	-	3.90	9.78	7.88	-	77.34	0.09
$7a_1$	0.90	3.26	14.88	5.24	2.56	72.86	0.16
$5b_2$	-	5.67	6.82	10.86	0.48	75.21	0.04

Table 5.10: Partial Gross Population Analysis for selected MOs of the $^2B_2$ state of ThO_2^+ using the Gaussian geometry (Th-O = 1.906 Å, O-Th-O = 118.75°)

	Gross Atomic Populations				
Atom	s	p	d	f	Total
Th	2.066	6.139	11.812	0.863	20.976
O	3.670	9.336	0.0177	0.000	13.024

Table 5.11: Mulliken Population Analysis for the SCF wave function of the $^1A_1$ state of ThO_2 using the Gaussian geometry (Th-O = 1.906 Å, O-Th-O = 118.75°)

	Gross Atomic Populations				
Atom	s	p	d	f	Total
Th	2.054	6.051	11.525	0.678	20.406
O	3.743	8.831	0.0197	0.000	12.594

Table 5.12: Mulliken Population Analysis for the SCF wave function of the $^2B_2$ state of ThO_2^+ using the Gaussian geometry (Th-O = 1.906 Å, O-Th-O = 118.75°)

	Initial State		Final State		IE
	State	Total Energy (Hartree)	State	Total Energy (Hartree)	(eV)
Gaussian	$^1A_1$	-206.04872	$^2B_2$	-205.73994	8.402
B3LYP	$^1A_1$	-206.04849	$^2B_2$	-205.73963	8.404
Hartree-Fock	$^1A_1$	-206.04853	$^2B_2$	-205.73969	8.404

Table 5.13: Vertical Ionization Energy (eV) for ThO_2 based on Hartree-Fock calculations

	Initial State		Final State		IE
	State	Total Energy (Hartree)	State	Total Energy (Hartree)	(eV)
Gaussian	$^1A_1$	-206.79394	$^2B_2$	-206.48235	8.479
B3LYP	$^1A_1$	-206.79382	$^2B_2$	-206.48194	8.487
Hartree-Fock	$^1A_1$	-206.79384	$^2B_2$	-206.48200	8.486

Table 5.14: Vertical Ionization Energy (eV) for ThO_2 based on single-reference CISD calculations without spin-orbit

CHAPTER 6

THEORETICAL CALCULATIONS FOR THE HIGH-LYING EXCITED LEVELS AT THE OXYGEN K-EDGE FOR $Cs_2UO_2Cl_4$

6.1 Introduction

X-ray photoelectron spectroscopy has been performed on a wide range of uranium compounds [133-139] in order to gain insight into the electronic structure and the spatial extent of the adjoining atoms. Both experimental study and theoretical calculations have been performed to study the spectral features near the threshold region [133,134,140] and also in the region of a few electron volts extending above the edge [133, 134, 136, 139].

In this chapter we present a theoretical calculation of the X-ray absorption spectrum at the oxygen K-edge for $Cs_2UO_2Cl_4$, which extends over 20 eV from 530 eV to 550 eV going beyond the ionization potential of oxygen 1s. In this spectrum, the oxygen 1s core electron is excited into valence and Rydberg orbitals by the absorption of soft x-rays with their polarization vector aligned parallel and perpendicular to the uranyl O-U-O bond axis. This spectrum was taken by Denning *et al.* [141] and a portion of it is shown in Figure 6.1. The S polarization includes transitions where the polarization vector is both parallel and perpendicular to the bond axis and the absorption in the R orientation is dominated by the transitions polarized perpendicular to the uranyl bond axis. According to the dipole selection rule for linear UO_2^{2+} ion the parallel and perpendicular transitions will be σ → σ and σ → π respectively. Both the gerade and ungerade final states will be allowed from the O1s ($1\sigma_g$ and $1\sigma_u$) initial states. The bonding and antibonding O1s molecular orbitals are separated by ~0.35 meV.

The paper by Denning *et al.* [141] also provides the x-ray emission spectra in the R and S configuration for four different excitation energies, which are 531.4, 534.1, 536.5, and 550.2 eV. The selection rules to assign the x-ray emission spectra used are as follows: during the emission from valence orbitals with σ character, the intensity will be a maximum when the polarization vector is aligned parallel to the molecular axis and during emission from the valence orbitals with π character, the maximum intensity will be obtained when the polarization vector is aligned perpendicular to the molecular axis. The emission spectrum data was further used to estimate the ionization potential of oxygen 1s around 536eV [141]. As is well known, the K-absorption edge can be approximated as the sum of the ionization energy of the valence state and the K-emission line of this valence state. But this procedure is expected to give some error, since due to the creation of a core hole, the valence MOs will experience the attractive potential of a larger effective nuclear charge and also the reduced U-O overlap will decrease the energy of the unoccupied valence orbtials as they are derived from the overlap of the unoccupied uranium 5f and 6d orbital and the occupied oxygen 2s and 2p orbitals (discussed in detail later in the chapter).

Once we have located the information regarding the O K-edge, the photoabsorption spectrum of $Cs_2UO_2Cl_4$ shown in Figure 6.1 can be characterized by five lines of absorption below and three lines of absorption above the ionization threshold.

The salient features of our analysis are the intense lines of absorption above the ionization limit for the oxygen K-edge at 541 eV and 550 eV respectively. Above the ionization threshold, one expects the core hole state to ionize directly rather than by Auger relaxation. The implication is that above the ionization threshold, the excitation occurs to pseudo-bound states in which an electron is temporarily trapped by a potential barrier, through which it will eventually tunnel and escape. Based on the fact that sharp autoionizing resonances can be attributed to the occupation of an orbital with a high angular momentum [142-143], in this chapter we have assigned shape resonances to the unoccupied MOs with a large angular momentum and embedded in the continuum. In addition one cannot refute that multiexcitation processes can overlap with the one-electron shape-resonance structure and strongly modify the shape of the absorption bands in the energy range above the threshold region [144-145].

The subsequent sections of this chapter are organized as follows. Section 6.2 details the theoretical approach and computational methods employed in performing the *ab initio* electronic structure calculations. Section 6.3 presents the expected results of the calculations performed along with a comparison of our calculations with the experimental data. Finally, section 6.4 provides some conclusions that may be drawn from the proposed research.

6.2 Calculation Details

In the case of uranium, the inner 68 electrons (1s-5p) were replaced by an RECP. The chlorine core consisted of 10 electrons 1s-2p and for cesium an all-electron core potential was used. No core potentials were used in case of oxygen since we are interested in analyzing the K-absorption spectrum of oxygen in $Cs_2UO_2Cl_4$. For the UO_2^{2+} ion there are 68 core electrons and 38 valence electrons and for $Cs_2UO_2Cl_4$ there are 133 core electrons and 70 valence electrons.

The basis sets used were contracted Gaussian basis sets following the correlation-consistent method of Dunning and coworkers [32-39]. In the case of uranium, the 5d, 6s, 6p core orbitals, as well as the 5f, 6d, 7s 7p, 7d, 8s and 8p valence and Rydberg orbitals, were treated explicitly using contracted Gaussian basis sets. The basis for including all these valence and Rydberg orbitals in the calculations was the following: The salient feature of this proposal is the investigation is Denning's suggestion that the peak at 550 eV might correspond to excitations to U5g orbitals. When we included the 5g states we found states lower than 5g states that were not described by the basis sets of U5f, U6d, U7s and U7p. In order to describe these states we added basis functions for U8p, U8s, and U7d Rydberg states. The orbital energies in the presence of relativistic effects for the 5f, 6d, 7s 7p, 7d, 8s and 8p states is shown in Figure 6.1.

For uranium, the basis sets were generated for the U^{+2} ion and the RECP used in the calculations were also derived for the U^{+2} ion. The (9s4p1d)/[2s2p1d] correlation-consistent double-zeta (cc-pVDZ) basis set was used for oxygen to represent the 1s, 2s and 2p electrons. The s and p primitives were obtained by optimizing the s and p exponents in the Hartree-Fock calculation on the ^3P ground state. The d polarization function was obtained by optimizing the exponents in SO-CISD calculations on the $^3P_2$ ground state. Since the effective charge of the oxygen atoms in UO_2^{2+} is -0.08e we did not use the augmented basis set for oxygen. Calculations indicated that oxygen diffuse functions play little role in the bonding description [146] Similarly for chlorine the chlorine (4s4p1d) primitive basis sets were contracted to [2s2p1d] to represent 3s and 3p orbitals. The s and p primitives were obtained by optimizing the s and p exponents in the Hartree-Fock calculation on the ^2P ground state. The d polarization set was obtained by optimizing the exponents in SO-CISD calculations on the $^2P_{3/2}$ ground state. The above-mentioned choice of basis set resulted in a total of 120 and 172 symmetry orbitals for free UO_2^{2+} and for the crystal respectively.

The SCF calculations were carried out mainly to obtain the initial-guess MOs that were used in the subsequent CI calculations. The initial-guess MOs used for the excited-state calculations were SCF orbitals derived from the complex with a hole on the oxygen center thereby allowing the valence and the Rydberg states to adjust to the presence of the hole on the oxygen 1s centers. The lifetime of the x-ray excited state is $\sim 10^{-15}$ sec [147] and the electronic motion of the electron for a unit order of magnitude (1eV) is $\sim 10^{-17}$ sec. Since the time scale of the electronic motion is comparable to that of the lifetime of x-ray excited states it further strengthens the use of hole-state MO's for the CI calculations to allow for the rearrangement of other electrons following the creation of vacancy in the oxygen 1s shells.

A single-excitation CI (CIS) calculation was used to obtain the excited-state energies with a convergence criterion of 10^{-8} Hartree. Given the size of the system (172 basis functions and 70 non-core electrons), it is only possible to calculate the lowest energy roots at the CISD level. Since the relative magnitude of the excitation energies is of greater significance in describing the spectrum, one can expect a better analysis of the spectrum if all the roots are calculated at the same order of approximation. In addition the relaxation and correlation effects have very little effect on the relative spacing between the states and only significantly change their absolute positions [148]. There are two vital arguments which further validates our result even at the CIS level: firstly for spectra acquired in the region of oxygen K-edge excitations for uranyl complexes, the role of the correlation effect will be comparatively small since its magnitude will be very small in comparison to the range of the excitation energy (530-550 eV) and the secondly we'll be performing the calculation under both the symmetry broken and adapted calculations (discussed in detail in the later paragraphs). It has been shown in the literature [148] that symmetry-broken solutions are more accurate at a lower level of approximation since for these cases the correlation effects are smaller in magnitude in comparison to the relaxation effects.

Our spin-orbit CI calculations for the free uranyl ion were carried out using 19 orbitals containing 38 electrons. Of these 19 orbitals, only 6 orbitals involving U5d and U6s orbitals were used as frozen orbitals, which were doubly occupied in all the CSFs. Then 12 orbitals involving U6p orbitals and bonding MOs derived from the mixing between the O2p orbitals with some U5f and U6d components were used as the inactive orbitals, which were doubly occupied in all the reference CSFs, but were correlated in the CI expansion. The active orbitals (orbitals with variable occupancy) consist of oxygen 1s orbitals in the reference CSFs and the selected set of virtual orbitals. The reason for choosing the following reference space (active and inactive orbitals) is as follows: 1. The U6p orbitals are included in the reference space, as there is a considerable hybridization between the 5fσ and 6pσ orbitals. 2. The presence of a O1s hole will lower the orbital energy and reduce the radial extent of the O2p orbital, changing the extent of mixing between the O2p orbitals and the U5f and U6d orbitals that constitutes the σ_u, π_u, σ_g and

π_g bonding MOs. Since the makeup of these orbitals changes significantly on core-electron excitation one will expect the correlation energy involving these orbitals to change significantly.

Similarly the spin-orbit CI calculations for the $Cs_2UO_2Cl_4$ crystal were carried out using 35 orbitals containing 70 electrons. For the excited state calculation, an additional constraint was imposed, where only the CSFs containing an excitation out of a oxygen 1s orbital were generated. The excitation-energy values reported in this chapter are the vertical excitation energy. Since the lifetime of the x-ray excited state (~ 10^{-15} sec) [147] is shorter than the vibronic motions, it can be assumed that the molecular structure is frozen during the process. Just for the sake of the argument, following the hole formation the nuclear relaxation energy for uranyl ion was 0.02 Hartree accompanied by an increase in the U-O bond length.

In addition to gaining an insight into the wave-function character of the excited state, we were also interested in studying the nature of the hole in the final state since at the level of theory (limited CI) for which we are constrained to perform the calculations, these descriptions are liable to give different results. To this end, we performed calculations under two conditions: (1) the hole being localized on one oxygen atom and, (2) the hole being delocalized over both oxygens. In the delocalized state SCF calculation the core hole was assigned to symmetry adapted molecular orbital formed by the linear combination of two oxygen 1s orbtials. The basic idea of localized holes means that the two oxygen atoms in UO_2^{2+} cannot be related by a symmetry operator in the symmetry group used or else you are liable just to get the "delocalized hole" result again. In the localized state SCF calculation one should be aware of the fact, that the calculation might collapse to the SCF state where the hole is delocalized state, since the SCF procedures can converge to a to a local minimum. On going from a delocalized to a localized solution the symmetry restrictions on the system were lowered to allow for the localization of a hole on one oxygen. For UO_2^{2+} the point group symmetry was lowered from D_{2h} to C_{2v} and similarly for the crystal the symmetry was lowered from C_{2h} to C_s.

Although the uranyl ion has $D_{\infty h}$ point-group symmetry, all the calculations were carried out using D_{2h} symmetry and its subgroups due to the complications in CI code of using the higher symmetry. But the flexibility of using the fractional population in the SCF calculations allows us to use the solutions derived from higher symmetry.

Since the experiment was performed on a single crystal of $Cs_2UO_2Cl_4$, we performed the calculation with the crystal model previously developed by our group [149-151]. The model that has been used is a cluster model with a central actinyl ion and the four neighboring chloride ions. The following layer consisting of six cesium atoms, on which no valence basis functions were used; they were instead described by an all-electron core potential. Then this cluster was embedded in a set of 1180 ions, which were approximated as point charges. The potentials of these point charges were added to reproduce the Madelung potential in the region of the central atoms. This scheme accounts for both the short and long-range interactions. In the subsequent section this large cluster model is used to assign the absorption bands of the spectrum of the uranyl ion in the crystalline state.

Since in our calculations the states are being studied well above the ionization potential, they are actually resonances and methods must be used so that do not collapse to lower energy continuum states. Of all the single excitations that were generated from the desired reference configurations, there were no CSFs where the O1s orbitals were fully occupied.

6.3 Results and Discussion

The electronic spectrum of UO_2^{2+} has been studied extensively both at the theoretical and experimental level. The theoretical calculations performed on uranyl ions and the ions in the condensed phase are mostly concentrated on studying the spectra in the optical region. This work is an effort to theoretically analyze the experiment data of oxygen K-spectrum in $Cs_2UO_2Cl_4$.

UO_2^{2+} is a linear molecule with a closed-shell ground state configuration of $\sigma_u^2(\delta_u, \varphi_u)^0$. The U^{6+} ions split the 2p states of the nearest neighbor O^{2-} ions into σ and π orbitals in the following order: $\pi_u < \pi_g < \sigma_g < \sigma_u$. In turn, due to the presence of the O^{2-} ligand field the 5f orbital will split with energies in the order $f\delta \sim f\varphi << f\pi < f\sigma$ and, similarly, the 6d orbital will split with energies in the order $d\delta < d\pi << d\sigma$. The splitting of 6d is more than that of 5f because the former is more radially expanded than the latter and overlaps better with the oxygen orbtials. These states then form linear combinations appropriate for the desired symmetry of the UO_2^{2+} site. The highest occupied electrons in the valence shell are the bonding electrons occupying the σ_u, π_u, σ_g and π_g molecular orbitals of the form $C_1(O2p) + C_2(U5f \text{ or } U6d)$ where $C_1 > C_2$. The lowest unoccupied orbtials are uranium-centered $5f\delta$ and $5f\varphi$ nonbonding orbitals, followed by orbitals derived from U5f and U6d orbitals with a small antibonding O2p contribution. In the uranyl ion, the 7s, 7p, 7d, 8s, 8p and 5g orbitals are too diffuse to participate in the U-O molecular bonding.

In the presence of a core hole in the O1s shell, one can expect a significant variation in the result. Due to the presence of the hole on the oxygen center, the effective nuclear charge experienced by the O2p will increase significantly which will lower the orbital energy and the radial expectation value of the O2p orbital. This will result in a decrease in the overlap between the empty uranium centered orbitals and the O2p orbitals. The decreased orbital overlap results in a reduction in the charge transfer from oxygen to uranium in the UO bonds. In the presence and absence of an oxygen 1s hole, uranium has a partial charge of +2.88 and +2.16 respectively. The Mulliken population analysis, displaying the populations of all the occupied levels is presented in Table 6.1.

6.3.1 Ionization Potential

Table 6.2 shows the ionization potential of the oxygen 1s orbital based on the self-consistent-field (SCF) approximation. From Table 6.2, it is clear that the ionization potential of O1s orbital is not only sensitive to the nature of the hole in the final state but also to a large extent on the chemical environment of the uranyl ion.

From the data in Table 6.2, it is evident that the ionization energy was lowered by 11-12eV when the symmetry restrictions were released in the 1s hole state. Under the frozen-core approximation, the result is 20eV higher than when the symmetry-broken wave functions are used, since this approximation ignores the orbital relaxation accompanying the ionization step. The theoretical study of the core-hole states of O_2^+ performed by Bagus and Schaefer, [152] obtained a similar result. According to their result for O_2, the localized Hartree-Fock wave function resulted in an ionization energy

12eV below the delocalized solution. This paper provides the seminal work addressing the topic of localized and delocalized core-hole picture. The self-consistent-field values for the ionization potential in the case of a symmetry-broken solution should give results in better agreement with experiments, as discussed in a paper by Cederbaum *et al.* [148] and mentioned in the subsequent section that correlation effects are much smaller than the relaxation effect when symmetry-broken wave functions are used. The CI calculations are predicted to give higher values for the ionization potential, as the correlation effects are higher in the ground state in comparison to the hole state.

6.3.2 Hole State Calculation

The problem of symmetry breaking involving both core hole states [7, 148, 152-154] and valence-hole states [11] has been a subject of investigation for many years. For localized solutions, from limited CI calculations, there are two equivalent non-orthogonal solutions with similar energy. This method has been widely favored in the past for problems that involve excitations from core electrons, since in this method the relaxation effects play a more significant role than correlation effects. Thus by performing the localized-core calculation, one can get an energetically favored result at a lower order of approximation. In the case of symmetry-adapted solutions, however, both relaxation and correlation effects are important. Hence one has to involve contributions from multiple excitations to obtain results in agreement with experiments [147].

As discussed in the previous section, at the level of the theory with which we are performing the calculation, the localized and delocalized hole descriptions are expected to give different results. To date, it is been shown on many different molecules that one can expect a lowering of the energy in the case of symmetry-broken solutions [7, 11,148, 152-154] due to the increased localization offered by the reduction in the symmetry constraint. According to the quantitative framework provided by Snyder [153] the relaxation energy is in an inverse relationship with the number of equivalent sites a hole can occupy. Therefore, in the case of core excitation from the oxygen 1s in uranyl complexes, we expect that the screening energy for the symmetry-adapted case will be approximately half the value obtained in the localized case.

In the event that a full CI calculation is performed, there would be a 50%-50% probability for the hole to localize on oxygen A or B. Hence, with the increase in the level of approximation, one can expect a convergence in the results obtained from localized and delocalized calculations.

6.3.3 Free-Ion Results

The results for the free uranyl ion were obtained at the geometry with the following parameters: R(U-O) = 3.155 Bohr v(U-O) = 1059 cm^{-1}[24]. The UO_2^{+2} ion has ground-state symmetry of $D_{\infty h}$ ($^1\Sigma_g^+$), D2h (^1A_g), $C_{\infty v}$($^1\Sigma^+$), and C_{2v}($^1A_1$) under various point-group symmetries.

The calculated vertical excitation energies are shown in Tables 6.3 and 6.4. Table 6.4 contains the list of the states with ungerade symmetry. The states with gerade symmetry are close to those of the ungerade symmetry since the separation between the $1\sigma_g$ and $1\sigma_u$ initial states is of the order of 0.35 meV. Although for the linear UO_2^{2+} ion the calculation was carried out using D_{2h} and C_{2v} point-group symmetries, the $D_{\infty h}$ and $C_{\infty v}$ notation has been used to describe the wave function in case of the delocalized and localized calculations respectively. As mentioned in the previous section however, the flexibility of using the fractional population in the SCF calculations has allowed us to obtain a wave function of higher symmetry.

In Table 6.5, we compare our localized free-ion results with previous calculations, obtained by Denning *et al*. [141] using the Amsterdam Density Functional program suite [155] ADF2000.2 [156]. Despite the difference in the theoretical approaches used, the comparison shows that not only is the relative ordering of the energy levels qualitatively similar, but also that the relative magnitude of the excitation energies is quantitatively equivalent with a maximum variation of 0.14%.

In the case of the uranyl ion, the ligand-field splitting experienced by the Rydberg orbitals is small due to their diffuse nature since they interact only weakly with the oxygen atoms. For example, in the case of p orbitals based on simple ligand-field considerations, the energy ordering of $p\pi < p\sigma$ the will be expected. For 7p, the $7p\pi$ state is 2.19 eV lower than the $7p\sigma$ state, but in case of 8p orbital, the $8p\pi$ state is lower than the $8p\sigma$ by only 0.42 eV.

Comparisons of the experimental results with our calculated results in Table 6.5 show that all the antibonding orbitals ($5f\pi^*$, $5f\sigma^*$ and $6d\pi^*$) are overestimated and the 7s orbital is underestimated by the theoretical calculations. Hence the free uranyl ion calculation does not agree with the experimental result.

6.3.4 Crystal Calculation

The crystal model used to perform the calculation is discussed in the previous section. In this model, we used U-O and U-Cl distance of 3.251 bohr and 5.0469 bohr respectively to represent the central $UO_2Cl_4^{2-}$ entity.

The U-O bond lengths in free UO_2^{2+} and UO_2^{2+} embedded in the crystal are 1.67 Å and 1.73 Å respectively. This increased U-O bond distance in the presence of the chloride ions further results in a decreased partial delocalization of charge from O→U. This decrease is evident from the fact that the effective charge on each oxygen center in the case of UO_2^{2+} is -0.08, and in case of $Cs_2UO_2Cl_4$ it is -0.405. This increase in the negative charge on the oxygen, is accompanied by the decrease of positive charge on the central uranium ion ($q_U = +2.16$ for UO_2^{2+} and $q_U = +1.49$ for $Cs_2UO_2Cl_4$), as we move from UO_2^{2+} to $Cs_2UO_2Cl_4$. This reduced positive charge on the uranium is due to the polarization of chloride orbitals to the uranium ion.

The uranium-oxygen overlap in excited states will be reduced not only due to the presence of an electronegative group but also due to the increase in effective nuclear charge seen by the O2p orbitals, preceding the formation of the hole. Due to the reduced U-O overlap, the energy of the lowest occupied bonding orbitals will increase and that of the corresponding antibonding orbitals will decrease. This further explains why the energies of antibonding orbitals ($5f\pi^*$, $5f\sigma^*$ and $6d\pi^*$) are overestimated for the free uranyl ion.

The most accurate description [77] of the energy terms in uranyl complexes seems to expressed by the order $V_{ax} > e^2/r_{ij} > H_{so} > V_{eq}$, where V_{ax} describes the axial field of the oxygen atoms of the uranyl entity, H_{so} stands for the spin-orbit interaction and V_{eq} describes the equatorial field of other atoms such as chloride ions in the complex of $UO_2Cl_4^{2-}$. Pitzer and Matsika have provided results on the magnitude of the splitting [25], where the calculations where performed at the CISD level. The CIS calculation performed in this chapter however, will also account for crystal field effects with reasonable accuracy. This is because the crystal field is a one-electron operator and we know that molecular properties that involves only one-electron operators are well described by CI singles. In the presence of the chlorides in the equatorial plane, 5fδ and 5fφ are still low-lying orbitals. Under C_{2h} symmetry the 5fφ ($11b_u$ and $12b_u$), 5fδ ($7a_u$ and $8a_u$), 5fπ ($13b_u$ and $15b_u$), 5fσ ($9a_u$) orbitals can interact with the chloride 3p orbitals based on symmetry arguments. However, this interaction with the equatorial chloride orbitals is quite minimal. According to the Mulliken overlap population for each U-Cl bond, the U(5f) population is ~0.059 (which is only 3% of the total U5f population in the ground state of $Cs_2UO_2Cl_4$ crystal). The ligand field splitting of 5fδ orbital is calculated as 0.61 eV and that for 5fφ is 0.67eV at the CIS level. The 5fφ splits more than 5fδ since it lies in a region of higher electron density.

The chloride ions will affect the Rydberg states more than the valence states. This is because the more diffuse the orbital is, the more strongly it will interact with the negatively charged ligands. For the free uranyl ion, the 8pπ state is 0.42eV lower than the 8pσ state, but, in the presence of chlorides, there is a reversal in the order and the $17b_u$ (8pσ) state is 3.70eV lower than the $11a_u$ (8pπ) state.

In addition to the short-range repulsive interaction with the neighboring chloride ions, diffuse orbitals will also experience the long-range Madelung potential due to the neighboring ions. It is the interplay between the two that will decide the radial extent and the energy of the diffuse orbitals.

6.3.5 Transition Assignments For Bands Below the Ionization Threshold

Since the experiment was performed on the crystal, we have used our crystalline-state calculation result for the assignment of the peaks in Figure 6.1. The symmetry-broken results are displayed in Tables 6.6 and 6.7. The values shown in these tables are averages of all the double-group states resulting from the respective electronic states.

For the assignment of peaks in the lowest energy side of the spectrum, we can use the model of the active-electron approximation, since in this energy range the single-electron excitation process dominates [144]. Hence we have assigned the broad peaks at 534 and 536 eV to overlap between more than one one-electron process. The presence of many eigenstates in this region (534 and 536 eV) further validates the assignment of these bands to the superposition of the excitation to various unoccupied orbitals.

The strong and sharp peak at 531 eV corresponds to the transition to the state with mostly 5fπ character. The assignment for this peak is consistent with Denning *et al.*'s [141] result using ADF. The agreement for the first peak gains importance as the relative difference between the states will also aid in the assignment of the other peaks. Along the same line, peaks in Table 6.6 and Table 6.7 are decreased by 0.56 eV in order to align the very first theoretical and experimental peaks.

The perpendicularly polarized peak at 536 eV is broad enough to be assigned to an excitation involving one allowed transition. This band comprised of the excitation where the core electron is excited to a state with the following configurations: $1\sigma^1 6\pi^1$ (536.17eV), $1\sigma^1 7\pi^1$ (536.95 eV) and $1\sigma^1 8\pi^1$ (537.92). The wave-function character corresponding to the 6π, 7π and 8π states is listed in Table 6.6.

The unexpected result we encountered for uranyl embedded in the crystal was the spacing between the 5π (U5fπ) and the 10σ (U5fσ) orbital. For the free uranyl ion, the composition of the 10σ orbital formed by the antibonding interaction between U5fσ and O2pσ is 40%U5fσ + 33.95% O2pσ + 22.95%U6pσ + 2.4% O2sσ, but in the crystal, the corresponding wave function has the makeup of 93.45%U5fσ + 5.5%O2pσ + 0.27%U6pσ. According to Denning *et al.* [141], it is the U6p, U5f and O2p mixing that contributes strongly to the spacing between the 5π (U5fπ) and the 10σ (U5fσ) orbital. From the compositions of the 10σ orbital, it is evident that with the increase in the U-O bond length, there is a reduced interaction of the 6p orbital with the oxygen orbitals, which is further accompanied by a decrease in the magnitude of the hole on U6p [157]. At the SCF level of theory, the energy difference between the 5fπ and 5fσ in free uranyl ion is of the order of 3.7eV and in case uranyl ion embedded in the crystal this difference is reduced to 0.41 eV. The parallel polarized peak centered at ~531 eV is ascribed to the transition to the 10σ state (U5fσ) state as shown in Table 6.7.

The parallel-polarized band at 534.1 eV is broad and has a small bump on the high-energy side around 536 eV. Based on our calculated results we have assigned this structure to the wave functions involving the $1\sigma^1 11\sigma^1$, $1\sigma^1 12\sigma^1$ and $1\sigma^1 13\sigma^1$ configurations (Table 6.7).

6.3.6 Assignments Above the Ionization Threshold

Shape resonances have been a topic of contention for some time. For a more through background of the topic, the reader is referred to the following papers that discuss the phenomenon in both atomic and molecular systems [142-145, 147, 158, 159].

The term shape resonance simply means that the resonance behaviors arises from the "shape", i.e., the potential barrier which is formed due to the interaction between the repulsive centrifugal force (varies as $1/r^2$) and the attractive columbic potential (varies as $1/r$). Although in atomic systems the barrier is known for states with d- and f angular momentum [142-143], in molecular fields, due to the larger spatial charge distribution, the resonances are expected to be associated with states with even larger angular momentum.

In our work we assign shape resonances to the unoccupied valence or Rydberg type MOs with large angular momentum embedded in the continuum. The direction of the polarization vector has facilitated the assignment. The σ and π shape resonances will contribute, when the polarization vector is parallel to and perpendicular to the O-U-O molecular axis. In the spectrum (Figure 6.1) there are two peaks corresponding to the parallel transition and one peak corresponding to the perpendicular transition above the threshold at 540 and 551 eV respectively. Similar shape resonance profiles have also been observed for the O K-edge photoionization spectra of CO_2 [159]. For the O K-edge X-ray spectrum of CO_2 also, only the shape resonance associated with σ symmetry is observed at 540 eV. In fact, the occurrence of only the σ shape resonance state has been the most common case in the literature [145]. Since there is no firm basis behind this, we have not used it as the basis for assignments in this chapter.

From Table 6.7 (based on a single excitation process), we can see that the band at 541 eV corresponds to the 5g states with heavy mixing with U7d, U8s, U8p and Cl3p states, which is in line with the analysis that the auto-ionizing states are usually only sharp for the states with higher angular momenta under the one-electron description. In this region of the spectrum, the band structure can also be partly or fully a result of multiple-excitation processes. To quantify its magnitude with respect to resonance states is rather difficult. This is due to two reasons: (1) many configurations of doubly excited states are possible and (2) there are many orbitals in the valence and Rydberg state with varying screening power.

Finally, in order to investigate the band at 551eV, we included the 6h orbital in our calculation to check if we can assign a one-electron shape resonance structure to this parallel and perpendicular polarized peak. At the SCF level, the energy difference between the 5g and 6h orbitals was of the order of 1-1.5eV. Due to this small difference between the two orbitals, we did not ascribe the band at 551eV to the autoionizing 6h shape resonance.

The band at 551eV is polarized (change in position and intensity with change in direction of the polarization vector) and it has a corresponding emission spectrum [141]. Hence this band cannot be a result of multiple scattering of the excited electron by the atoms surrounding the emitting atom

Multiple-scattering calculations have been performed to examine the X-ray absorption spectrum at the oxygen K-edge for UO_2 [133,134]. Using the Multiple Scattering (MS) Simulation they have assigned the band at 562 eV to multiple scattering with the neighboring shells from the central oxygen atoms. It is not appropriate to compare the results for UO_2 with the results shown in Figure 6.1 based on following reasons; firstly the U-O bond length is 2.37 Å and 1.77 Å in UO_2 and $Cs_2UO_2Cl_4$ respectively. Hence the U-O scattering in uranyl should be even higher than 562 eV. Secondly the compounds have different crystalline structure. $Cs_2UO_2Cl_4$ has a monoclinic structure whereas UO_2 crystallizes in the fluorite structure. Hence a MS calculation performed on the X-ray absorption spectra of $Cs_2UO_2Cl_4$ can only determine whether the structure at 551 eV is a fingerprint of the geometric structure or it is as a result of a double excitation-ionization process.

6.4 Conclusions

The Soft X-ray spectrum of Denning and co-workers for the high-lying excited levels at the oxygen K-edge for $Cs_2UO_2Cl_4$ is studied theoretically. We performed calculations with uranyl as a free ion and as an ion embedded in the crystal. The calculations in the crystalline environment were done using the crystal model previously developed by our group. The states are being studied well above the ionization potential and so they are resonances and methods must be used that do not collapse to lower energy continuum states. At this level of theory, localized and delocalized hole description gives different results so we have computed both sets of values. An important part of the investigation is the intensities of the polarized bands near and well above the ionization threshold of the oxygen 1s orbital. According to our results the band at 551 eV is not due to autoionizing 5g and 6h shape resonance. As a result this structure might be a result of a multiple excitation-ionization process

Our calculation provides the wave-function character and excitation energies for the experimentally observed features, which extends from 530 eV to 550 eV. The calculated results for states below the oxygen 1s ionization threshold display an error magnitude of 0.5-1 eV when compared with the experimental results. This is expected, as there were a limited number of active orbitals and a limited length of CI expansions. The assignment of the states can be further strengthened by transition-moment calculations since the experimental data on the relative intensities for different states is available.

	Ground	Localized Hole State	Delocalized Hole State
Oxygen Centered Orbitals			
$O1s_A$	1.999	1.999	1.500
$O1s_B$	1.999	1.001	1.500
$O2s_A$	1.881	1.910	1.921
$O2s_B$	1.881	1.930	1.921
$O2p_A$	4.174	3.921	4.487
$O2p_B$	4.174	4.993	4.487
Total Population	16.164	15.814	15.878
Charge q_o	-0.082	-0.407	-0.439
Uranium Centered Orbitals			
Us	2.037	2.018	2.018
Up	5.814	5.800	5.791
Ud	11.492	11.138	11.134
Uf	2.496	2.233	2.183
Ug	-0.004	-0.004	-0.005
Total Population	21.836	21.185	21.122
Charge q_u	+2.164	+2.815	+2.878

Table 6.1. Mulliken Population analysis for U and O centers of UO_2^{2+} for a U-O distance of 3.155 bohr

Species	R (U-O) (bohr)	O1s Ionization Potential (eV)				
		Symmetry Broken (I)	Symmetry Adapted (II)	Frozen-orbital (III)	ΔE (II – I)	ΔE (III – I)
UO_2^{2+}	3.156	554.91	565.93	574.56	11.02	19.65
$UO_2Cl_4^{2-}$	3.252	531.53	542.66	552.69	11.13	21.16
$Cs_2UO_2Cl_4$	3.252	537.29	548.47	558.49	11.18	21.20

Table 6.2: Oxygen 1s Ionization energies at the SCF approximation

Configuration	Wavefunction Character	Polarization	Excitation Energies (eV)
$1\sigma^1\ 1\varphi^1$	U5fφ	-	529.8996
$1\sigma^1\ 2\delta^1$	U5fδ	-	529.5219
$1\sigma^1\ 5\pi^1$	U5fπ*	⊥	531.3086
$1\sigma^1\ 10\sigma^1$	U5fσ*	‖	536.9938
$1\sigma^1\ 3\delta^1$	U6dδ	-	533.5056
$1\sigma^1\ 6\pi^1$	U6dπ*	⊥	538.0691
$1\sigma^1\ 9\sigma^1$	U7sσ + U6dσ*	‖	534.3760
$1\sigma^1\ 12\sigma^1$	U6dσ* + U7sσ	‖	543.4209
$1\sigma^1\ 7\pi^1$	U7pπ	⊥	539.5639
$1\sigma^1\ 11\sigma^1$	U7pσ	‖	541.7565
$1\sigma^1\ 4\delta^1$	U7dδ	-	544.2288
$1\sigma^1\ 8\pi^1$	U7dπ	⊥	544.3552
$1\sigma^1\ 13\sigma^1$	U7dσ	‖	544.9750
$1\sigma^1\ 9\pi^1$	U8pπ	⊥	545.6728
$1\sigma^1\ 14\sigma^1$	U8pσ	‖	546.0937
$1\sigma^1\ 1\gamma^1$	U5gγ	-	548.1392
$1\sigma^1\ 2\varphi^1$	U5gφ	-	548.1448
$1\sigma^1\ 5\delta^1$	U5gδ	-	548.1717
$1\sigma^1\ 10\pi^1$	U5gπ	⊥	548.2474
$1\sigma^1\ 15\sigma^1$	U5gσ	‖	548.3196

Table 6.3: Vertical excitations energies of the UO_2^{2+} ion at U(R-O) = 3.155 bohr. (symmetry-broken solution)

Configuration	Wavefunction Character	Polarization	Excitation Energies (eV)
$1\sigma_g^1\ 1\varphi_u^1$	U5fφ	-	531.7871
$1\sigma_g^1\ 1\delta_u^1$	U5fδ	-	531.2847
$1\sigma_g^1\ 3\pi_u^1$	U5fπ∗	$\perp$	533.0766
$1\sigma_g^1\ 5\sigma_u^1$	U5fσ∗	$\parallel$	538.0638
$1\sigma_u^1\ 2\delta_g^1$	U6dδ	-	534.4716
$1\sigma_u^1\ 3\pi_g^1$	U6dπ∗	$\perp$	538.3920
$1\sigma_u^1\ 5\sigma_g^1$	U7sσ + U6dσ∗	$\parallel$	535.0923
$1\sigma_u^1\ 6\sigma_g^1$	U6dσ∗ + U7sσ	$\parallel$	543.7263
$1\sigma_g^1\ 4\pi_u^1$	U7pπ	$\perp$	540.2403
$1\sigma_g^1\ 6\sigma_u^1$	U7pσ	$\parallel$	542.2359
$1\sigma_u^1\ 3\delta_g^1$	U7dδ	-	544.5676
$1\sigma_u^1\ 4\pi_g^1$	U7dπ	$\perp$	544.7706
$1\sigma_u^1\ 7\sigma_g^1$	U7dσ	$\parallel$	545.2114
$1\sigma_g^1\ 5\pi_u^1$	U8pπ	$\perp$	546.0049
$1\sigma_g^1\ 7\sigma_u^1$	U8pσ	$\parallel$	546.4502
$1\sigma_u^1\ 1\gamma_g^1$	U5gγ	-	548.4944
$1\sigma_u^1\ 1\varphi_g^1$	U5gφ	-	548.5091
$1\sigma_u^1\ 5\delta_g^1$	U5gδ	-	548.6035
$1\sigma_u^1\ 4\pi_g^1$	U5gπ	$\perp$	548.6238
$1\sigma_u^1\ 8\sigma_g^1$	U5gσ	$\parallel$	548.7566

Table 6.4: Vertical excitations energies of the UO_2^{2+} ion at U(R-O) = 3.155 bohr. (symmetry-restricted solution)

Assigned Transition	Wavefunction Character of the Excited State	This work (eV)	Denning *et al.* ref [144] (eV)
$1\sigma \rightarrow 5\pi$ $1\sigma \rightarrow 9\sigma$ $1\sigma \rightarrow 10\sigma$ $1\sigma \rightarrow 6\pi$	$5f\pi$ $5f\sigma$ $7s\sigma + 6d\sigma$ $6d\pi$	531.31 536.99 534.15 538.06	531.9 536.8 533.8 537.3

Table 6.5: Comparison of Excitation Energies for UO_2^{2+} (symmetry-broken results)

	Experimental Peaks (eV)	Theoretical Result (I) (eV)	I – 0.56 eV	Configuration $C_{\infty v}$	Wave function Character
I	531.4 (strong and sharp)	531.96	531.4	$1\sigma^1 5\pi^1$	$5f\pi$ + O2p
II	536 (strong and Broad)	536.73 537.51 538.48	536.17 536.95 537.92	$1\sigma^1 6\pi^1$ $1\sigma^1 7\pi^1$ $1\sigma^1 8\pi^1$	$6d\pi$ $7p\pi$ $7d\pi$

Table 6.6: Assignment of Peaks for Perpendicular Polarization (symmetry-broken results)

	Experimental Peaks (eV)	Theoretical Result (I) (eV)	I – 0.56 eV	Con-figuration $C_{\infty v}$	Wave function Character
III	531.4 (strong and sharp)	531.98	531.42	$1\sigma^1 10\sigma^1$	5fσ + O2p
IV	533-538 (strong and Broad with a hump at 536 eV)	535.34 536.09 537.35	534.78 535.53 536.79	$1\sigma^1 11\sigma^1$ $1\sigma^1 12\sigma^1$ $1\sigma^1 13\sigma^1$	7sσ + 6dσ 7pσ 6dσ + 7sσ
V	541 (weak and broad)	540.24 – 543.71	539.68 –543.15		5g (+ U7d, U8s, U8p and Cl3p) and Double excitation process

Table 6.7: Assignment of peaks for Parallel Polarization (symmetry-broken results)

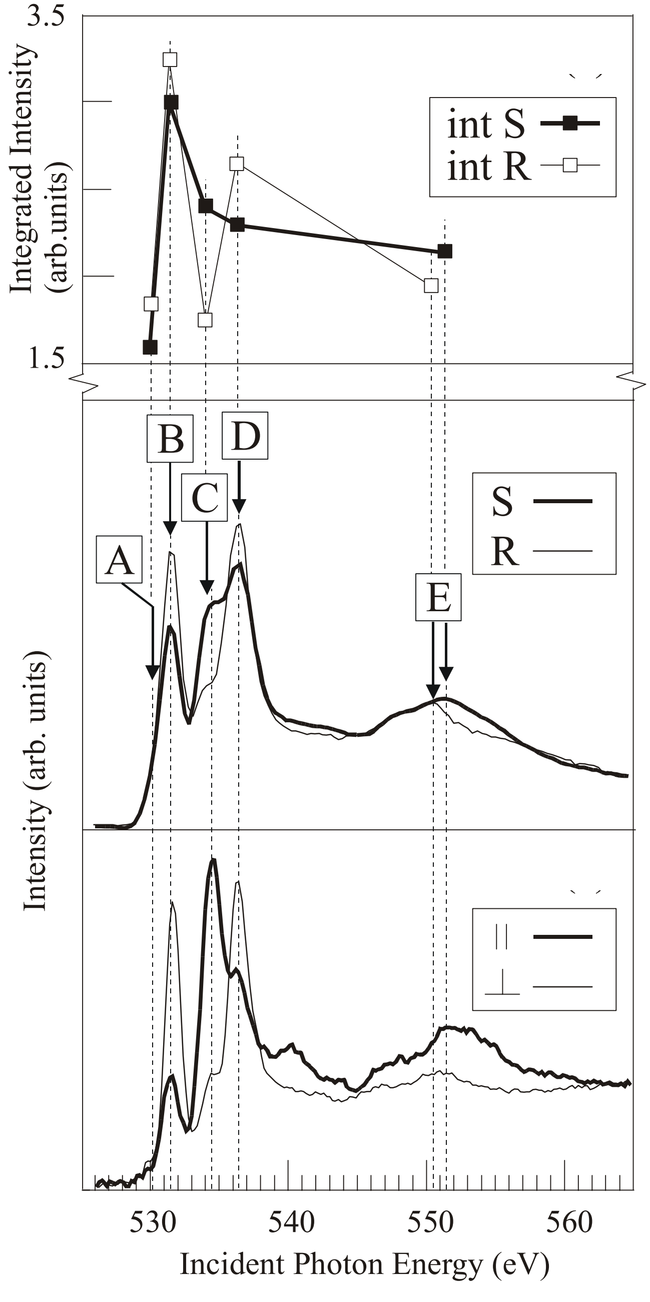

Figure 6.1: X-ray absorption spectrum at the oxygen K-edge for $Cs_2UO_2Cl_4$ (ref [144])

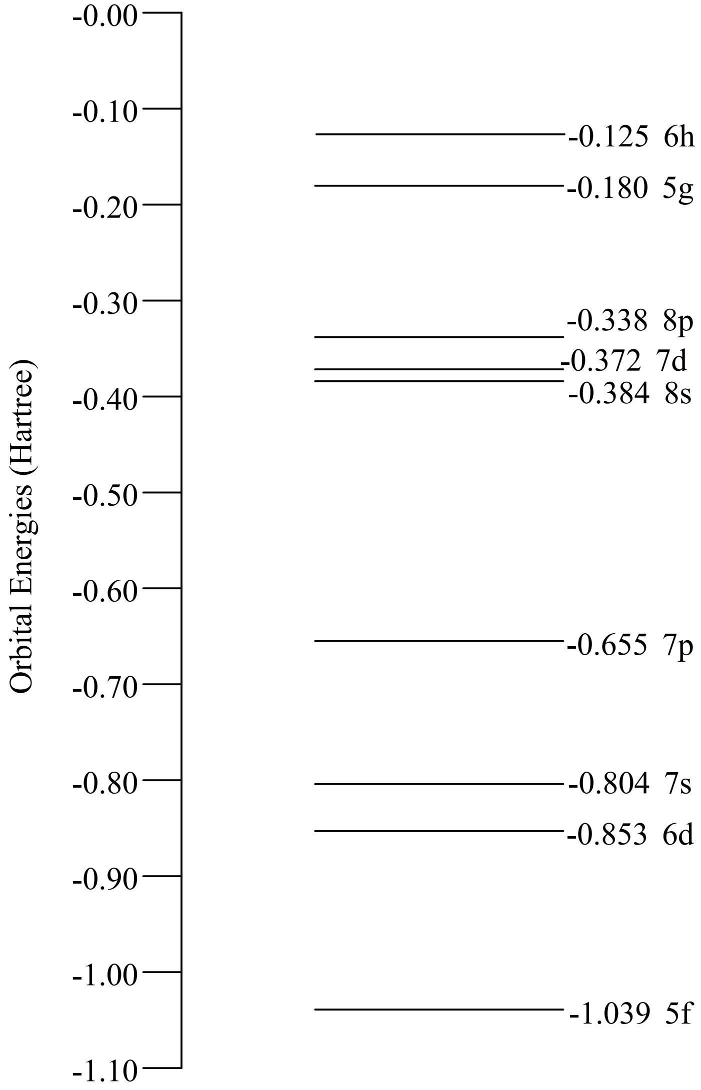

Figure 6.2: Orbital Energies of the valence orbitals of U^{+2} ion from relativistic Hartree-Fock wave functions

BIBLIOGRAPHY

[1] N. W. Winter, R. M. Pitzer, and D. K. Temple, *J. Chem. Phys.*, **86,** 2945 (1987)

[2] R. Shepard, I. Shavitt, R. M. Pitzer, D. C. Comeau, M. Pepper, H. Lischka, P. G. Szalay, R. Ahlrichs, F. B. Brown and J. G. Zhao, *Int. J. Quantum Chem.*, **22**, 149 (1998)

[3] S. Yabushita, Z. Zhang and R. M. Pitzer, *J. Phys. Chem.*, **103**, 5791 (1999)

[4] H. L. Hsu, R. M. Pitzer and E. R. Davidson, *J. Chem. Phys.*, **65,** 609 (1976)

[5] T. H. Fischer, and J. Almlöf, *J. Chem. Phys.*, **96,** 9768 (1992)

[6] S. P. Bagus, and H. F. Schaefer, *J. Chem. Phys.*, **56,** 224 (1975)

[7] H. Ågren, P. S. Bagus, B. O. Roos, *Chem. Phys. Lett.*, **82,** 505 (1981)

[8] R. L. Lozes, O. Goscinski and U. I. Wahlgren, *Chem. Phys. Lett.*, **63(1),** 77 (1979)

[9] P. J. Hay, L. R. Kahn, R. C. Raffenetti and D. H. Phillips, *J. Chem. Phys.*, **71,** 1767 (1979)

[10] A. M. Bernard, *Theor. Chim. Acta.*, **61(4),** 379 (1982)

[11] R. Broer and W. C. Nieuwpoort, *Theor. Chim. Acta.*, **73,** 405 (1988)

[12] *Relativistic Electronic Structure Theory*, Part 2, edited by P. Schwerdtferger (Elsevier)

[13] D. D. Koelling and A.J. Freeman, *Phys. Rev. B.*, **7**, 4454 (1973)

[14] M. Krauss and W. J. Stevens, *Ann. Rev. Phys. Chem.*, **35**, 357 (1984).

[15] P. A. Christiansen, W. C. Emler and K. S Pitzer, *Annu. Rev. Phys. Chem.*, **71,** 1767 (1979)

[16] K. Balasubramanium, *Chem. Rev.*, **90**, 93 (1990)

[17] P. A. Christiansen, Y. S. Lee and K. S Pitzer, *J. Chem. Phys.*, **72,** 4445 (1979)

[18] L.F. Pacios and P.A. Christiansen, *J. Chem. Phys.*, **82**, 2664 (1985)

[19] M.M. Hurley, L.F. Pacios, P.A. Christiansen, R.B. Ross and W.C. Ermler, *J. Chem. Phys.*, **84**, 6840 (1986)

[20] L.A. LaJohn, P.A. Christiansen, R.B. Ross, T. Atashroo and W.C. Ermler, *J. Chem. Phys.*, **87**, 2812 (1987)

[21] R.B. Ross, J.M. Powers, T. Atashroo, W.C. Ermler, L.A. LaJohn and P. A. Christiansen, *J. Chem. Phys.***,** **93**, 6654 (1990)

[22] W. C. Ermler, R. B. Ross and P. A. Christiansen, *Int. J. Quant. Chem.*, **40**, 829 (1991)

[23] R. B. Ross, G. Gayen and W. C. Ermler, *J. Chem. Phys.*, **100**, 8145 (1994)

[24] M. Dolg, *J. Chem. Phys.*, **104**, 4061 (1996)

[25] M. Dolg, *Chem. Phys. Lett.*, **250**, 75 (1996)

[26] E. V. Beck, L. W. Burggraf, S. R. Brozell, J. P Blaudeau and R. M. Pitzer, Manuscript in Preparation (2005)

[27] C. C. J. Roothaan and P. S. Bagus, *Meth. Comp. Phys.*, **2,** 47 (1963)

[28] B. Roos, C. Salez, A. Veillard, and E. Clementi, *IBM Research RJ518* (1968)

[29] R. M. Pitzer, *QCPE*, 10, 587 (1990)

[30] R. M. Pitzer, *Comp. Phys. Commun.*, **170(3)**, 239 (2005)

[31] S. F. Boys, G. B. Cook, C. M. Reeves and I. Shavitt, *Nature*, **178**, 1207 (1956)

[32] T. H. Dunning, Jr., *J. Chem. Phys.*, 55: 716-723, 1971

[33] T. H. Dunning, Jr., *J. Chem Phys.*, 90, 1007 (1989)

[34] D. E. Woon, and T. H. Dunning, Jr., J. Chem Phys., **98**, 1358 (1993)

[35] D. E. Woon, and T. H. Dunning, Jr., J. Chem Phys., **100**, 2975 (1994)

[36] D. E. Woon, and T. H. Dunning, Jr., J. Chem Phys., **103**, 4572 (1995)

[37] A. K. Wilson, and T. H. Dunning, Jr., J. Chem Phys., **106**, 8718 (1997)

[38] K. A. Peterson, and T. H. Dunning, Jr., J. Phys. Chem A., **106**, 6280 (1997)

[39] T. H. Dunning, K. A. Peterson, A. K. Wilson, *J. Chem Phys.*, **114**, 9244 (2001)

[40] J. P Blaudeau and L. A. Curtis, *Int. J. Quant. Chem.*, **61**, 943 (1997)

[41] S. Matsika and R. M. Pitzer, *J. Phys. Chem. A.*, **102**, 1652 (1998)

[42] P. A. Christiansen, *J. Chem. Phys.,* **112,** 10070 (2000)

[43] J. P Blaudeau, S. R. Brozell, S. Matsika, Z. Zhang and R. M. Pitzer, *Int. J. Quant. Chem.*, **77**, 516 (2000)

[44] T. Yang, R. Tyagi and R M. Pitzer, Manuscript in Preparation (2005)

[45] R. D. Brado, and K. Ruedenberg, *J. Chem Phys.*, **60**, 918 (1974)

[46] R. D. Brado, and K. Ruedenberg, *J. Chem Phys.*, **60**, 932 (1974)

[47] S. Huzinaga and M. Klobukowski, *Chem. Phys. Lett.*, 120, 509 (1985)

[48] G. A. Petersson, S. Zhong, J. A. Montgomery, Jr. and M. J. Frisch, *J. Chem Phys.*, **118(3)**, 1101 (2003)

[49] P. O. Lowdin, *Advan. Chem. Phys.*, **2**, 207 (1959)

[50] C. C. J. Roothaan, *Rev. Mod. Phys.*, **32**, 179 (1960)

[51] S. R. Langhoff and E. R. Davidson, *Int. J. Quant. Chem.*, **8**, 61 (1974)

[52] E. A. Hylleraas, *Z. Physik*, **48**, 469 (1928)

[53] S. F. Boys, *Proc. Roy. Soc. (London)*, **A201**, 125 (1950)

[54] P.-O. Löwdin, *Phys. Rev.*, **97**, 1474 (1955)

[55] P.-O. Löwdin, *Phys. Rev.*, **97**, 1490 (1955)

[56] I. Shavitt, *Methods of Electronic Structure Theory*, ed. H. F. Schaefer III (Plenum, New York (1977), p. 189

[57] B. R. Brooks, and H. F. Schaefer, *J. Chem. Phys.*, **70**, 5092 (1979)

[58] K. A. Brueckner, *Phys. Rev.*, **97**, 1353 (1955)

[59] K. A. Brueckner, *Phys. Rev.*, **100**, 36 (1955)

[60] J. Goldstone, *Proc. Roy. Soc. (London)*, **A239**, 267 (1957)

[61] R. J. Bartle and G. D. Purvis, *Int. J. Quantum Chem.***,** **16**, 561 (1978)

[62] Cizek, J., and Paldus, J., *Int. J. Quantum Chem.,* **5(4)**, 359 (1971)

[63] F. E. Harris, *Int. J. Quantum Chem.*, **11**, 403 (1977)

[64] F. E. Harris, *"Electrons in Finite and Infinite Structures"* (P. Phanseau and L. Scheive, eds.). Plenum, New York (1977)

[65] K. Hirao, and Y. Ishikawa, *Recent Advances in Relativistic Molecular Theory*, pages 47–109, World Scientific Publishing, (2004)

[66] R. J. Buenker, G. Hirsch, Y. Li, J.-P. Gu, A. B. Alekseyev, H.-P. Libermann, and Mi. Kimura, *Computational Molecular Spectroscopy*, John Wiley, Chichester (2000)

[67] http://www.itc.univie.ac.at/~hans/Columbus/columbus_parallel.html

[68] L. A. Kaledin, J. E. McCord and M. C. Heaven, J. Mol. Spectrosc. **164**, 27 (1994)

[69] K. P. Huber and G. Herzberg, *Spectroscopic Constants of Diatomic Molecules*, Van Nostrand Reinhold, Princeton, NJ, 1979

[70] V. Goncharov, and M. C. Heaven, *J. Chem. Phys.*, **122**, 204311 (2005)

[71] S. D. Gabelnick, G. T. Reedy, and M. G. Chassanov, *J. Chem. Phys.*, **60,** 1167 (1974)

[72] E. U. Condon and G. H. Shortley, *The Theory of Atomic Spectra*, Cambridge University Press, London, 1935, 1963

[73] J. C. Slater, *Quantum Chemistry of Atomic Structure*, McGraw-Hill, New York, 1960

[74] http://www.nist.gov

[75] J. Paulovič, T. Nakajima, K. Hirao, R. Lindh and P. Å. Malmqvist, *J. Chem. Phys.*, **119**, 798 (2003)

[76] J. B. Newman, *J. Chem. Phys.*, **47,** 85 (1967)

[77] C. Görller-Walrand and L. G. Vanquickenborne, *J. Chem. Phys.*, **57,** 1436 (1972)

[78] S. Matsika, Z. Zhang, S. Brozell, J. Blaudeau, Q. Wang and R. M. Pitzer, *J. of Phys. Chem. A*, **105**, 3825 (2001)

[79] J. Han, V. Goncharov, L. A. Kaledin and A. V. Komissarov, *J. Chem. Phys*, **120**, 5155 (2004)

[80] C. J . Lue, J. Jin, M. J. Ortiz, J. C. Rienstra-kiracofe and M. C. Heaven, *J. Am. Chem. Soc.*, **126**, 1812 (2004)

[81] M. Zhou, L. Andrews, N. Ismail and C. Marsden, *J. Phys. Chem. A*, **104**, 5495 (2000)

[82] E. G. Rauh and R. J. Ackerman, J. Chem. Phys, **60,** 1396 (1974)

[83] J. Han, L. A. Kaledin, V. Goncharov, A. V. Komissarov and M. C. Heaven, *J. Am. Chem. Soc.*, **125**, 7176 (2003)

[84] L. Gagliardi, M. C. Heaven, J. W. Krogh, J. Wisborg and B. O. Roos, *J. Am. Chem. Soc.*, **127(1)**, 86 (2005)

[85] Q. Chang, Master's Thesis, Ohio State University, 2002

[86] L. Gagliardi, B. O. Roos, P. Å. Malmqvist and J. M. Dyke, *J. Phys. Chem. A*, **105**, 10602 (2001)

[87] P. Pyykkö and L. Laaksonen, *J. Phys. Chem.*, **88**, 4892 (1984)

[88] Z. Zhang and R. M. Pitzer, *J. Phys. Chem. A*, **103**, 6881 (1999)

[89] S. Matsika and R. M. Pitzer, *J. Phys. Chem. A*, **104**, 4064 (2000)

[90] B. R. Judd, *Phys. Rev.*, **125**, 613 (1962)

[91] The Chemistry of Uranium, edited by J. Katz and E. Rabinowitch (McGraw-Hill, New York, 1951)

[92] M. C. Heaven, J. P. Nicolai, S. J. Riley and E. K. Parks, *Chem. Phys. Lett.*, **119,** 229 (1985)

[93] L. A. Kaledin, E. A. Shenyavskaya and L. A. Gurvich, *Russ J. Phys. Chem.*, **60**, 633 (1986)

[94] L. A. Kaledin, A. N. Kulikov, A. I. Kobyliansky, E. A. Shenyavskaya and L. A. Gurvich, *Russ J. Phys. Chem.*, **61**, 712 (1987)

[95] J. M. Dyke, A. M. Ellis, M. Feher and A. Morris, *Chem. Phys. Lett.*, **145**, 159 (1988)

[96] L. A. Kaledin, A. N. Kulikov and L. A. Gurvich, *Russ J. Phys. Chem.*, **63**, 439 (1989)

[97] L. A. Kaledin, J. E. McCord and M. C. Heaven, *J. Mol. Spectrosc.*, **164**, 27 (1994)

[98] L. A. Kaledin and M. C. Heaven, *J. Mol. Spectrosc.*, **185**, 1 (1997)

[99] S. D. Gabelnick, G. T. Reedy and M. G. Chasanov, *J. Chem. Phys.*, **58,** 4468 (1973)

[100] R. D. Hunt and L. Andrews, J. Chem. Phys., **98**, 3690 (1993)

[101] V. Goncharov and M. C. Heaven, MG14 International Symposium on Molecular Spectroscopy 60th Meeting (2005)

[102] J. J. Katz, G. T. Seaborg, and I. R. Morss (Eds). The Chemistry of Actinide Elements, Second Edition, Vol. 2, Chapman and Hall, London (1986)

[103] R. W. Field, *Ber. Bunsen-Ges. Phys. Chem.*, 86, 771 (1982)

[104] D. D. Koelling and A.J. Freeman, *Phys. Rec. B.*, **7**, 4454 (1973)

[105] M. Krauss and W.J. Stevens, *Chem. Phys. Lett.*, **99**, 417 (1983)

[106] M. Krauss and W.J. Stevens, *Mol. Phys.*, **101**, 125 (2003)

[107] G. L. Malli, In The Challenge of d and f Electrons, Theory and Computation; D. R. Salahub, and M. C. Zerner, Eds.; ACS Symposium Series 394; American Chemical Society: Washington, DC, 1989

[108] C. M. Marian, U. Wahlgren, O. Gropen and P. Pyykkö, Theochem, **169**, 339 (1988)

[109] W. Küchle, M. Dolg, H. Stoll and H. Preuss, *J. Chem. Phys.*, **100**, 7535 (1994)

[110] J. Paulovič, T. Nakajima, K. Hirao, R. Lindh and P. Å. Malmqvist, J. *Chem. Phys.*, **119**, 798 (2003)

[111] V. Goncharov and M. C. Heaven, *J. Chem. Phys.*, **122**, 204311 (2005)

[112] G. Edvinsson and A. Lagerqvist, *J. Mol. Spectrosc.*, **113**, 93 (1985)

[113] G. Edvinsson and A. Lagerqvist, *J. Mol. Spectrosc.*, **122**, 428 (1987)

[114] G. Edvinsson and A. Lagerqvist, *Phys. Scr.*, **41**, 316 (1990)

[115] G. W. Lehman, *Phys. Rev.*, **116**, 846 (1959)

[116] J. Han, L. A. Kaledin, V. Goncharov, A. V. Komissarov and Michael C. Heaven, *J. Am. Chem. Soc.*, **125**, 7176 (2003)

[117] E. G. Rauh and R. J. Ackerman, *J. Chem. Phys.*, **60,** 1396 (1974)

[118] F. Capone, Y. Colle, J. P. Hiernaut and C. Ronchi, *J. of Phys. Chem. A*, **103**, 10899 (1999)

[119] J. K. Gibson, *Radiochim. Acta*, **81**, 83 (1998)

[120] X. Cao, M. Dolg and H. Stoll, *J. Chem. Phys.*, **118(2),** 487 (2003)

[121] J. J. Katz, G. T. Seaborg, and I. R. Morss (Eds). The Chemistry of Actinide Elements, Second Edition, Vol. 2, Chapman and Hall, London (1986)

[122] L. Gagliardi, B. O. Roos, P. Malmqvist and J. M. Dyke, *J. Phys. Chem. A*, **105**, 10602 (2001)

[123] Zhou, M.; Andrews, L.; Ismail and N.; Marsden, *J. Phys. Chem. A*, **104**, 5495 (2000)

[124] G. H. Igel-Mann, H. Stoll and H. Preuss, *Molec. Phys.*, **65**, 1321 (1988)

[125] M. Dolg and H. Soll, *Theor. Chem. Acta*, **75**, 369 (1989)

[126] M. Dolg, *J. Chem. Phys.*, **104,** 4061 (1996)

[127] H. H. Cornehl, C. Heinemann, J. Marcalo, A. P. de Matos and H. Schwarz, Angew. Chem., *Int. Ed. Engl.*, **35**, 891 (1996)

[128] E. A. Boudreaux and E. Baxter, *Int. J. Quantum Chem.*, **90**, 629 (2002)

[129] S. Köhler, R. Deiβenberger, E. Eberhardth, N. Erdmann, G. Herrmann, G. Huber, J. V. Kratz, M. Nunnemann, G. Passler, P. M. Rao, J. Riegel, N. Trautmann and K. Wendt, *Spectrochem. Acta, Part B*, **52,** 717 (1997)

[130] S. G. Lias, J. E. Bartmess, J. F. Liebman, J. L. Homes, R. D. Levin and W. G. Mallard, *J. Phys. Chem. Ref. Data,* 17 (1988).

[131] S. D. Gabelnick, G. T. Reedy and M. G. Chassanov, *J. Chem. Phys.*, **60,** 1167 (1974)

[132] W. R. Wadt, *J. Am. Chem. Soc.*, **103**, 6053 (1981)

[133] Z. Y. Wu, F. Jollet, N. Thromat, M. Gautier-Soyer and T. Petit, *J. Phys. Condensed Matter*, **11**, 7185 (1999)

[134] F. Jollet, T. Petit, S. Gota, N. Thromat, M. Gautier-Soyer and A Pasturel, *J. Phys. Condensed Matter*, **9**, 9393 (1997)

[135] B. W. Veal, D. J. Lam, W. T. Carnall, and H. C. Hoekstra, *Phys. Rev. B*, **12(12)**, 5651 (1975)

[136] J. Guo and D. E. Ellis, *Phys. Rev. B*, **39(9)**, 6125 (1989)

[137] E. A. Hudson, P. G. Allen, and L. J. Terminello, M. A. Denecke and T. Reich, *Phys. Rev. B*, **54**, 156 (1996)

[138] G. Kalkowski, G. Kaindl, W. D. Brewer, and W. Krone, *Phys. Rev. B*, **35**, 2667 (1987)

[139] E. A. Hudson, J. J. Rehr and J. J. Bucher, *Phys. Rev. B*, **52**, 13815 (1995)

[140] J. Petiau, G. Calas, D. Petitmaire, A. Bianconi, M. Benfatto and A. Marcelli, *Phys. Rev. B*, **34(10)**, 7350 (1986)

[141] R. G. Denning, C. J. Green, T. E. Hutchings, C. Dallera, A. Tagliaferri, K. Giarda, N. B. Brookes and L. Braicovich, *J. Chem. Phys.*, **117**, 8008 (2002)

[142] S. T. Manson and J. W. Cooper, *Phys. Rev.*, **165**, 126 (1968)

[143] U. Fano and J. W. Cooper, *Rec. Mod. Phys.*, **40**, 441 (1968)

[144] F. A. Gianturco, G. Guidotti and L. Lamanna, *J. Chem. Phys.*, **57**, 840 (1972)

[145] M . N. Piancastelli, Journal of Electron Spectroscopy and Related Phenomenon, **100**, 167 (1999)

[146] Z. Zhang and R. M. Pitzer, *J. Phys. Chem. A*, **103**, 6880 (1999)

[147] J. L. Dehmer, *J. Chem. Phys.*, **56**, 4495 (1972)

[148] L. S. Cederbaum and W. Domcke, *J. Chem. Phys.*, **66**, 5084 (1977)

[149] N. W. Winter, R. M. Pitzer and D. K. Temple, *J. Chem. Phys.*, **86**, 3549 (1987)

[150] N. W. Winter, R. M. Pitzer and D. K. Temple, *J. Chem. Phys.*, **87**, 2945 (1987)

[151] S. Matsika and R. M. Pitzer, *J. Phys. Chem. A*, **105**, 637 (2001)

[152] P. S. Bagus and H. F. Schaefer, *J. Chem. Phys.*, **56**, 224 (1975)

[153] L. C. Snyder, *J. Chem. Phys.*, **55**, 95 (1971)

[154] R. Broer and W. C. Nieuwpoort, *TheoChem*, **458**, 19 (1999)

[155] J. Baerends, ADF Program System, 2000.02 (Vrije Universiteit, Amsterdam, 2000)

[156] E. J. Baerends, E. G. Ellis and P. Ros, *J. Chem. Phys.*, **2**, 41 (1973) ; B. te Velde and E. J. Baerends, *J. Comput. Phys.*, **99**, 84 (1992)

[157] P.Pyykkö and L. Lohr, *Inorg. Chem.*, **20**, 1950 (1981)

[158] M. N. Piancastelli, D. W. Lindle, T. A. Ferrett and D. A. Shirlely, *J. Chem. Phys.*, **86**, 2765 (1987)

[159] N. Watanabe, J. Adachi, K. Soejima, E. Shingemasa, and A. Yagishita, N. G. Fomiykh and A. A. Pavlychev, *Phys. Rev. Lett.*, **78**, 4910 (1997)